

**Contributions to the FEL2001 Conference,
August 20-24, 2001 in Darmstadt, Germany**



October 2001, TESLA-FEL 2001-09

Contents

<i>M. Abo-Bakr^a, W. Anders^a, J. Bahr^a, R. Bakker^a, W. Eberhardt^a, B. Faatz^b, R. Follath^a, A. Gaupp^a, M. von Hartrott^a, E. Jaeschke^a, D. Krämer^a, P. Kuske^a, M. Martin^a, R. Müller^a, H. Prange^a, S. Reiche^c, W. Sandner^d, F. Senf^a, I. Will^d, G. Wüstefeld^a, ^a(BESSY, Berlin, Germany), ^b(DESY, Hamburg, Germany), ^c(UCLA, Los Angeles, USA), ^d(MBI, Berlin, Germany)</i>	
The BESSY FEL Project	1
<i>J. Bähr, K. Flöttmann, F. Stephan (DESY Zeuthen and Hamburg)</i>	
Development of a TV Diagnostics System for the Photoinjector Test facility at DESY Zeuthen	5
<i>V. Balandin, N. Golubeva, M. Körfer (DESY, Hamburg, Germany)</i>	
Studies of Beam Optics in the Collimation System for the Future Soft X-Ray User Facility	7
Number: Mo-P-38	
<i>I. Bohnet, J. Bähr, D. Lipka, F. Stephan, M. Winde, Q. Zhao (DESY Zeuthen), K. Flöttmann (DESY Hamburg)</i>	
Photo Injector Test Facility in the commissioning phase at DESY Zeuthen	15
<i>W. Brefeld^a, B. Faatz^a, J. Feldhaus^a, M. Körfer^a, J. Krzywinski^b, T. Möller^a, J. Pflüger^a, J. Rossbach^a, E.L. Saldin^a, E.A. Schneidmiller^a, S. Schreiber^a, M.V. Yurkov^c, ^a(DESY, Hamburg, Germany), ^b(IP PAS, Warszawa, Poland), ^c(JINR, Dubna, Russia)</i>	
Generation of High Power Coherent Soft X-ray Pulses by Subharmonically Seeded FEL at DESY	17
<i>W. Brefeld^a, B. Faatz^a, J. Feldhaus^a, M. Körfer^a, J. Krzywinski^b, T. Möller^a, J. Pflüger^a, J. Rossbach^a, E.L. Saldin^a, E.A. Schneidmiller^a, S. Schreiber^a, M.V. Yurkov^c, ^a(DESY, Hamburg, Germany), ^b(IP PAS, Warszawa, Poland), ^c(JINR, Dubna, Russia)</i>	
Development of a Femtosecond Soft X-ray SASE FEL at DESY	30
<i>W. Brefeld^a, B. Faatz^a, J. Feldhaus^a, K. Flöttmann^a, M. Körfer^a, J. Krzywinski^b, T. Limberg^a, T. Möller^a, J. Pflüger^a, J. Rossbach^a, E.L. Saldin^a, E.A. Schneidmiller^a, S. Schreiber^a, M.V. Yurkov^c, ^a(DESY, Hamburg, Germany), ^b(IP PAS, Warszawa, Poland), ^c(JINR, Dubna, Russia)</i>	
Linac-Based Synchrotron Radiation Facility with Femtosecond Soft X-ray Pulses ..	40
<i>W. Brefeld^a, B. Faatz^a, J. Feldhaus^a, M. Körfer^a, J. Krzywinski^a, T. Möller^a, J. Pflüger^a, J. Rossbach^a, E.L. Saldin^a, E.A. Schneidmiller^a, S. Schreiber^a, M.V. Yurkov^c, ^a(DESY, Hamburg, Germany), ^b(IP PAS, Warszawa, Poland), ^c(JINR, Dubna, Russia)</i>	
Generation of High Power Femtosecond Pulses by Sideband-Seeded X-ray FEL ...	49
<i>M. Brunken^a, H. Genz^a, C. Hessler^a, M. Hüning^b, H. Loos^a, A. Richter^a, P. Schmüser^b, S. Simrock^b, M. Tonutti^c, D. Türke^c, ^a(Darmstadt University of Technology, Darmstadt, Germany), ^b(DESY, Hamburg, Germany), ^c(RWTH Aachen, Aachen, Germany)</i>	
Electro-Optic Experiments at the TESLA Test Facility	60

<i>B. Faatz^a, A.A. Fateev^b, J. Feldhaus^a, C. Gerth^a, U. Hahn^a, U. Jastrow^a, M. Jurek^c, J. Krzywinski^c, N.I. Lebedev^b, M. Meschkat^a, V.A. Petrov^b, T.V. Rukoyatkina^b, E.L. Saldin^a, E.A. Schneidmiller^a, S.N. Sedykh^b, V.S. Shvetsov^b, W. Sobala^d, K.P. Sytchev^b, V.V. Tarasov^b, K. Tiedke^a, R. Treusch^a, M.V. Yurkov^b</i> , ^a (DESY, Hamburg, Germany), ^b (JINR, Dubna), ^c (IP PAS, Warszawa, Poland), ^d (Institute of Nucl. Physics, Cracow, Poland)	
Use of micro-channel plate for nondestructive measurement of VUV radiation from SASE FEL at the TESLA Test Facility	62
<i>B. Faatz^a, A.A. Fateev^b, J. Feldhaus^a, C. Gerth^a, U. Hahn^a, U. Jastrow^a, J. Krzywinski^c, N.I. Lebedev^b, J. Lewellen^d, L. Malkinski^c, M. Meschkat^a, V.A. Petrov^b, J. Rossbach^a, T.V. Rukoyatkina^b, E.L. Saldin^a, E.A. Schneidmiller^a, S. Schreiber^a, S.N. Sedykh^b, V.S. Shvetsov^b, R. Sobierajski^c, K.P. Sytchev^b, V.V. Tarasov^b, K. Tiedke^a, R. Treusch^a, M.V. Yurkov^b</i> , ^a (DESY, Hamburg, Germany), ^b (JINR, Dubna), ^c (IP PAS, Warszawa, Poland), ^d (APS-ANL, Argonne, USA)	
Alignment of the optical feedback system of VUV Regenerative FEL Amplifier at the TESLA Test Facility at DESY	68
<i>B. Faatz^a, A.A. Fateev^b, V.I. Kobets^b, I.N. Meshkov^b, S. Reiche^c, E.L. Saldin^a, E.A. Schneidmiller^a, M.V. Yurkov^b</i> , ^a (DESY, Hamburg, Germany), ^b (JINR, Dubna), ^c (UCLA, Los Angeles, USA)	
A concept of a 150 nm FEL oscillator driven by rf linear accelerator with a thermionic gun	76
<i>P. Gippner^a, E. Grosse^a, J. Pflüger^b, A. Schamlott^a, W. Seidel^a, U. Wolf^a, R. Wünsch^a</i> , ^a (Institut für Kern- und Hadronenphysik, FZ Rossendorf), ^b (HASYLAB, DESY Hamburg)	
Magnetic Characterization of the Hybrid Undulator U27 for ELBE	83
<i>M. Hüning, P. Schmüser</i> (DESY, Hamburg, Germany)	
Wake Fields Excited by a Rough Surface	85
<i>M. Körfer</i> for the TTF FEL Group (DESY, Hamburg, Germany)	
The TTF-FEL Status and its Future as a Soft X-ray User Facility	89
<i>D. Lipka^a, J. Bähr^a, I. Böhner^a, K. Flöttmann^b, D. Richter^c, F. Stephan^a, Q. Zhao^a</i> , ^a (DESY Zeuthen, Germany), ^b (DESY Hamburg, Germany), ^c (BESSY Berlin, Germany)	
Measurement of the longitudinal phase space for the Photo Injector Test Facility at DESY Zeuthen	94
<i>J. Pflüger, M. Tischer</i> (HASYLAB at DESY, Germany)	
Undulator Systems for the TESLA X-FELs	96
<i>Sven Reiche</i> (UCLA, Los Angeles, USA), <i>Bart Faatz</i> (DESY, Hamburg, Germany)	
Status of the 3D Time-Dependent FEL Simulation Code GENESIS 1.3	107
<i>E.L. Saldin, E.A. Schneidmiller</i> (DESY), <i>M.V. Yurkov</i> (JINR, Dubna)	
An Analytical Description of Longitudinal Phase Space Distortions	109
<i>M. Tischer^a, P. Ilinski^b, U. Hahn^a, J. Pflüger^a, H. Schulte-Schrepping^a</i> , ^a (HASYLAB at DESY, Hamburg, Germany), ^b (APS ANL, USA)	

Photon Diagnostics for the X-ray FELs at TESLA	118
<i>M.V. Yurkov for TTF FEL Team</i> ¹	
Statistical Properties of Radiation From SASE FEL: Experimental Results From SASE FEL at DESY	127

¹V. Ayvazyan, N. Baboi, I. Bohnet, R. Brinkmann, M. Castellano, L. Catani, P. Castro, M. Dohlus, H.T. Edwards, B. Faatz, A.A. Fateev, J. Feldhaus, K. Flöttmann, A. Gamp, T. Garvey, C. Gerth, V. Gretchko, B. Grigoryan, U. Hahn, C. Hessler, K. Honkavaara, M. Hüning, R. Ischebeck, M. Jablonka, T. Kamps, M. Körfer, M. Krassilnikov, J. Krzywinski, J. Lewellen, M. Liepe, A. Liero, T. Limberg, H. Loos, C. Magne, J. Menzel, P. Michelato, M. Minty, A. Mosnier, U.-C. Müller, D. Nölle, A. Novokhatski, C. Pagani, F. Peters, J. Pflüger, P. Piot, L. Plucinski, K. Rehlich, I. Reyzl, A. Richter, J. Rossbach, E.L. Saldin, W. Sandner, H. Schlarb, G. Schmidt, P. Schmüser, J.R. Schneider, E.A. Schneidmiller, H.J. Schreiber, S. Schreiber, D. Sertore, S. Setzer, S. Simrock, R. Sobierajski, B. Sonntag, B. Steeg, F. Stephan, K.P. Sytchev, K. Tiedtke, M. Tonutti, R. Treusch, D. Trines, D. Türke, V. Verzilov, R. Wanzenberg, T. Weiland, H. Weise, I. Will, K. Wittenburg, M.V. Yurkov, K. Zapfe

The BESSY* FEL Project

M. Abo-Bakr^a, W. Anders^a, J. Bahrdt^a, R. Bakker^a, W. Eberhardt^a, B. Faatz^b, R. Follath^a,
 A. Gaupp^a, M. von Hartrott^a, E. Jaeschke^a, D. Krämer^a, P. Kuske^a, M. Martin^a, R. Müller^a,
 H. Prange^a, S. Reiche^c, W. Sandner^d, F. Senf^a, I. Will^d, G. Wüstefeld^a

^aBESSY, Albert-Einstein-Straße 15, D-12489 Berlin, Germany

^bDESY Hamburg, Notkestraße 85, D-22607 Hamburg, Germany

^cUCLA, Particle Beam Physics Lab, CA 90095, USA

^dMax-Born-Institut, Max-Born-Straße 2A, D-12489 Berlin, Germany

Abstract

BESSY plans to construct a linac-based single-pass FEL as an addition to its existing third generation storage-ring based light-source. The project aims to obtain an FEL-based user-facility that covers the VUV and soft X-ray spectral range ($0.01 \leq \hbar\omega \leq 1$ keV). At present the design-stage is funded as a collaboration between BESSY, DESY, the Hahn-Meitner-Institute (HMI) in Berlin, and the Max-Born-Institute (MBI) in Berlin. The design stage focuses on optimization of the FEL as a user light-source, both with respect to its capabilities and in its performance. Important issues are stability, seeding options of the SASE FEL, wavelength-tunability, synchronization with external laser sources and, on a longer time-scale, the generation of ultra-short (< 20 fs RMS) optical pulses.

PACS: 41.60.Cr, 42.72.Bj, 07.85.Fv, 29.17.+w,

Keywords: Single-pass Free-Electron Laser, User facility, VUV, Soft X-ray, Proposal

1. Introduction

The Berliner Elektronenspeicherring-Gesellschaft für Synchrotronstrahlung (BESSY) operates storage-ring based synchrotron light-source since 1981. BESSY II started user operation in January 1999, delivering world class high brilliance photon beams in the VUV to XUV spectral range [1]. Based on its experience BESSY now proposes the construction of a SASE FEL as an addition to BESSY II, both for its traditional user-community and for the laser community, which has expressed a broad scientific interest. The target photon energy range is 10 eV to 1 keV ($120 \geq \lambda \geq 1.2$ nm) with a peak-brilliance of (at least) 10^{31} photons/sec/mm²/mrad²/0.1 % BW, i.e., a peak power up to 10 GW. The pulse-duration is foreseen to be less than 200 fs (RMS) and ultimately possibly less than 20 fs.

Presently the design-stage of the project is funded as a collaboration between BESSY, DESY, HMI and MBI.

2. Machine Description

A view of the site with the existing BESSY II storage-ring based light-source and the proposed FEL is shown in fig. 1. The synchrotron facility is located in the circular building in the center of the triangularly shaped 60,000-m² site. The FEL will be placed at the southwest side. Central part is the 260-m long accelerator based on the 1.3-GHz super-conducting linear accelerator technology developed at the TESLA-DESY collaboration [2]. At the

right end, a “magnifying glass” enlarges the laser driven photo-injector with the gun, the first linac module and a third harmonic cavity. The latter in combination with a set of bunch-compressors ensure sufficient peak-current to sustain the SASE process at the desired wavelength.

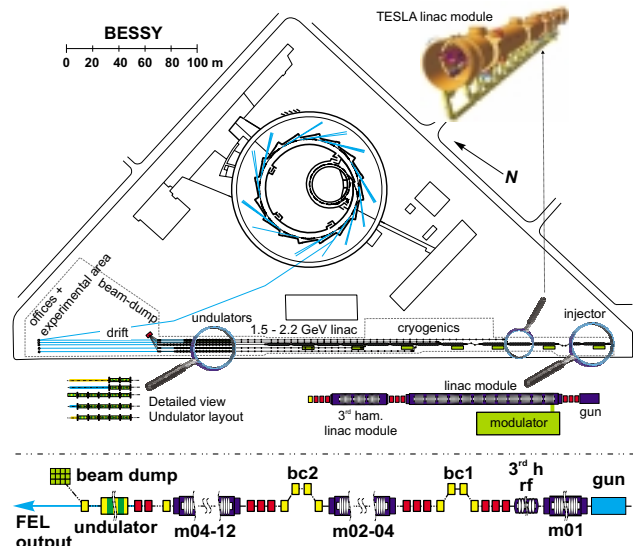


Fig. 1. **Top:** View to the BESSY site at Berlin Adlershof with the planned SASE below. **Bottom:** Schematic overview. On the right, the photo-injector RF-gun followed by a TESLA accelerating module and a 3rd harmonic cavity for efficient bunch-compression in bc1 and bc2. Twelve modules boost the electron beam to sufficient energy for lasing at $\hbar\omega = 1$ keV.

* Funded by the Bundesministerium für Bildung, Wissenschaft, Forschung und Technologie (BMBF), the Land Berlin and the Zukunftsfonds des Landes Berlin.

In the first phase of the project, three undulators will be fed with an electron beam extracted from the linac at a maximum energy of 700 MeV, 1.1 GeV and at the full energy of 2.25 GeV. This ensures a flexible selection of photon energy range from (at least) 10 eV to 1 keV.

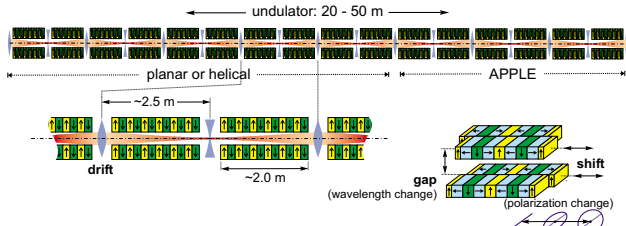


Fig. 2. Design concept for a combination of a planar and an APPLE II type variable-gap undulator based on the insertion device technology presently installed in BESSY II [3]. The drift spaces between undulator-sections are used to focus the electron beam, phase matching and diagnostics.

To achieve saturation undulators of up to 50 m in length are needed. For economical and technical reasons, the device will be split into individual undulator-sections of approximately 2 m each. Quadrupole magnets for beam focussing, orbit correctors and beam position monitors as well as phase shifters will be placed in-between the successive undulators. Planar hybrid undulators and helical undulators, based on the APPLE II design, are being used extensively at BESSY II and a long years experience in the design and construction exists [3]. Using APPLE II devices at the end gives the advantage of generating circular-polarized light (see fig. 2).

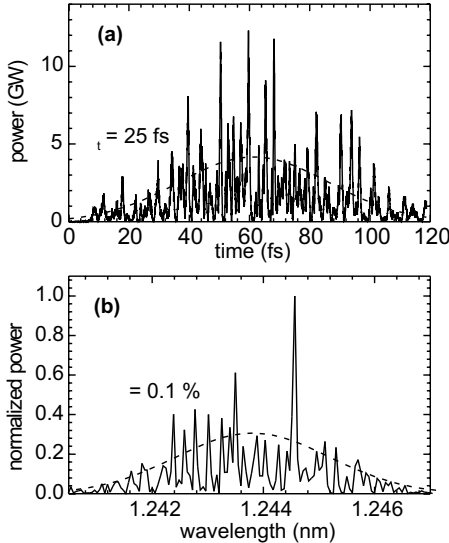


Fig. 3. GENESIS 1.3 [4] calculation for the shortest wavelength target of the BESSY FEL for a 50-m long planar undulator ($\lambda_u = 2.75$ cm) and electron beam parameters according to tab. 1. (a) The time-resolved- and (b) the spectral resolved distribution. The dashed curve represents a Gaussian fit of the distribution.

3. Peak Performance

The electron beam properties defining the SASE FEL process are summarized in tab. 1. The main challenge is

the peak current of 5 kA, needed to sustain the SASE process at the shortest possible wavelength. These values are obtained by magnetic compression of a $\sigma_t = 6$ ps long bunch emerging from the gun, see fig. 1. For longer wavelength, it is planned to reduce the compression and, hence, reduce the peak-current and energy-spread. A GENESIS 1.3 [4] calculation for the highest photon energy ($\hbar\omega = 1$ keV) for a 50-m long planar undulator as shown in fig. 2 is presented in fig. 3. The spiking in both the temporal and spectral domain as shown is typical for a short-wavelength SASE FEL [5]. Note that the SASE process shortens the micro-pulse duration as compared to the electron bunch length ($\sigma_t \approx 85$ fs).

Tab. 1. Electron beam parameters.

Beam Energy	E	0.70 – 2.25	GeV
Bunch Charge	Q	1.0	nC
Bunch Length	σ_t	265 – 85	fs
Peak Current	I	1.5 – 5.0	kA
Norm. Emittance	ϵ_n	1.5	π mm mrad
Energy spread	σ_E	0.5 – 2.0	MeV

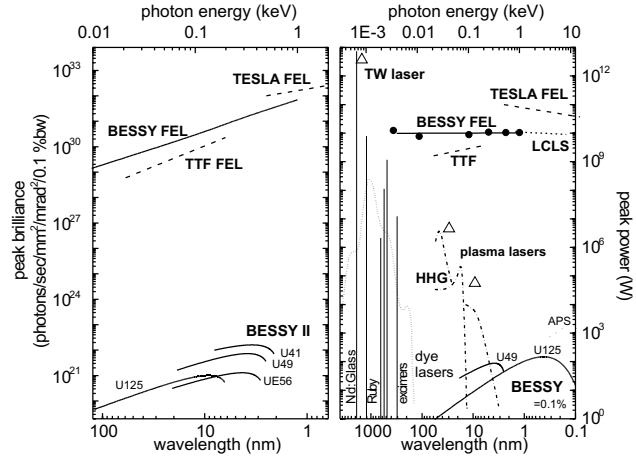


Fig. 4. Peak brilliance (left) and peak-power (right) vs. wavelength compared to BESSY II in single-bunch mode (10 mA), DESY TTF [6], TESLA-FEL [2], and the LCLS [7]. The output power (right) is also compared to present high power lasers [8] and sources using higher harmonic generation (HHG) [9].

Fig. 4 displays the range of peak brilliance. The curves represent a summary of results obtained from analytical formulas on the SASE FEL performance [5]. For the most relevant parameter combination, for example, the performance at the shortest wavelength, the results have been verified by six-dimensional numerical simulations [4], e.g., see fig. 3. More detailed performance analyses are presented in fig. 5. For high beam-energy a somewhat shorter period undulator is foreseen to ensure lasing at $\hbar\omega = 1$ keV, while at lower beam-energy a longer period undulator permits higher output power and a wider tuning range. The latter reflects the typical operational mode where at fixed beam energy the wavelength of the FEL may be changed by changing the magnetic field-strength, or K -parameter of the undulator.

The operational mode shown has the advantage that wavelength tuning by a user is somewhat decoupled from

the accelerator settings, i.e., the beam energy. As it is foreseen to provide beam to a multiple of undulators this is an important factor to decouple the different user experiments in the initial stage of the project. For later stages, it is foreseen to permit a more flexible mode of operation where slow wavelength scans with a duration of minutes or more can be achieved by undulator gap changes. Fast scans on the millisecond time-scale or below over a few percent might be possible by small adjustments of the electron beam energy.

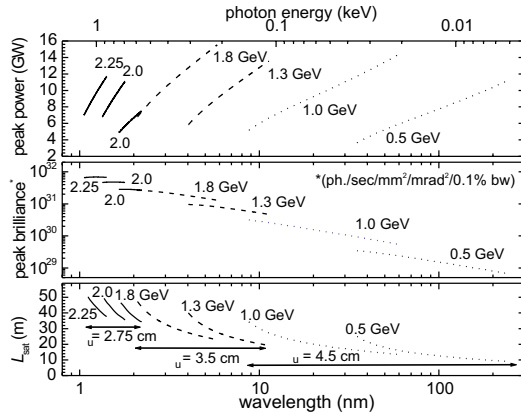


Fig. 5. Peak FEL performance (top) and the required planar undulator length (bottom), including drift-sections. Note that a multiple set of undulators with different periods is assumed.

4. Timing

As the electron-beam parameters define the peak performance of the laser, the timing defines the time-averaged specifications. For the timing three different operational scenarios are being considered (fig. 6):

1. a "CW" FEL with room-temperature photo injector, i.e., operating the linac in continuous wave mode and generating 1 to 25 micro bunches minimally spaced 100 ns in trains at a repetition rate of up to 1 kHz
2. a "CW" FEL with super-conducting photo injector, i.e., operating the linac in continuous-wave mode and generating 1 micro-bunch in multiples n of the BESSY II revolution time, i.e., every $n \times 800$ ns.
3. a "pulsed" FEL: micro-bunch trains of 7200 bunches, each bunch spaced by 100 ns are generated at a repetition rate of 10 Hz, similar in bunch pattern to the DESY TESLA project [2].

BESSY has chosen to follow in two developmental steps the solutions 1) and 2) because there is a considerable flexibility in the bunch to bunch spacing to tailor the bunch patterns for the needs of the users. Furthermore, the improvement in stability of the RF-system will be a definite advantage. The fundamental limitation will be set by the mean electron current, e.g. maximum beam loading, determined by the available RF power. Both versions have in common that the electron beam from a RF-photo-injector, - normal- (1) or super-conducting (2) - is accelerated in the CW-operated super-conducting linac to an energy of 2.25 GeV. For scenario 1), which is envisioned to be the initial scheme, the total electron beam power is

less than 200 kW. Hence, the electron beam can be dumped in locally shielded beam dump. Scenario 2) which employs a super-conducting photo-injector will require recovery of the electron beam energy for n - values smaller or equal to 10, see tab. 2.

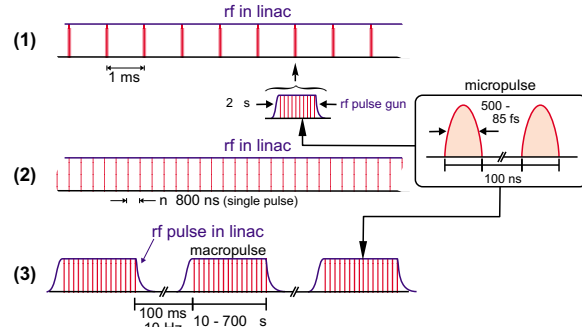


Fig. 6. Possible timing patterns for the BESSY FEL for the 3 different scenarios. See text for details.

Performance data corresponding to scenario 1) are presented in fig. 7. From the figure it follows that the SASE FEL not only has a superior peak-performance as compared to modern synchrotron light-sources but also the average flux is impressive. In the case scenario 2) gets implemented the curves in fig. 7 are still expected to increase by three orders of magnitude.

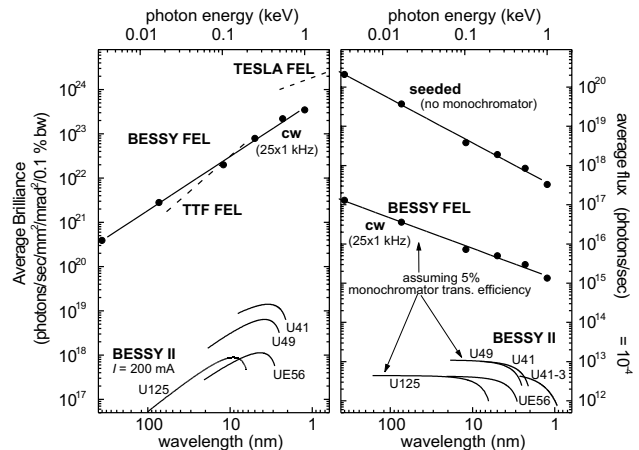


Fig. 7. Time-averaged brilliance (left) and flux (right) vs. wavelength for timing scenario 1). The average flux has been reduced to a relative band-width of 10^{-4} . The seeded FEL, operating at the transform limit, does not use a monochromator.

Note that solution 3) remains open as an fall-back alternative. That is, to obtain sufficient accelerating gradient the CW solution requires a large amount of cryogenic cooling, see tab. 2, and possibly a redesign of the cryogenic modules of the TESLA project [2]. Even with the proposed accelerating gradient of 15 MV/m the target photon energy of 1 keV is only barely in reach. Moreover, at these higher accelerating gradients an increase in dark-current from the cavity walls might impede the effectiveness of the accelerator for the relatively low repetition rates as with scenario 2. Also the development of a CW injector with sufficient electron beam quality still needs to be investigated in more detail.

Tab. 2. Main parameters for the proposed BESSY-FEL for the three different scenarios described in Sec. 4.

		CW _{NL} (1)	CW _{SL} (2)	Pulsed (3)	
Bunch spacing	τ	$10^{-7} - 10^{-3}$	$n^* \times 8 \times 10^{-7}$	10^{-7}	s
Macro-pulse duration	T	8.5	-	720	μ s
Micro-pulse duration (e-beam)	σ_i	200 (85)	2000 (85)	200 (85)	fs
Number of bunches	N	$1 - 25 \cdot 10^3$	$1.25 \cdot 10^6 / n$	72000	1/s
Photon energy range	$\hbar\omega$	0.01 – 1	0.02 – 1	0.01 – 1	keV
Number of photons/pulse	N	$1.3 \cdot 10^{13}$	$1.3 \cdot 10^{13}$	$1.3 \cdot 10^{13}$	
Peak brilliance #	B_p	7	7	7	10^{31} **
Average brilliance #	B_a	0.9	45 / n	2	10^{23} **
Average flux #	Φ_a	$3.2 \cdot 10^{17}$	$1.6 \cdot 10^{18} / n$	$9.4 \cdot 10^{17}$	ph/s
Average beam current	I_a	1 – 25	1250 / n	72	μ A
Maximum accelerating gradient	G	15	15	20	MV/m
Maximum beam-energy	E	2.25	2.25	2.5 ##	GeV
Maximum average beam-loading	P_{bl}	56	+ 2810 / n	180	kW
Cryogenic loss @ 2K	P_c	3.5	3.5	0.8	kW
Undulator period	λ_u	2.75	2.75	3.5	cm
Undulator length	L_u	50	50	55	m
Tuning range	$\Delta\lambda/\lambda$	30	30	100	%

* Sub-harmonic of the BESSY II roundtrip time ** Photonen/sec/mm²/mrad²/0.1% bw

at $\hbar\omega = 1$ keV

10 instead of 12 TESLA modules

+ Requires energy recovery

5. Enhancements

Feedback from potential users [10] has indicated an interest for enhancements of the FEL performance to broaden the scientific scope as a user-facility. The most important request involve:

- synchronized secondary sources to enable pump-probe experiments.
- shorter optical pulses down to the $\sigma_i \leq 20$ fs range.
- an improvement of the spectral purity.

The last aspect is anticipated to have a clear solution where a two-stage FEL scheme, as proposed for the TTF-FEL [11], may reduce the band-width of the FEL to the transform limit of the micro-pulse duration. The seeded option in fig. 7 reflects the expected performance enhancement for the BESSY FEL employing this scheme.

Synchronization of a secondary external laser in the visible with the FEL pulse down to (at least) 200 fs is the goal of a joint project financed by the EU undertaken at the TESLA TTF by DESY, MBI, BESSY, the Lund Laser Center, LURE and the university of Dublin.

Alternative seeding schemes to reduce the pulse-duration have been proposed at SLAC [12] and at DESY [13]. Especially the DESY proposal, which involves pulse slicing with the aid of a visible laser system, is interesting since it might be implemented such that it auto-synchronizes a fs FEL pulse with a fs visible laser. A collaboration between BESSY and MBI is on its way to investigate the feasibility and the limits of such a scheme.

References

- [1] D. Krämer, Proc. of the European Part. Acc. Conf., Wien, (2000), p. 640
- [2] TESLA-Technical Design Report, DESY 2001-011, ECFA 2001-209, CD-ROM, March 2001

- [3] J. Bahrtdt, A. Gaupp, G. Ingold, M. Scheer, W. Gudat, J. of Synchr. Rad. **5-3** (1998) 443
- [4] S. Reiche, Nucl. Instrum. Meth. **A429** (1999) 243
- [5] *The Physics of Free Electron Lasers*, E.L. Saldin, E.A. Schneidmiller, M.V. Yurkov, Springer, Berlin-Heidelberg (2000).
- [6] J. Rossbach, Nucl. Instr. Meth. **A375** (1996) 269
- [7] SLAC report R-521, Dec. 1998
- [8] Brookhaven National Laboratory, BNL-48565, Feb. 1993
- [9] M. Schnürer, Z. Cheng, M. Hentschel, F. Krausz, T. Wilhein, D. Hambach, G. Schmahl, M. Drescher, Y. Lim, U. Heinzmann, Appl. Phys. B. **70** [Suppl.], S227 (2000)
- [10] Workshop related to the BESSY FEL, BESSY internal publication, Holzhau Germany, Jan. 2001
- [11] E.L. Saldin, E.A. Schneidmiller, M.V. Yurkov, Nucl. Instrum. Meth. **A445**, 178 (2000)
- [12] C. B. Schroeder, C. Pellegrini, S. Reiche, J. Arthur, P. Emma, Proc. Of the 2001 Particle Accelerator Conference, Chicago, USA (2001) WPPH121
- [13] W. Brefeld, B. Faatz, J. Feldhaus, M. Körfer, T. Möller, J. Pflueger, J. Rossbach, E.L. Saldin, E.A. Schneidmiller, S. Schreiber, J. Krzywinski, and M.V. Yurkov, DESY report 01-063 (2001)

Development of a TV diagnostics system for the Photo Injector Test facility at DESY Zeuthen

J.Bähr,^a K.Flöttmann^b, F.Stephan^a

^aDESY Zeuthen, Platanenallee 6, 15738 Zeuthen, Germany

^bDESY Hamburg, Notkestrasse 85, 22607 Hamburg, Germany

A Photo Injector Test facility is under commissioning at DESY Zeuthen (PITZ). The aim is to develop and operate an optimized photo injector for future free electron lasers and linear colliders. The optimization of an electron gun is only possible based on an extended diagnostics system including a TV-system. The goal of the TV-system is measuring the electron beam position and beam profile at different positions along the beam line. Several demands of the system are described, for example the alternative of object size and high optical resolution. Radiation damage of the components has to be avoided. Solutions for the depth-of-field problem will be given. The optical system will be optimized concerning different effects on optical resolution as diffraction, depth of field, pixel size of the camera and effects of different elements of the optical system.

1. Introduction

A Photoinjector Test Facility is in commissioning phase at DESY Zeuthen (PITZ)[1]. The project was originated by a collaboration of BESSY (Berlin), DESY (Hamburg and Zeuthen), Max-Born-Institute (Berlin) and Technische Universität (Darmstadt) and is funded partially by the HGF-Vernetzungsfonds. The goal of PITZ is to operate a test facility for laser driven RF guns and to optimize photo injectors for the operation of Free Electron Lasers (FEL) and the TESLA linear collider. First photoelectrons will be produced in autumn 2001 [2].

To provide an optimization of the setup and its components a complex diagnostics system will be used [3]. One of the most flexible and universal diagnostics subsystems is the TV-system which is under development.

2. Characteristics of the TV-system

Several channels of the TV-system will be used to analyse the light distribution produced by an electron beam hitting a YAG-powder (Yttrium-Aluminium-granate) screen. Beam position, beam profile and intensity distribution will be measured. Furthermore, it is foreseen to measure the light intensity distribution behind

an Emittance Measurement System (EMSY). In the dispersive arm of the magnet spectrometer the beam energy spectrum will be measured analysing the corresponding light distribution detected by the TV-system. The virtual cathode system of PITZ is also based on a TV-readout.

Basing on these general tasks, several characteristics of the PITZ TV-system can be specified. The light distribution created by a YAG screen is to be projected by lenses at different magnifications onto the camera sensor. The range of magnification is defined between an overview over the whole screen (magnification 0.24) and a “microscopic” view (magnification 10) where a resolution of $< 10 \mu\text{m}$ should be reached. It is aimed to reach a resolution of the order of $1 \mu\text{m}$ for analysing the pattern behind the EMSY system. Consequently, the object field is restricted in the operation mode of high resolution. The measurement of magnification should be possible in all operation modes basing on a grid in the screen plane. The YAG screen can be illuminated for this purpose. The resolution can be measured in all operation modes using an illuminated grid in a second arm of the system which can be activated by a movable mirror. Radiation damage and a direct illumination of the camera by X-rays will be avoided by projection in a 90° scheme using one mirror. A schematic of the system is shown in

Fig. 1. The video signal is read out and analysed

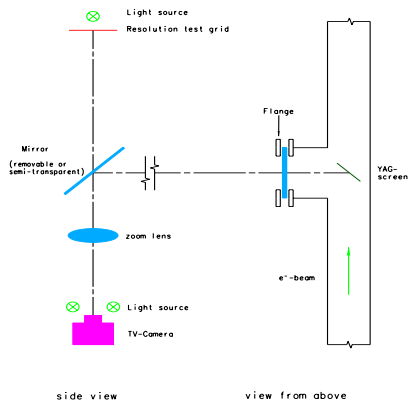


Figure 1. Schematic of the setup optical System of the TV-System.

by a computer based framegrabber (BESSY) over a distance of about 40 m. The camera of the type JAI M10RS has a 1/2" black/white sensor and is read out in the progressive scan mode. The sensor consists of 782×582 pixels. The pixel dimensions are $8.3 \mu\text{m} \times 8.3 \mu\text{m}$. External gain control and external trigger are foreseen. The control of the camera is realized via a RS 232 interface. The characteristic curve of the sensor is linear.

The depth-of-field problem which arises because of the 45° position of the YAG screen relative to the electron beam and the optical axis can be solved using the view screen camera geometry. In this case the image plane is inclined relative to a normal position to the optical axis.

To overcome the problems of distance and of access to the setup, several functions of the TV-system as focus, diaphragm and focal length will be remotely controlled. At the present stage of the project investigations to perform a choice of lenses is performed. Especially different influences on resolution are under investigation. In Fig. 2 the influence of diffraction, depth of field, lens resolution and camera resolution are plotted to evaluate the process for different param-

eters of imaging. In this example the depth of

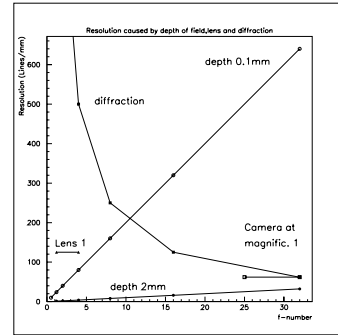


Figure 2. Influence of several effects on optical resolution

field of 2 mm is the hardest limitation for resolution. One could overcome this problem applying the viewscreen camera principle. In this case the drawback is a non-uniform magnification in the field. In the case of small defocusing one can find the optimum of the combined effects of defocusing and diffraction at a f-number of about 10. In this case, the limitation of resolution is caused by lens and camera. The limitation of the camera (pixel size) can be eliminated by higher magnification, which leads to a smaller object field. Obviously, one can match f-number and magnification such, that the resolution of the lens remains the limiting factor. Hereby, the solution of the depth-of-field problem is assumed.

REFERENCES

- 1 F. Stephan et al., Photo Injector Test Facility under Construction at DESY, FEL 2000, Durham.
- 2 I. Bohnet et al., Photo Injector Test Facility in the Commissioning Phase at DESY Zeuthen, FEL 2001, Darmstadt.
- 3 J. Bähr et al., Diagnostics for the Photo Injector Test Facility in DESY Zeuthen, DIPAC 2001, Grenoble.

Studies of the collimation system for the TTF FEL at DESY

V. Balandin, N. Golubeva and M. Körfer

Deutsches Elektronen-Synchrotron (DESY), Hamburg, Germany

Abstract

A collimation scheme for the protection of the undulators at the TESLA Test Facility phase 2 (TTF2) is discussed. The transverse and energy collimation, and the protection against off-energy and mis-steered bunches are proposed in a beam line which, besides of collimation elements, integrates the fast feedback system and matches the beam to the undulator entrance.

Key words: Beam dynamics, collimators, apertures, free electron laser

PACS: 41.75. i, 42.79.Ag, 41.60.Cr

1 Introduction

The experience of the TTF phase I indicates that a protection system for the undulator is desirable [1]. In this paper studies of the collimation system for the TTF phase 2 [2] are presented and discussed.

Due to limitations of available space it is proposed to place the TTF2 collimation system in the beam line with a dogleg of $\sim 20 m$ length (Figure 1), which, besides the collimation elements, has to contain the fast feedback system and to match the beam to the undulator entrance [2]. So it was impossible to use the advantages of the popular spoiler-absorber scheme, and having only a limited number of available free positions, all proposed collimators are considered as primary collimators. Energy collimation and passive protection against off-energy bunches are achieved in the dogleg with horizontal dispersion.

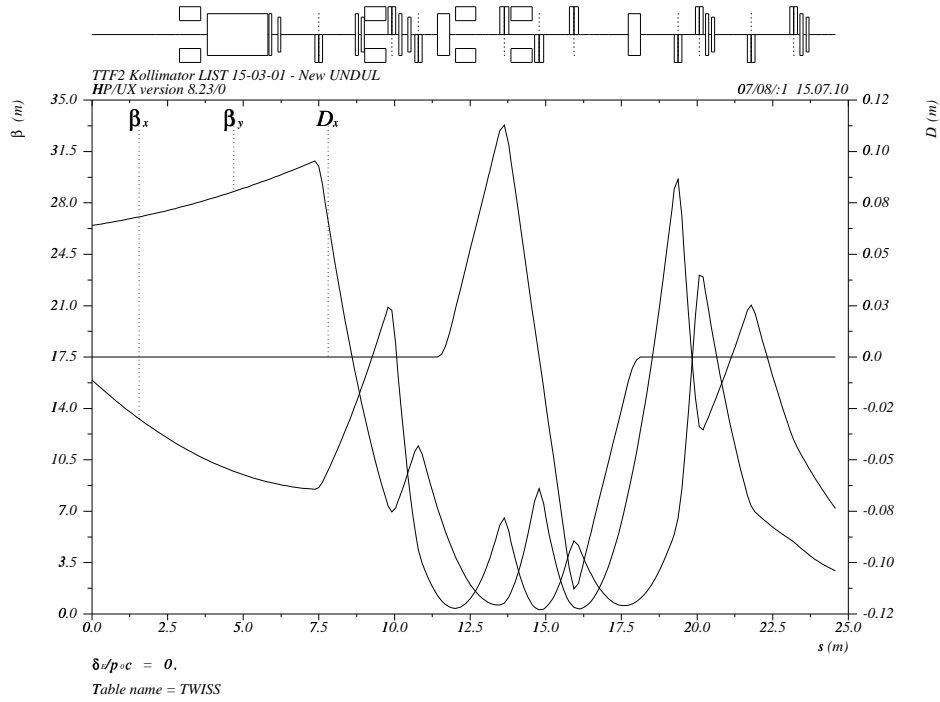


Fig. 1. Optical functions of the TTF2 collimator section.

2 Protection against primary particles

In the first step of our studies we have used the "black absorber" model for the collimators - any particle touching them is considered lost. The purpose was to find the collimator locations and to determine the set of apertures which will stop all particles which can hit the undulators without touching the collimators (protecting apertures). It is clear that only such apertures can be the subject of further studies which will take into account secondary particles and those rescattered into the beam. Because of two strong sextupoles which were used in the dogleg for the correction of the second order dispersion, it was not possible to limit the calculations to linear optics only. In addition it was desirable to avoid uncontrolled losses of the primary particles on the beam pipe in the collimation section.

It is not possible to describe the whole set of protecting apertures constructively. However if we restrict ourselves to practically valuable apertures (for example, with elliptical or rectangular shape), it can be achieved. After choosing for each collimator the totally ordered scale of apertures (see details in [3]), the distribution of the particles coming into the collimation section, and the particle tracking algorithm, it becomes possible to map the set of protecting apertures

into a simply connected subset in the finite dimensional space. A special numerical procedure has been developed which allows us to find the borders of this subset and then to make some additional optimization within this subset, if necessary.

In this study we have used circular holes as apertures, the requirement to maximize the minimum collimator radius is an additional optimization criteria, and as particle tracking algorithm the symplectic numerical integration of the exact Hamiltonian equations of motion in the SCOFF approximation was used (thus all geometrical and chromatic aberrations were taken into account).

Because the distribution of the incoming particles, which need to be collimated, is difficult to predict precisely (it depends on how well the upstream system has been tuned, on emission of dark current, and so on) the initial distribution was modeled by 4-dimensional slices (x, p_x, y, p_y) , with a transverse extent over the radius of the vacuum chamber at the collimation section entrance (the maximum values for momentum p_x and p_y were chosen so as to fully populate the acceptance of the transport line), and with the same value of energy deviation $\Delta E/E_0$ for all particles in each slice (monochromatic $\Delta E/E_0$ - fractions). The above mentioned optimization procedure was performed for each slice separately and the results are presented as a function of the energy deviation.

Figure 2 shows the resulting maximized minimal aperture radius in the energy deviation range of $-50\% \leq \Delta E/E_0 \leq +25\%$. The collimation scheme considered includes 4 collimators, 2 collimators in the first straight part of the collimation section and 2 collimators in the dogleg (see Figure 1). The minimum value of $\sim 2 \text{ mm}$, seen in Figure 2, means that at least one collimator must stay within such aperture radius. With careful additional optimization it was shown that 3 collimators must keep this value as aperture radius, and the radius of the first energy collimator (placed just after the first dipole magnet in the dogleg) can be safely increased to 6 mm .

Note that the maximized minimal aperture radius can be increased up to $\sim 3.2 \text{ mm}$ by shifting one of the two first collimators placed in the straight section before the dogleg into the straight section after the dogleg (this was the first scheme considered). But in this case we will have uncontrolled losses of primary particles on the beam pipe between the collimators, which can lead to beam pipe damage if the beam is off-energy or (and) mis-steered. In order to avoid these losses one needs to reduce the aperture radius of two energy collimators to $\sim 1 \text{ mm}$.

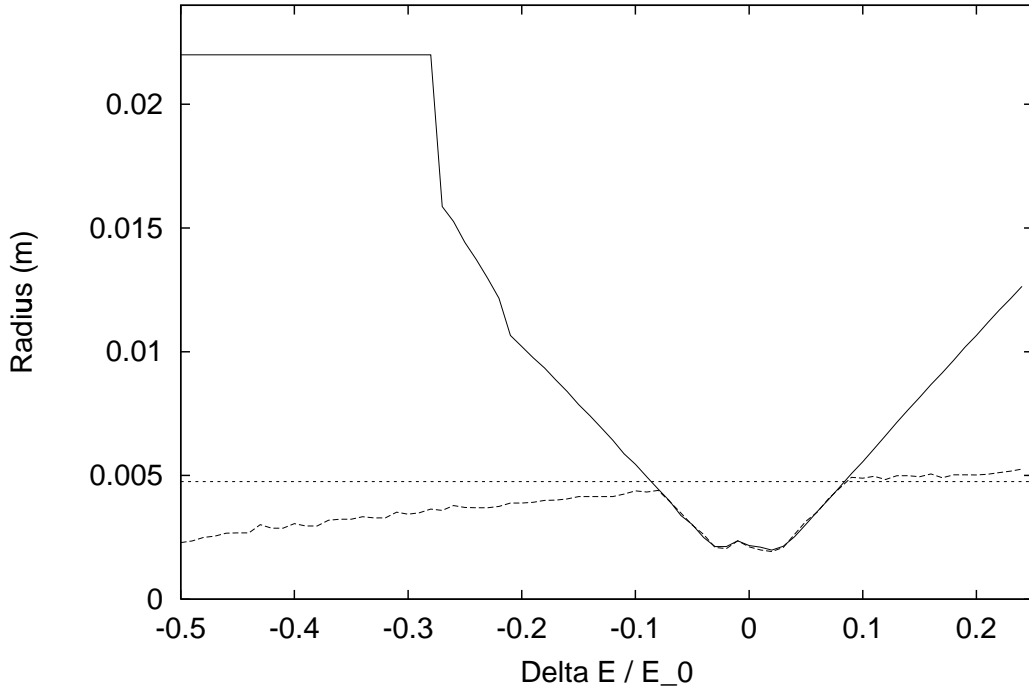


Fig. 2. Maximized minimal aperture radius as a function of the energy deviation. Dashed curve: there are no uncontrolled losses on the beam pipe in the full collimation section. The straight line shows the undulator aperture.

3 Additional tracking studies with primary particles

After fixing the aperture radii (6 mm for the first energy collimator and 2 mm for the remaining collimators) the collimators were tapered on both sides to reduce the wakefield effects (the length of each collimator including tapers is chosen to be 50 cm) [4].

Additional tracking simulations, important for further evaluation of collimation efficiency, were performed with tapered collimators to study: how lost primary particles are distributed between the four collimators and along the collimator length; to find the maximum and average angles at which primary particles heat the collimator surface; and which monochromatic $\Delta E/E_0$ - fractions of incoming particles will be stopped by the collimation system completely. As an example, Figure 3 shows the loss distribution of primary particles on the second energy collimator. We see that most of the captured particles are intercepted by the face surface and the entrance taper, and only less than 1% of all particles absorbed by this collimator hit the inner surface, which is parallel to the beam line axis (the main part of the collimator).

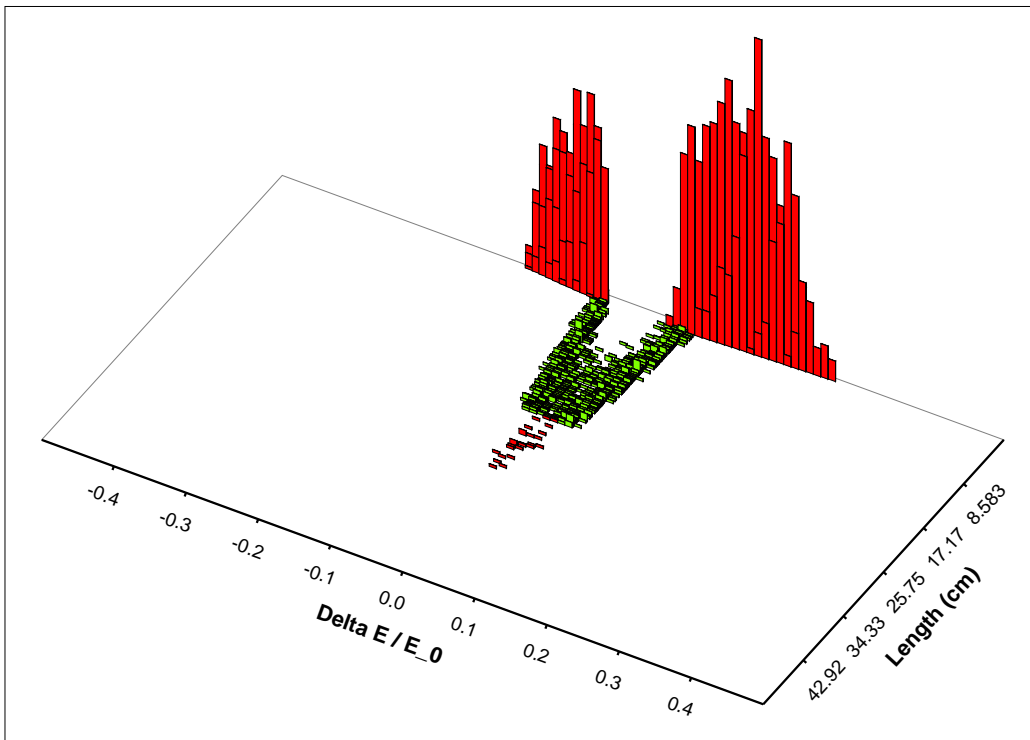


Fig. 3. Loss distribution of primary particles along the collimator length on the second energy collimator as a function of the energy deviation. Losses on the face surface, the entrance taper, and the main part of the tapered collimator are seen.

4 Choice of collimator material

The properties of copper and titanium as possible candidates for the collimator material have been investigated and compared. Both the survival of the material in the emergency case, when a few design bunches of the train can directly hit the collimator, and the heat load under normal operating conditions, when only the beam halo is intercepted by the collimators, were considered. Here we list briefly the main directions of those studies, all details can be found in [3].

For the study of the survival of collimator material in the emergency case the direct impacts of design bunches on the collimators were simulated using the EGS4 code [5]. The energy-density deposition in both materials as a function of longitudinal and transverse positions has been calculated for all possible locations of collimators in the beam line, taking into account the changing beam spot size with energy and the relative energy spread within the bunch (which is important for collimators placed in the dispersive section of the beam line). In both materials in the energy range of 0.3 – 1.0 GeV the maximum energy-density deposition occurs in the

first few millimeters from the material surface. The thermal and stress analyses have been performed which have shown that the main problem of material survival comes from the energy collimators, because they are located in the dogleg, where the betatron functions are small.

Under normal operating conditions the distribution of temperature in the collimator has been obtained as a solution of the heat conduction equation for stationary and nonstationary cases assuming that the outer collimator surface is cooled by circulating water, and $\sim 2\%$ of the average power, that is about 1.5 kW , is absorbed by a single collimator.

As the result, we have chosen copper for the collimator-absorbers, because a copper collimator gives us better thermal behaviour and better collimation efficiency under normal operating conditions than a titanium one. To improve survival, the first few centimetres of the collimator could be made from titanium.

5 Secondary particles and rough estimation of collimation efficiency

To study the effect of secondary and rescattered particles, we have used a combination of the TrackFMN [6] and the EGS4 [5] programs so that, between collimators, particles (electrons, positrons and photons) were transported using the TrackFMN code, and the passage through the beam line sections containing tapered copper collimators was simulated with EGS4 Monte-Carlo code. Figure 4 shows an example of such simulations when 10 electrons hit the inner surface of the collimator. One sees the rescattered particles, the secondary particles produced (both will be then picked up by TrackFMN code and tracked further through the beam line), and the development of the electromagnetic shower in the collimator material.

For the estimation of the collimation efficiency, the collimators have been hit by pencil beams at different points on the surface at angles which are possible for each collimator and which were calculated in the black absorber model. The resulting rescattered and secondary particles were then tracked further through the downstream beam line and the undulator according to the above described procedure. These studies have shown that the main problem is the scattered electrons from the second energy collimator after which there are no more collimators. The problems start when particles hit the inner surface of the main part of this collimator with small entrance angles. In the worst case the scattered electrons transmit $\sim 20\%$ of the input energy,

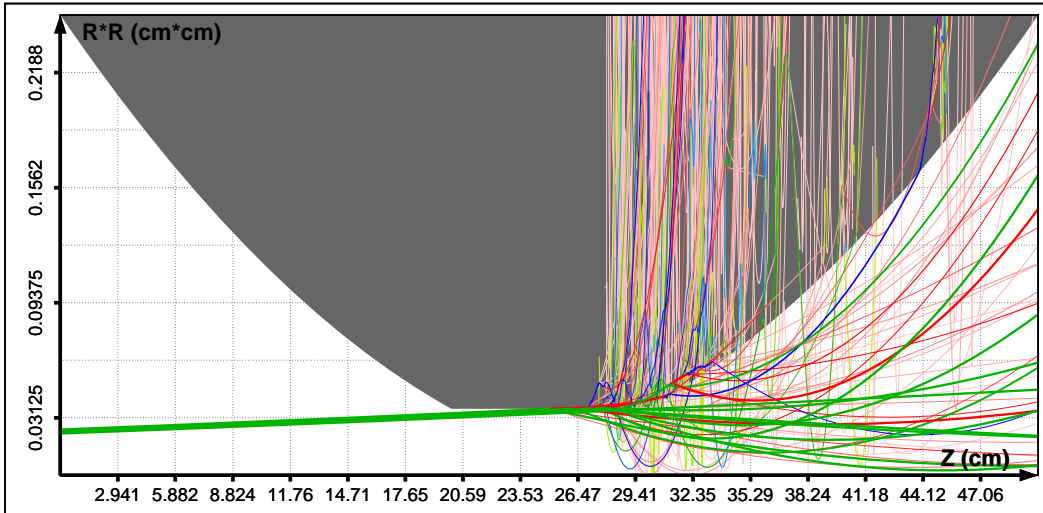


Fig. 4. Scattering, production of secondary particles, and development of the electromagnetic shower in the copper collimator.

but only $\sim 1\%$ of the input energy is recorded to be lost in the undulator.

The accurate estimation of the collimation efficiency requires the knowledge of the beam halo distribution and the following convolution of this distribution with the results of the pencil beam investigations (in the spirit of [7]). How can we estimate the collimation efficiency without a knowledge of the beam halo distribution? We can assume that 1% of the beam particles hit the last collimator, so, taking into account that only less than 1% of those particles reach the inner surface of the main part of that collimator, we may conclude that a routine collimation efficiency (defined as the ratio of energy deposited in the undulator to total beam energy) will not exceed $\sim 10^{-6}$.

6 Acknowledgements

We would like to thank J. Rossbach for the suggestion of this work, continuous support and many valuable discussions. We thank R. Brinkmann, M. Seidel and H. Schlarb for their interest and helpful discussions. We are grateful to K. Flöttmann for his help with the EGS4 code. We thank S. Wipf for carefully reading the manuscript.

References

- [1] H. Schlarb, Collimation System for the VUV-FEL at TTF, DESY thesis in preparation.
- [2] M.Körfer, for the TTF FEL Group, The TTF-FEL Status and its Future as a Soft X-ray User Facility, these proceedings.
- [3] The collimation system for the TTF FEL at DESY, DESY report in preparation.
- [4] M. Dohlus, R. Wanzenberg, unpublished note.
- [5] W.R. Nelson, H. Hirayma, D.W.O.Rogers, The EGS4 code system, SLAC Report 265, 1985.
- [6] V. Balandin, The TrackFMN Program, User's Reference Manual, unpublished.
- [7] W.R. Nelson, S. Ecklund and S. Rokhi, A Convolution Method for Determining Temperature Rise in Targets Struck by Beams of Various Size, Proc. of the Second Inter. Workshop on EGS, KEK Proceedings 200-20, pp.182-192.

Photo Injector Test Facility in the Commissioning Phase at DESY Zeuthen*

I. Bohnet^a, J.Bähr^a, D.Lipka^a, F.Stephan^a, M.Winde^a, Q.Zhao^a, K.Flöttmann^b

^aDESY, Platanenallee 6, 15738 Zeuthen, Germany

^bDESY, Notkestr.85, 22603 Hamburg, Germany

A photo injector test facility is in the commissioning phase at DESY Zeuthen within a cooperation of BESSY, DESY, MBI and TU-Darmstadt. The aim is to develop and operate an optimized photo injector for future free electron lasers and linear accelerators which require extraordinary beam properties. The scientific goals, the planned and existing hardware and the developments for the photo injector facility are briefly described. First operation of the rf gun is expected for autumn 2001. Even higher gradients are aimed for in Zeuthen than achieved today in similar rf guns, so that in the near future more conditioning work of the rf gun needs to be done. The effects which might happen during conditioning based on the experiences gained so far in Hamburg (at the FEL and the FNAL guns) are briefly described. Information about diagnostic elements at the rf gun and the requirements for a simplification of the upcoming conditioning work are given.

1. Introduction

A photo injector test facility is in the commissioning phase at DESY Zeuthen in order to optimize injectors for different applications like free electron lasers, production of flat beams for linear colliders and polarized electron sources [1]. The experimental setup in the start up phase is shown in Fig. 1. A primary goal is the stable production of short electron bunches (≈ 20 ps) with a transverse emittance of $\approx 1\pi$ mm mrad at 1 nC and a small energy spread. We expect to produce first photoelectrons with energies up to 5 MeV in autumn 2001.

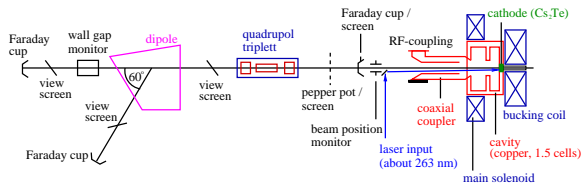


Figure 1. The present electron beamline corresponding to a total length of ≈ 5 m. The electron beam is accelerated from right to left.

2. Plans

Measurements of the transverse and longitudinal phase space will allow a detailed comparison between experimental results and simulations after the commissioning of the facility. The integrated optimization of all components of the photo injector is also foreseen, especially for the subsequent operation at the TESLA Test Facility - Free Electron Laser (TTF-FEL). Presently we work on the development and improvement of beam diagnostics [2,3], and on the development of an automatic conditioning program for rf guns [4].

3. Conditioning of the cavity

Conditioning of a normal conducting cavity is the successive increase of rf power in the cavity in order to achieve high gradients. It is a time consuming and boring work. To increase the efficiency and to protect the rf gun it is planned to develop an Automatic Conditioning Program (ACP). The aim is to get even higher gradients (> 35 MV/m) in the rf gun than achieved today in similar normal conducting cavities.

3.1. Which effects could happen?

A fundamental process in a high gradient cavity is field emission of electrons from protrusions on the surface. Electrons which hit the cavity with some

*The project is partially funded by the HGF Vernetzungsfond.

keV can produce secondary electrons. If the trajectory of those secondaries terminates close to the emission side of the primary electron a resonant phenomenon can appear called multipacting. A different effect is a spark which is accompanied by a strong light emission, a strong reflected power signal and an increase of the vacuum pressure. Probably it can be explained by an exponentially increasing emission of electrons from a protrusion due to field emission and the heating of the protrusion. All these effects guide to an increase of vacuum pressure and can destroy cathode, cavity, rf window or rf coupler. The details of these processes are not well understood. For example during conditioning of the rf gun at TTF it has been observed that the probability for an event which happens in the beginning of an rf pulse is influenced by the length of the previous rf pulse. It seems to be a memory effect of the cavity with respect to the rf pulse structure.

3.2. Automatic Conditioning Program

The ACP has to control the rf power and to react appropriately on interlock signals. Several detectors are installed close to the rf coupler, rf window and cavity. Fast signals from photomultipliers interrupt the rf power within an rf pulse so that the conditioning can be continued with the next rf pulse. Slow signals from temperature or vacuum pressure sensors interrupt the conditioning to offer a recovering time for the rf gun. The ACP works on the rf power P . The gradient \vec{E} can be obtained by the relation $\vec{E}^2 \propto P$. After resetting an interlock the program increases the power rapidly. To condition multipacting effects the program can sweep the solenoidal field additionally. Within the dangerous power region the power is increased slowly until the alarm threshold is reached just below the level at which the interlock occurred. The power could be turned down by a significant step and than slowly increased again for a while to improve the vacuum (see Fig. 2). Then the alarm threshold is increased.

3.3. Data acquisition and analysis

During the conditioning process of the cavity slow and fast signals will be read out, so that a huge amount of data will grow up. Reasonable selections of recorded data and analysis programs are required. A solution is offered with ROOT which is an object

oriented data base for large scale data analysis developed at CERN. Root is based on C++ and offers also capabilities for data compression and analysis during standard operation, especially for a use at TTF-FEL at a later date. However, presently a deeper analysis of the ACP data will be realized by an event recorder reading out the fast signals just in case of significant data content.

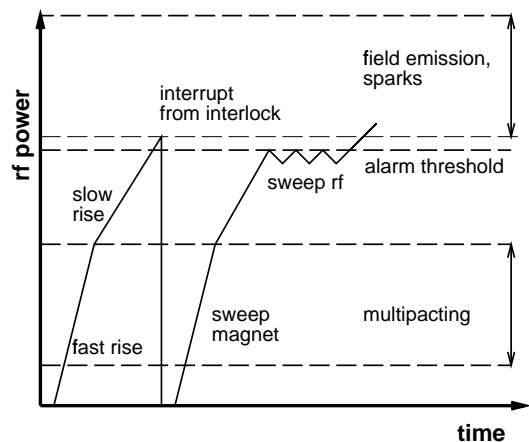


Figure 2. Sketch of rf power control of the ACP.

Acknowledgements

It is to thank several colleagues from Hamburg and Zeuthen for strong help and useful discussions, especially P. Castro, A. Gössel, W.-D. Möller, S. Schreiber, T. Thon, F. Tonisch. We want to thank J. Möller for technical support.

REFERENCES

1. F. Stephan et al., Photo Injector Test Facility under Construction at DESY, FEL 2000, Durham.
2. J. Bähr et al., Diagnostics for the Photo Injector Test Facility in DESY Zeuthen, DIPAC 2001, Grenoble.
3. Q. Zhao et al., Design of the Bunch Length Measurement for the Photo Injector Test Facility at DESY Zeuthen, PAC 2001, Chicago.
4. <http://desyntwww.desy.de/pitz/>

Study of Frequency Multiplication Process in Multistage HGHG FEL

W. Brefeld^a, B. Faatz^a, J. Feldhaus^a, M. Körfer^a, J. Krzywinski^b,
T. Möller^a, J. Pflueger^a, J. Rossbach^a, E.L. Saldin^a,
E.A. Schneidmiller^a S. Schreiber^a and M.V. Yurkov^c

^a*Deutsches Elektronen-Synchrotron (DESY), Notkestrasse 85, D-22607 Hamburg,
Germany*

^b*Institute of Physics of the Polish Academy of Sciences, 02688 Warszawa, Poland*

^c*Joint Institute for Nuclear Research, Dubna, 141980 Moscow Region, Russia*

Abstract

A new design for multistage High-Gain Harmonic Generation (HG HG) scheme is proposed. The main difference with previous HG HG schemes is that in our scheme the HG HG technique can be applied more than once in a HG HG chain (single bunch scheme). This is consequence of the fact that the growth of the energy spread due to the HG HG process in our case is much less than initial energy spread, and exponential growth rate in the main undulator is practically the same as without stage sequence. Problems relating to X-ray HG HG FEL are discussed. Our studies have shown that the frequency multiplication process produces a noise degradation proportional to at least the square of the multiplication ratio. This prevents operation of HG HG FEL at a very short wavelength range. The results presented in this paper have demonstrated that the HG HG FEL approach is quite adequate for the VUV coherent source, but not scalable to X-ray devices.

1 Introduction

The improvement of the longitudinal coherence of the X-ray SASE FEL is of great practical importance. At present two ways to overcome this problem are under development. One of them is based on an idea to use a self-seeding scheme [1,2]. Another approach to produce completely coherent radiation consists in utilizing a high-gain harmonic generation (HG HG) FEL scheme. In the HG HG FEL the radiation output is derived from a coherent subharmonic seed pulse. Consequently, the optical properties of the HG HG FEL are expected to be a map of the characteristics of the high-quality seed laser. This has the benefit of providing radiation with a high degree of stability and control of the central wavelength, bandwidth energy and pulse duration which is absent from the SASE FEL source [3–7]. An idea of using two undulators, with the second undulator resonant to one of the harmonics of the first one, has been proposed in [3]. The next step in this direction was taken in [4], where dispersion section is introduced

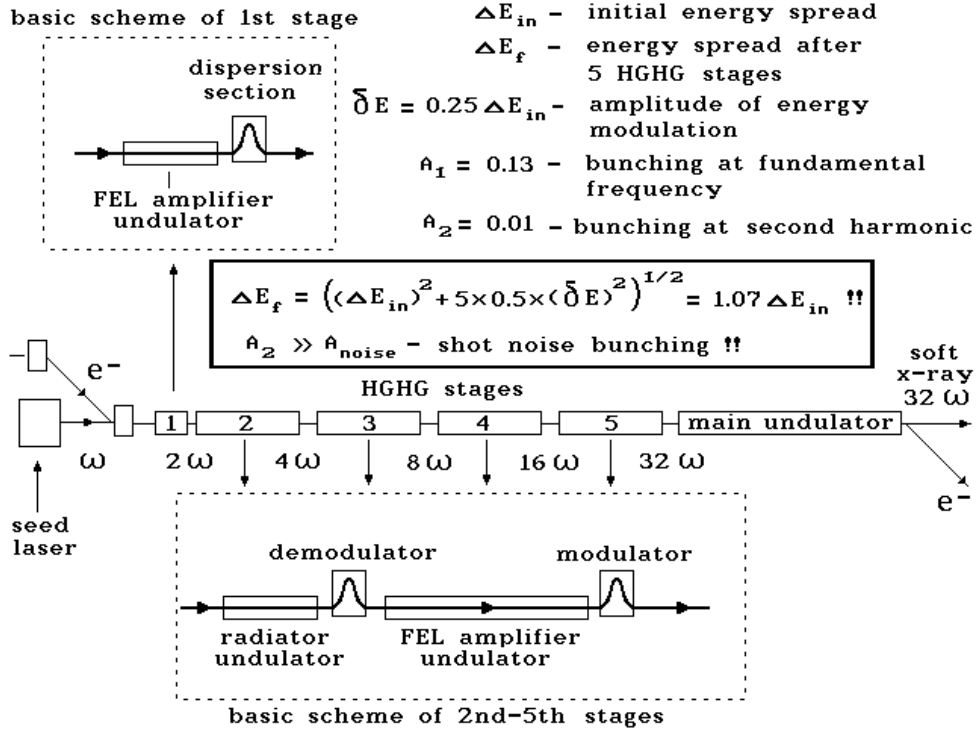


Fig. 1. Single bunch HGHG FEL scheme proposed in this paper

between the two undulators. Recently, an approach utilizing a HGHG scheme, which is capable of producing longitudinally coherent pulses, was demonstrated experimentally [8,9].

To generate short wavelengths we have to go to a high harmonic number. In order to obtain an efficient coherent harmonic generation, the energy modulation δE , introduced by the modulator, needs to be larger than the initial energy spread by the factor of harmonic number N . Therefore, for very high harmonics, the energy modulation becomes very large and this makes the exponential growth gain length too large. This problem can be solved with a multistage HGHG scheme [10]. A simple solution to solve the energy spread problem, which has been proposed in [10], is to use fresh electron bunches in each stage. Once the coherent harmonic generation process in the first stage is over, the resulting radiation at frequency 4ω is guided to the next amplifier/radiator unit for interaction with a fresh electron bunch. Following the second stage the radiation at frequency 16ω enters the third stage. Like the second stage, the third stage makes use of fresh electron bunches, etc. The results of these studies are considered very promising because they indicate that the HGHG FEL technique could allow the production of fully coherent X-rays [10].

In this paper we propose an idea for a single-bunch, multistage HGHG FEL scheme (see Fig. 1). Each stage (except the first stage) consists of a radiator undulator, first dispersion section (demodulator), FEL amplifier undulator and end-stage dispersion section (modulator). The proposed scheme operates as follows. The first stage is a conventional FEL amplifier seeded by an external laser. The seed laser pulse is timed to overlap with the electron bunch. This laser pulse interacts with the electron beam in the first undulator, which is tuned to be resonant to the seed radiation wavelength. The undulator is followed by a dispersion section to increase spatial bunching. In contrast to usual the HGHG approach [4], in our scheme the density modulation at the fundamental frequency at the exit of the dispersion section is about 10% only. Nevertheless,

at the chosen parameters, the amplitude of the second harmonic of the density modulation is high enough, about 1%, and dominates significantly over the amplitude of shot noise harmonics (about 0.01 %). This modulation density serves as an input signal for the second stage which is resonant to the second harmonic. An important feature of our design is that a very small energy modulation is sufficient to produce 10% microbunching in the dispersion section. In particular, the amplitude of the energy modulation δE can be much smaller than the natural (local) energy spread in the electron beam ΔE_{in} . The analysis of the parameters of the subharmonically seeded FEL has shown that it will operate reliably even for an energy modulation amplitude equal to $\delta E = 0.25\Delta E_{\text{in}}$ (see Sec.2 for more details).

Figure 1 illustrates how the soft X-ray wavelength range may be reached by successive multiplication ($\omega \rightarrow 2\omega \rightarrow 4\omega \rightarrow 8\omega \rightarrow 16\omega \rightarrow 32\omega$) in a stage sequence. Following the first stage (FEL amplifier undulator and dispersion section) the electron beam and the seed radiation enter a short undulator (radiator) which is resonant with the second harmonic of the seed radiation. In the radiator the seed radiation plays no role and is diffracted out of the electron beam, while the bunched beam generates radiation with frequency 2ω . At the exit of the radiator undulator the radiation power exceeds significantly the effective power of shot noise. After leaving the radiator the electron beam is guided through a dispersion section (demodulator). The function of this dispersion section consists in suppressing the density and energy modulation of the electron bunch produced in the first stage. The problem of suppressing the beam modulation can be solved quite naturally due to the presence of the local energy spread in the electron beam. After passing the dispersion section, the demodulated electron beam enters the FEL amplifier and amplifies in exponential regime the radiation with frequency 2ω produced by the radiator undulator. The length of the FEL amplifier undulator is chosen in such a way that the energy modulation at the undulator exit has the same value of $\delta E = 0.25\Delta E_{\text{in}}$ as at the exit of the first stage. This energy modulation is then converted to spatial bunching while the electron beam traverses the end-stage dispersion section (modulator). The values of the 2nd and the 4th harmonics of density modulation at the second stage exit are about 10% and 1%, respectively. These values are approximately the same as the amplitudes of the 1st and 2nd harmonics at first stage exit. Following the second stage the beam enters the third stage which is resonant with 4th harmonic of the seed radiation, etc. Finally, after the 5th stage the electron beam enters main undulator which is resonant to the 32th harmonic of the seed radiation. The process of amplification in the main undulator starts from the modulation of the beam density. By the time the beam is overbunched in the main undulator, the 32ω radiation reaches saturation. In order to reach saturation, the main undulator should be sufficient long. An important feature of the proposed scheme is that the energy modulation (i.e. correlated energy spread) induced in the n th stage, transforms to local (i.e. uncorrelated) energy spread in the $(n + 1)$ th stage. As a result, the dispersion of the electron energy distribution at the exit of the multistage scheme is calculated as the sum of induced dispersions. The small energy perturbation of the electron beam is one of the advantages of the adopted subharmonically seeded FEL design. For instance, the total energy spread generated to the end of the 5th stage, can be estimated as $\sqrt{\langle(\Delta E)^2\rangle} \simeq \sqrt{(\Delta E_{\text{in}})^2 + 5 \times 0.5 \times (\delta E)^2} \simeq 1.07\Delta E_{\text{in}}$ for $\delta E = 0.25\Delta E_{\text{in}}$ which does not differ much from the number obtained from numerical simulations (see Sec. 5 for more details). Such a small degradation of the energy spread allows effective generation of powerful radiation in the main undulator.

Up to now operation of HGHG schemes has been analyzed within the framework of ideal-

ized models which do not take into account shot noise effects [4–7]. The results of these studies were very promising and allowed the authors to make the conclusion that HGHG FEL technique would allow to reach the X-ray wavelength range starting from visible light. In this paper we take into account shot noise in the electron beam. It has been found that a general disadvantage of HGHG FEL schemes (as well as any frequency multiplication scheme) is due to strong noise degradation of the properties of output radiation with increasing harmonic number N . In the case of HGHG FEL this means that the effect of frequency multiplication by a factor of N results in multiplication of the ratio of noise power to carrier by a factor of N^2 . This prevents successful operation of HGHG FEL at very short wavelengths. On the basis of our study we can make the definite conclusion that the applicability region of the HGHG scheme is significantly narrower than claimed before. The results presented in this paper demonstrate that the HGHG scheme is quite adequate for the 10-100 nm coherent light source, but cannot be used to produce hard X-rays. It is explicitly shown that noise degradation prevents operation HGHG multistage scheme at Angstrom wavelength range.

2 General description of subharmonically seeded multistage HGHG FEL

The layout of the subharmonically seeded FEL is shown schematically in Fig. 1. Facility for production of fully coherent soft X-ray pulses consists of a seed laser, five stages of frequency doubling and main undulator. The first stage of frequency doubling (260 \rightarrow 130 nm) consists of FEL amplifier undulator, and dispersion section for the beam density modulation. The scheme operates as follows. The seed laser pulse of 5 ps duration and 10 MW peak power is timed to overlap with the electron bunch. This laser pulse interacts with the electron beam in the first undulator, which is tuned to be resonant to seed radiation wavelength. The top of the seed radiation pulse of 5 ps duration can be easily tuned to the arrival time of the short electron bunch at the predicted absolute jitter of about ± 1 ps. Radiation power is exponentially amplified upon passing through the first undulator. The amplitude of energy modulation of the electron beam at the undulator exit is equal to 0.3 MeV, while the beam density modulation is not sufficient to drive the second stage. The required value of the beam bunching at the second harmonic of about 0.01 is achieved when the electron beam passes through dispersion section. In this case the amplitude of the second harmonic of the density modulation dominates significantly over the amplitude of shot noise harmonic (of about 0.01 %), and it serves as input signal for the second stage.

Optimal parameters of the dispersion section can be calculated in the following way. The phase space distribution of the particles in the first FEL amplifier is described in terms of the distribution function $f(P, \psi)$ written in "energy-phase" variables $P = E - E_0$ and $\psi = k_w z + \omega_0(z/c - t)$, where E_0 is the nominal energy of the particle, $k_w = 2\pi/\lambda_w$ is the undulator wavenumber, and ω_0 is the frequency of the seed radiation. Before entering the first undulator, the electron distribution is assumed to be Gaussian in energy and uniform in phase ψ . The present study assumes the density modulation at the end of first undulator to be very small compared to the desired value (10 %) and there is an energy modulation $P_0 \sin \psi$ only. After passing through the dispersion section with dispersion strength $d\psi/dP$, the electrons of phase ψ and energy deviation P will come to a new phase $\psi + P d\psi/dP$. The integration of "energy-phase" distribution over energy provides the beam density distribution, and the Fourier

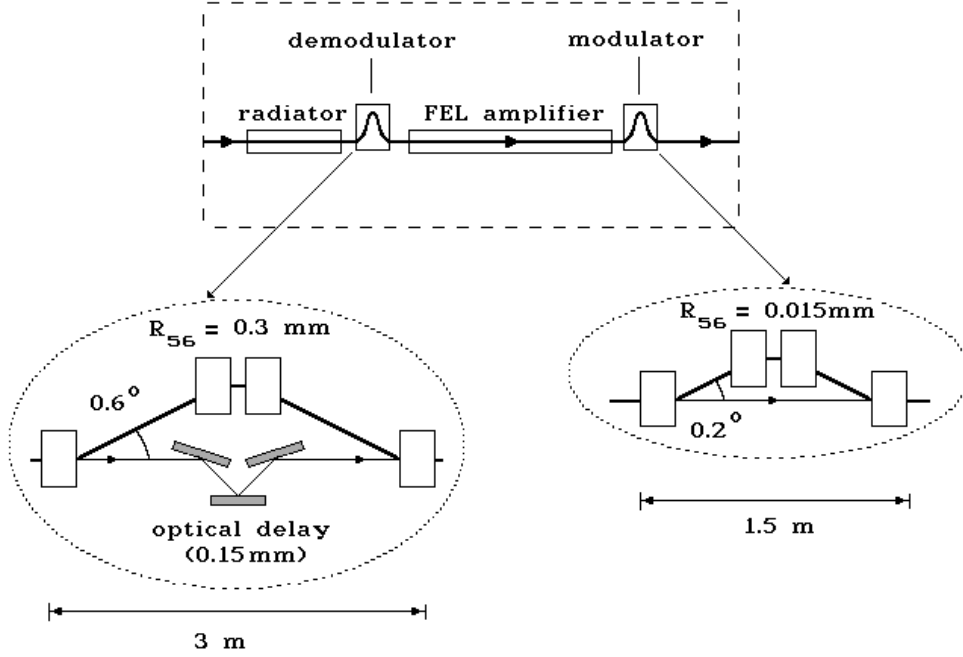


Fig. 2. Schematic illustration of design configuration for the second stage of subharmonically seeded soft X-ray FEL at TTF

expansion of this function gives the harmonic components of the density modulation converted from the energy modulation [4]:

$$\int_{-\infty}^{\infty} f(P, \psi) dP = 1 + 2 \sum_{n=1}^{\infty} \exp \left[-\frac{1}{2} n^2 \langle (\Delta E)^2 \rangle \left(\frac{d\psi}{dP} \right)^2 \right] \times J_n \left(n P_0 \frac{d\psi}{dP} \right) \cos(n\psi). \quad (1)$$

The Bessel function factor represents the microbunching. If its argument is much smaller than unity, the microbunching would be reduced proportionally to its n th power. Hence, $P_0 d\psi/dP$ must be comparable to a_1 , where a_1 is the desirable value of first harmonic bunching factor. The first exponential factor shows that the energy spread suppresses significantly the microbunching when $\Delta E d\psi/dP \simeq a_1 \sqrt{\langle (\Delta E)^2 \rangle} / P_0$ is larger or equal to unity. Hence, the energy modulation can be smaller than the energy spread in order to have a small first harmonic components ($a_1 \ll 1$). Parameters in our case are: $\sqrt{\langle (\Delta E)^2 \rangle} \simeq 1$ MeV, $P_0 \simeq 0.25$ MeV, $P_0 d\psi/dP \simeq 0.16$. Put these parameters in (1) we find the amplitudes of the first and the second harmonic of density modulation: $a_1 \simeq 0.13$, $a_2 \simeq 0.01$.

The above consideration of the bunching process has been treated within the framework of a single particle dynamic theory. One should care also about avoiding coherent synchrotron radiation (CSR) effects. The electric field of CSR induces an energy modulation along the bunch. Calculations of the correlated energy spread growth due to CSR shows that this should not be a limitation in our case (see [14] for more details).

Another harmful effect which may influence the operation of a HGHG scheme is the space

charge. Calculations of the space charge force in the beam bunched at 260 nm show that this should be a serious limitation in our case. The electric field of the space charge induces the additional energy modulation at 260 nm wavelength. If we calculate plasma oscillation along the HGHG scheme, the space charge induced energy modulation is predicted to be about 0.5 MeV. Specific design of the second stage is proposed for preparation of the electron beam with the required energy spread in order to overcome the problem of plasma oscillation. The design configuration of the second stage is shown in Fig. 2. The stage consists of a short undulator (radiator), dispersion section (demodulator), high-gain FEL amplifier and end-stage dispersion section (modulator).

Following the first stage the beam and seed radiation enter short undulator (radiator) which is resonant with second harmonic of seed radiation (130 nm). In the radiator the seed radiation plays no role and is diffracted out of the electron beam. However, a new 130 nm radiation is generated by the density-modulated electron beam and rapidly reaches MW-level peak power. After the radiator the electron beam is guided through a dispersion section (magnetic chicane) and the 130 nm radiation beam enters the grazing mirror system (see Fig. 2). The function of this chicane consists in suppressing the 260 nm modulation of the electron bunch produced in the first stage. The function of the mirror system consists in making the path length of the electron and the radiation beam to be equal. The trajectory of the electron beam in the chicane has the shape of an isosceles triangle with the base equal to L . The angle adjacent to the base, θ , is considered to be small. The problem of suppressing the beam modulation induced in the first stage can be solved quite naturally due to the presence of the local energy spread in the electron beam. Parameters in our case are: $\theta = 0.6^\circ$, $L = 3$ m, compaction factor $R_{56} = L\theta^2 \simeq 300\mu\text{m}$, $\sqrt{\langle(\Delta E)^2\rangle}R_{56}/E_0 \simeq 0.3\mu\text{m}$, $\lambda = 0.26\mu\text{m}$. This leads to the suppression of the electron beam modulation by a factor $\exp(-20)$ (for Gaussian energy distribution).

Passing the chicane the demodulated electron beam and seed 130 nm radiation enter the FEL amplifier undulator. Upon passing through the FEL amplifier radiation is exponentially amplified. This undulator is long enough to reach 0.25 MeV energy modulation at the wavelength of 130 nm. Since the density modulation at 130 nm is of about 4 times smaller than required value (0.2), one should use dispersion section at the exit of the second stage. After passing second dispersion section, the energy modulation induced in the beam by amplification in the FEL amplifier transforms into the density modulation.

Following the second stage the beam enters the third stage. Like the second stage, the third stage also consists of the radiator (which is resonant to the 4th harmonic of the seed radiation), demodulator, FEL amplifier and modulator. Now 65 nm density modulation serves as a seed for this radiator, etc. Main undulator, resonant with 32th harmonic of seed radiation (8 nm), follows immediately after the 5th stage. By the time the beam is overbunched in the main undulator, the 8 nm radiation reaches GW level. Calculations of the space charge effects show that they are negligible in the main undulator. The electric field of space charge is proportional to the wavelength of density modulation λ . As a result, the amplitude of energy modulation at 16 nm is much less than energy spread, and there is no need to install special chicane for suppressing the beam density modulation induced in the 5th stage. Table 1 lists some of the basic parameters of the magnetic system of HGHG FEL.

In our proposal soft X-ray pulses are produced by the multistage HGHG technique. Frequency multiplication can be an essential pulse shortening mechanism. Successive multiplica-

Table 1
Parameters of the magnetic system of HGHG FEL scheme

	Stage 1 256 nm	Stage 2 128 nm	Stage 3 64 nm	Stage 4 32 nm	Stage 5 16 nm	Main 8 nm
<u>Radiator undulator</u>						
length of undulator, m		1.4	1.7	1.9	2	
period, cm		5	4.5	4	3.3	
peak field, T		1.1	0.94	0.75	0.65	
K -value		5.5	4	2.8	2	
<u>Demodulator chicane</u>						
net momentum compaction, mm		0.3	0.3	0.3	0.03	
total chicane length, m		3	3	3	1.5	
length of each dipole magnet, m		0.25	0.25	0.25	0.25	
bend angle of each dipole, deg.		0.6	0.6	0.6	0.27	
magnetic field for each dipole, T		0.15	0.15	0.15	0.067	
<u>FEL amplifier undulator</u>						
length of undulator, m	1.95	1.6	2.4	2.8	4.6	13.1
period, cm	6.5	5	4.5	4	3.3	2.73
peak field, T	1.1	1.1	0.94	0.75	0.65	0.5
K -value	6.8	5.5	4	2.8	2	1.26
<u>Modulator chicane</u>						
net momentum compaction, μm	18	7.5	3.5	1.5		
total chicane length, m	1.5	1.5	1.5	1.5		
length of each dipole magnet, m	0.25	0.25	0.25	0.25		
bend angle of each dipole, deg.	0.2	0.13	0.09	0.06		
magnetic field for each dipole, T	0.05	0.033	0.023	0.015		

tion to the N th harmonic resulting in \sqrt{N} -fold compression of the N th harmonic pulse duration. In our case $N = 32$, and numerical simulations show that we can obtain 80 fs pulse at the wavelength of 8 nm.

3 Estimation of essential shot noise effects on basis of a simple model

As for the HGHG FEL operating in the short wavelength range, its noise properties are defined only by the shot noise. To describe the noise output quantitatively, we should define the quality criterion of the HGHG FEL. One possible definition can be made as follows. A HGHG FEL can be characterized by a noise factor F that related the input to output signal to noise ratio:

$$F = \frac{(P_s/P_n)_{\text{in}}}{(P_s/P_n)_{\text{out}}},$$

where P_s and P_n are the power of signal and noise, respectively. It is natural to describe the input signal and noise power by the radiation power of signal and noise at the first FEL amplifier exit. As a rule, the first FEL amplifier has gain of about 10-20 dB only which is insufficient for transverse mode selection. Nevertheless, for a long last (main) undulator the only fundamental TEM₀₀ mode, which has maximal gain, should survive. That is why the input noise power $(P_n)_{\text{in}}$

should be treated as a contribution to fundamental radiation mode only.

An intrinsic disadvantage in the short wavelength HGHG FEL is the enormous value of noise factor. This is the direct effect of the frequency multiplication. The dependence of a noise factor can be given as a function of a frequency multiplication factor N . Successive multiplication to the N th harmonic resulting in at least N^2 - fold increasing of the noise factor

$$F > N^2 \quad \text{at} \quad \omega_0 \rightarrow n_1\omega_0 \rightarrow n_1n_2\omega_0 \rightarrow \dots \rightarrow N\omega_0 ,$$

as one can expect from simple physical consideration (see below). This fundamental result is of great practical importance, because a crucial condition in HGHG FEL is that the output signal to noise ratio $(P_s/P_n)_{\text{out}}$ must be made much larger than unity, in order for the properties of the output radiation to be a map of the characteristics of the high-quality seed laser.

Simple physical consideration can lead directly to a crude approximation for the value of F . It should be noted that the method which can be applied to determine the output field perturbation is independent of a specific kind of HGHG technique. This calculation depends on the frequency multiplication factor N only. The field of amplified electromagnetic wave in the first FEL amplifier can be represented as

$$E_1 = E_s \exp(i\omega_0 t) + \sum_j u_j \exp(i\omega_0 t + \Delta\omega_j t) + \text{C.C.} , \quad (2)$$

where E_s is the amplitude of amplified seed signal. The quantities $u_j \exp(i\omega_0 t + i\Delta\omega_j t)$ represent the (small) signal changes due to the shot noise. Starting with a field at fundamental harmonic in the first stage (2) and omitting an inessential common factor, we find for the field in the main undulator at frequency $N\omega_0$:

$$E_N = E_s^N e^{iN\omega_0 t} + N E_s^{N-1} e^{i(N-1)\omega_0 t} \sum_j u_j e^{i\omega_0 t} e^{\Delta\omega_j t} + \text{C.C.} , \quad (3)$$

where we have assumed that at the end of each stage the amplitude of a higher harmonic density modulation is small. It is obvious, this is the situation that is encountered in any HGHG scheme. As we have seen in Sec. 2, the amplitude of the n th harmonic of the beam density modulation, a_n , is proportional to the n th power of the field amplitude at the fundamental frequency, i.e. $a_n \propto (E_1)^n$ at $a_n \ll 1$. Therefore, the field amplitude E_N in the main undulator is proportional to $E_N \propto a_N \propto (E_1)^N$. When derived (3), we also required the output signal to noise ratio to be much larger than unity. These two assumptions are quite general and do not reduce significantly the practical applicability of the result obtained. However, for simplicity presented derivation is limited to the case where only first FEL amplifier have significant contribution to the noise output.

In the frame of approximations discussed above the output signal to noise ratio can be represented as

$$\frac{\langle (E_s^N e^{iN\omega_0 t} + \text{C.C.})^2 \rangle}{\langle (N E_s^{N-1} e^{i(N-1)\omega_0 t} \sum_j u_j e^{i\omega_0 t} e^{\Delta\omega_j t} + \text{C.C.})^2 \rangle} = \frac{1}{N^2} \left(\frac{P_s}{P_n} \right)_{\text{in}} ,$$

where symbol $\langle \dots \rangle$ means the ensemble average over bunches. Thus, frequency multiplication by N degrades the signal/noise ratio by N^2 . Here we illustrated the essential shot noise effects on the basis of a simple model. Indeed, the present derivation assumes shot noise influence in the 2nd, 3rd and other stages to be negligible compared to the shot noise influence in the 1st stage. Nevertheless, the problem of calculation of HGHG FEL noise factor is more complicated and there are situations where, for instance, shot noise in the second stage can provide comparable or even larger output signal perturbation than shot noise in the first stage. As a result, we can conclude only that in practical situations noise factor satisfies inequality $F > N^2$.

4 Numerical study of the harmonic generation process in a multistage HGHG FEL

In this section we analyze possibilities of the HGHG FEL scheme described in the previous sections. To be specific, we consider numerical example for its possible realization at the TESLA Test Facility at DESY. However, this specific example highlights all general properties of the HGHG FEL schemes.

Numerical results presented in this paper are obtained with a version of code FAST upgraded for simulation of higher harmonics. This code allows one to perform three-dimensional simulations of the FEL process taking into account diffraction, space-charge, energy spread and slippage effects, and shot noise in the electron beam. An electron bunch of any transverse and longitudinal profile can be simulated. General features of the code FAST are described in [13]. In the present simulations we assumed both transverse and longitudinal profile of the electron beam to be gaussian. The simulation procedure of full HGHG scheme was described in citedesyp

All numerical results are illustrated for two cases: with and without taking into account shot noise in the electron beam. When we trace the behaviour of an idealized case (without taking into account shot noise), we obtain perfect quality radiation pulse (both in temporal and spectral domain) at the exit of HGHG FEL. However, taking into account noise effect results in a degradation of the quality of the radiation pulse from stage to stage. As we mentioned in the previous section, the HGHG FEL scheme, as well as any frequency multiplication scheme possesses significant intrinsic disadvantage. Namely, contribution of the shot noise power to the signal grows quadratically with the number of harmonic to be generated. The results of numerical simulations are in good agreement with simple physical estimations presented in the previous section. The growth of the noise contribution is clearly illustrated with the plots for the phase of the radiation field (see Fig. 3). The plots for radiation spectrum are presented in Fig. 4. Analysis of the present numerical example shows that the shot noise in the first stage gives relatively small contribution to the final value of the noise to signal ratio at the exit of the HGHG scheme. This is achieved by means of increase of the power of seed radiation. However, HGHG scheme does not allow to do this for the next stages when a small beam density modulation serves as input signal. In our case the main contribution of noise degradation comes from the second stage. The third stage also gives visible contribution to the noise.

The most critical issue of the single-bunch HGHG scheme is growth of uncorrelated energy spread. However, parameters of the stages can be optimized in such a way that this effect almost does not lead to degradation of output radiation. Calculations show that the increase of

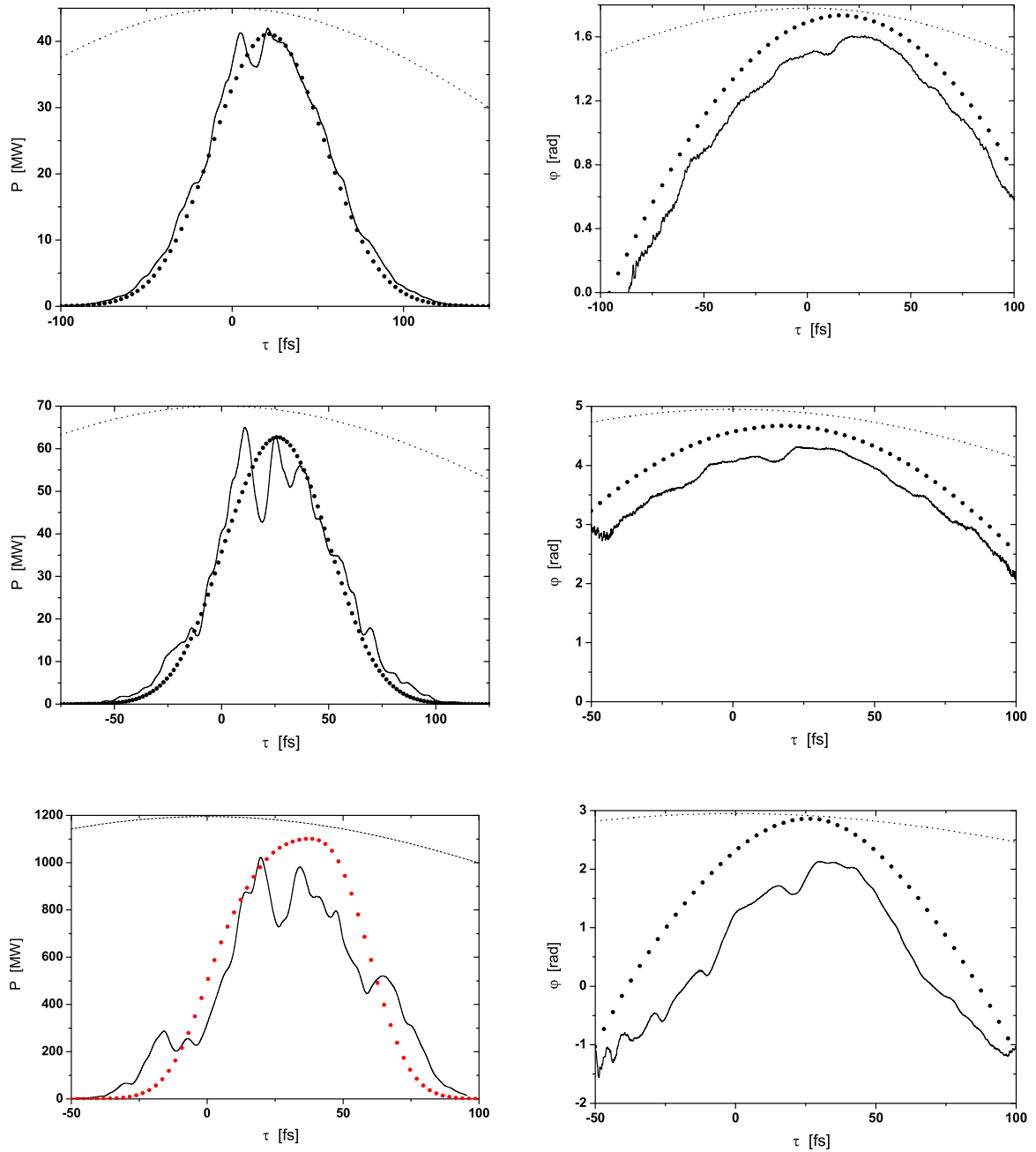


Fig. 3. Time structure of radiation power (left column) and phase of output radiation (right column) at the exit of different stages of HGHG scheme (upper, middle, and lower plots correspond to the 4th and 5th stages, and main undulator, respectively). Solid curves are calculated taking into account shot noise in the electron beam, and the circles present the results without noise effect. Dashed curves denote longitudinal profile of the electron bunch. The first stage is seeded by a long laser pulse.

uncorrelated energy spread is 20% only (see [14] for more details).

The results presented above allows us to make conclusion that shot noise degradation does not allow to reach very short wavelengths with the HGHG FEL scheme. A limit imposed by this fundamental effect seems to be around 8 nm when HGHG procedure starts from UV seeding

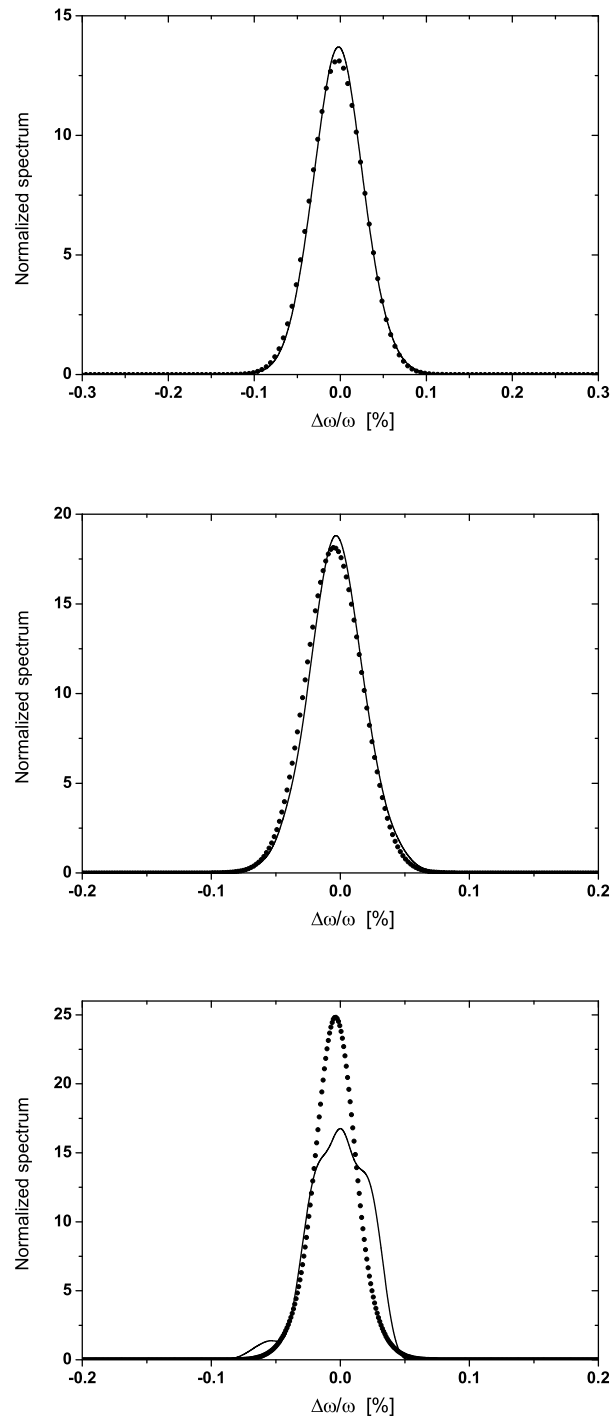


Fig. 4. Spectrum of output radiation at the exit of different stages of HGHG scheme (upper, middle, and lower plots correspond to the 4th and 5th stages, and main undulator, respectively). Solid curves are calculated taking into account shot noise in the electron beam, and the circles present the results without noise effect. The first stage is seeded by a long laser pulse.

laser (multiplication factor of about 30). Practical limit is reached for even longer wavelength. The reason for this is that HGHG FEL scheme is extremely sensitive to fluctuations of the beam

and seeding radiation parameters.

5 Discussion

In conclusion we would like to discuss some general aspects of noise influence on the HGHG FEL operation. It should be emphasized that despite the theory of HGHG FEL was developed over a decade, there are no papers devoted to the analysis of the noise properties of these sources. Here, it is relevant to remember that the analysis of the frequency multiplier chains and their effects on source noise in radar and similar systems has always been an important problem. The majority of communication and radar engineers are familiar with the fact that inserting the amplifier prior to frequency multiplication has the disadvantage that the phase noise contribution of the amplifier is multiplied by n^2 , where n is a frequency multiplication factor (see, for example, [15]). In the case of HGHG FEL this means that the effect of frequency multiplication by a factor of N multiplies the first FEL amplifier noise power to carrier ratio by N^2 . This prevents operation of HGHG FEL at very short wavelength range.

Let us give a more detailed discussion of problems relating to the X-ray HGHG FEL noise output. Frequency multiplication process produces a noise degradation proportional to at least the square of the multiplication ratio. As a result, HGHG FEL starting from optical wavelength range ($\lambda_{\text{in}} > 2000 \text{ \AA}$) cannot produce coherent radiation spanning to Angstrom wavelength range. The main problem is that the contribution of the noise to the output power increases drastically when approaching the X-ray band. Consider firstly an idealized case where only the first FEL amplifier has significant contribution to the noise output. Then the signal to noise ratio after an ideal frequency multiplier chain is smaller than the signal to noise ratio at the fundamental frequency by a factor of $F \simeq N^2 \simeq 10^7$ at $\lambda_{\text{out}} \simeq 1 \text{ \AA}$. If we want to make the ratio $(P_s/P_n)_{\text{out}}$ much larger than unity, $(P_s/P_n)_{\text{in}}$ must reach values of about 10^9 . To estimate the required value of the peak power of the seed laser pulse it is convenient to introduce the notion of an effective power of shot noise P_{sh} , which is usually used for numerical simulation of the SASE FEL with steady-state codes (see for example [12]). For the visible range of the spectrum the effective shot noise power for usual SASE FEL parameters is about $P_{\text{sh}} \simeq 10^2 \text{ W}$. This means that successful operation of the X-ray HGHG FEL requires a seed power of about 100 GW, but this value is beyond the output power of the FEL amplifier at saturation ($P_{\text{sat}} \simeq 10 \text{ GW}$). In principle, in this situation a laser pulse of 100 GW power level and a first undulator with a few periods only could be used. However, this does not solve the problem of the noise degradation, because the present analysis is based on assuming an ideal frequency multiplier chain. Considering the other contributions to the noise output, it is obvious that the 100 GW level power is not attainable in the radiator undulator operating at the second (or higher) harmonic. This means that the condition $(P_s/P_n)_{\text{out}} \gg 1$ will be violated when taking into account of the second HGHG stage contribution to the noise output.

Recently, various HGHG schemes have been proposed to improve the performance of X-ray FEL. The basic theory of these schemes does not take into account the shot noise effect, meanwhile it leads to a dramatic degradation of the quality of the output radiation when applying frequency multiplication schemes. The arguments discussed above, based on our results of numerical simulations, seem to be strong enough to suggest that the HGHG FEL schemes for reaching hard X-rays proposed in the literature so far will not work.

Acknowledgments

We thank J.R. Schneider and D. Trines for interest in this work and support.

References

- [1] J. Feldhaus et al., Optics Communications 140(1997)341
- [2] E. L. Saldin, E. A. Schneidmiller and M. V. Yurkov, Nucl. Instrum. and Methods A 445(2000)178
- [3] R. Bonifacio, L. De Salvo, and P. Pierini, Nucl. Instrum. and Methods A293(1990)627
- [4] L. H. Yu, Phys. Rev. A44(1991)5178
- [5] I. Ben-Zvi et al., Nucl. Instrum. and Methods A304(1991)151
- [6] I. Ben-Zvi et al., Nucl. Instrum. and Methods A393(1997)II-10
- [7] L. H. Yu and I. Ben-Zvi, Nucl. Instrum. and Methods A393(1997)96
- [8] L. H. Yu et al., Nucl. Instrum. and Methods A445(2000)301
- [9] A. Doyuran et al., "Characterization of a High-Gain Harmonic- Generation Free Electron Laser at Saturation" BNL-68031, submitted to Phys. Rev. Lett. January 2001
- [10] L. H. Yu "Seeded FELs and Expected performance", Proceedings of the ICFA Advanced Beam Dynamics Workshop on Future Light Sources, C. E. Eyberger, Ed., Argonne National Laboratory, Argonne, IL (1999).
- [11] J. Rossbach, Nucl. Instrum. and Methods A 375(1996)269
- [12] E. L. Saldin, E. A. Schneidmiller and M. V. Yurkov, "The physics of Free Electron Lasers" (Springer-Verlag, Berlin, 1999)
- [13] E. L. Saldin, E. A. Schneidmiller and M. V. Yurkov, Nucl. Instrum. and Methods A 429(1999)233
- [14] W. Brefeld et al., DESY-print 01-056 (2001)
- [15] W. P. Robins "Phase noise in signal sources" IEE Telecommunications series 9, Peter Peregrinus Ltd, 1982

Development of a Femtosecond Soft X-ray SASE FEL at DESY

W. Brefeld^a, B. Faatz^a, J. Feldhaus^a, M. Körfer^a, J. Krzywinski^b,
T. Möller^a, J. Pflueger^a, J. Rossbach^a, E.L. Saldin^a,
E.A. Schneidmiller^a, S. Schreiber^a, and M.V. Yurkov^c

^a*Deutsches Elektronen-Synchrotron (DESY), Notkestrasse 85, D-22607 Hamburg,
Germany*

^b*Institute of Physics of the Polish Academy of Sciences, 02688 Warszawa, Poland*

^c*Joint Institute for Nuclear Research, Dubna, 141980 Moscow Region, Russia*

Abstract

In this paper we describe the extension of the soft X-ray SASE FEL at the TESLA Test Facility (TTF) at DESY for generation of femtosecond pulses. The proposed scheme operates as follows. The first stage is a conventional FEL amplifier seeded by 523 nm external laser. A zero area optical pulse (i.e. the pulse with zero value of optical field in the central area of the pulse) is timed to overlap with the electron bunch. Radiation power is amplified up to the saturation level. Following the first stage the electron beam enters the main 6 nm SASE undulator. Large energy spread is induced in the significant fraction of the electron beam due to the FEL interaction process, and only a small part of the electron bunch (near the center of zero area light pulse) is capable to produce radiation in the 6 nm SASE FEL. The SASE FEL described in this paper will provide soft X-ray pulses with 30 fs (FWHM) duration. On the basis of the TTF parameters it should be possible to achieve an average brilliance of 10^{22} photons $s^{-1} \text{mrad}^{-2} \text{mm}^{-2}$ per 0.1% BW. The average number of photons can exceed 10^{12} photon/pulse.

1 Introduction

Phase transitions, surface processes, and chemical reactions are ultimately driven by the motion of atoms on the time scale of one vibrational period ($\simeq 100$ fs). Unfortunately, the pulse length of present synchrotron light sources is too long for resolving atomic motion on the 100 femtosecond time scale. Recent efforts at applying 300 fs X-rays pulses to probe structural dynamics have used a synchrotron source combined with a femtosecond optical quantum laser [1]. The same technique can be used to generate in the future 100 fs X-ray pulses with an average

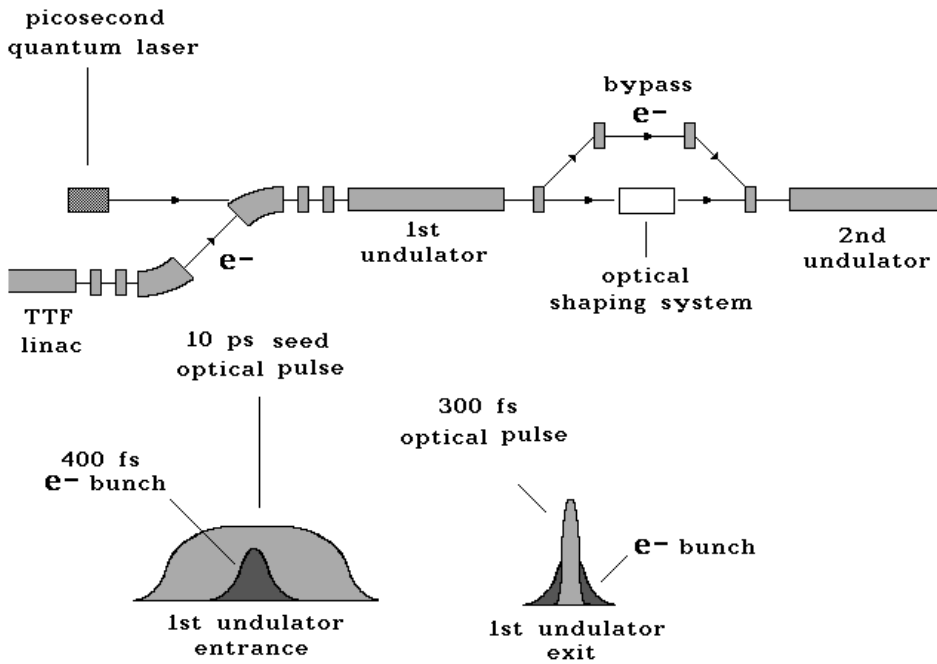


Fig. 1. The two stage scheme of the seeding system

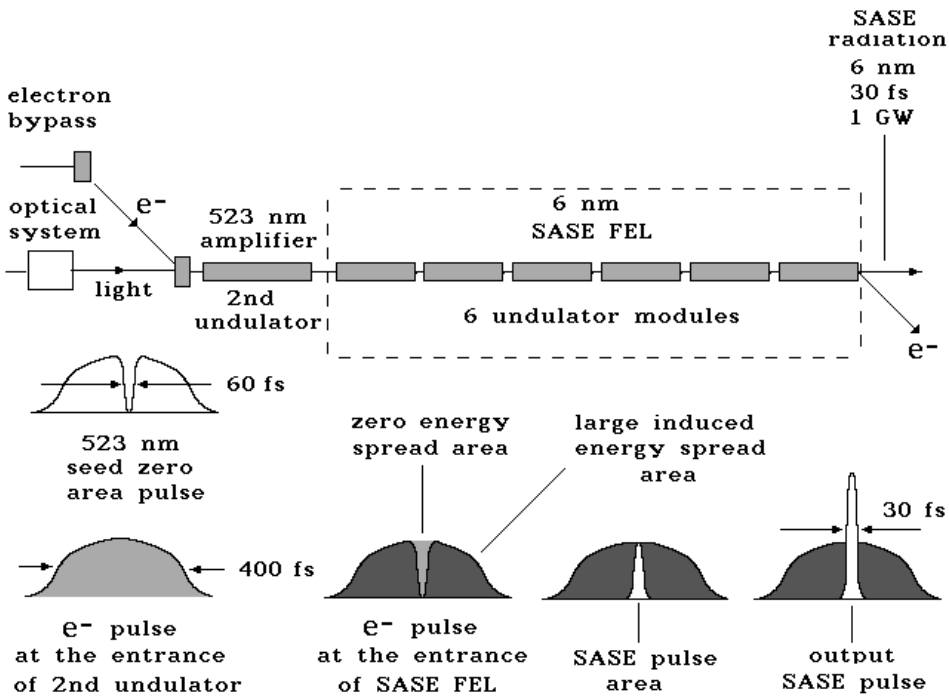


Fig. 2. Schematic diagram of zero area pulse technique for the generation of the soft X-ray femtosecond SASE pulses

brilliance of 10^{11} photons $s^{-1} \text{mrad}^{-2} \text{mm}^{-2}$ per 0.1% BW at the photon energy of 2 keV [1].

Femtosecond soft X-ray facility proposed in this paper is based on the use of soft X-ray SASE FEL. To be specific, we illustrate a new method of femtosecond X-ray pulses production with an example for the SASE FEL at the TESLA Test Facility (TTF) being under construction at DESY. The idea for production of very short X-ray pulses is based on a high sensitivity of the FEL gain on the energy spread in the electron beam. Thus, a technique best suited for the femtosecond SASE FEL consists of “manipulating” the energy spread along the electron bunch. The required shaping of the energy spread is performed by passing the electron beam through two-stage FEL amplifier (see Fig. 1) seeded by an optical pulse from existent TTF laser facility (pulse duration 10 ps, optical energy in the pulse $0.3 \mu\text{J}$, wavelength 523 nm – the 2nd harmonic of Nd:YLF laser). The first stage of the FEL amplifier operates in the linear regime and produces optical pulses of 300 fs pulse duration with peak power of about 60 kW which is strictly synchronized with the electron bunch. After the exit of the first stage the electron bunch is guided through a bypass, and the radiation enters the pulse shaping system. The functions of the electron bypass are to provide equal time delays for the electron and the light beams, and to suppress microbunching induced in the electron bunch in the first undulator due to the FEL process. The function of the optical pulse shaping system is to prepare zero area optical pulse. In pulse shaping system the input radiation is focused into a single-mode optical fiber. After the fiber exit, the linear chirped pulse is sent through spectral filtering system. The pulse is spectrally dispersed using a grating and directed through a mask which spectrally filters the pulse. The spectral components are recollimated into a beam by a second grating. The shaping system produces zero area pulses which are strictly synchronized with electron bunches at the entrance to the second undulator. Since the input optical pulse is produced by the same electron bunch, the proposed scheme tolerates electron pulse time jitter of about a few picoseconds. A zero area optical pulse produced by the shaping system is amplified up to the saturation level in the second undulator. Large energy spread is induced in the significant fraction of the electron beam due to the FEL interaction process, and only a small part of the electron bunch (near the center of the zero area light pulse) is capable to produce radiation in the 6 nm SASE FEL (see Fig. 2).

2 Scientific opportunities with the femtosecond soft X-ray SASE FEL

To date, the study of ultrafast dynamics in the field of physics, chemistry, and biology has relied largely on femtosecond optical pulses in the visible or infrared spectral range. Using fs optical lasers researches could collect a wealth of information on the details of reaction pathways in many molecular systems e.g. J_2 , CH_2J_2 , and even larger systems [3]. The importance of the field is underlined by awarding the Nobel Prize in chemistry to A. Zewail. Since all information in optical fs-experiments is obtained from spectroscopic results, e.g. ionization probability or kinetic energy of photoelectrons, a detailed knowledge on the involved - sometimes rather complex - energy surface is required for the interpretation and understanding

of the experimental data. Soft X-rays have several advantages compared to optical light pulse. Thanks to the element specific absorption of inner shell electrons well-defined atoms can be excited selectively. Moreover, chemical bonds can be selected by their well-known chemical shift, e.g. in inner shell photoelectron spectra (XPS). The latter can be used in order to identify surface and bulk states of condensed matter. Finally, the local excitation of tightly bound core levels allows the determination of structural information with various techniques (EXAFS, XANES, and photoelectron diffraction). Therefore, fs soft X-ray pulses hold great promises for new and exciting experiments in many fields of research which will give deep insight into the dynamics of nuclei and electrons on the time scale of vibrational motion.

The vibrational period of nuclear motion depends on the strength of chemical bonds and the mass of nuclei. In heavy molecules like J_2 the period is approximately 100-200 fs while for light molecules, especially hydrogen containing molecules it last about 10-50 fs. It is thus obvious, that the proposed new design for a soft X-ray FEL with 30 fs long pulses will have a considerable advantage compared to other proposed schemes [4,2] – some are already under construction or have emitted first light [5] - since their pulse duration of 200-300 fs is just at the limit for the studies on nuclear motion and lattice vibrations. Pump probe techniques which are commonly used with optical lasers, are highly desirable in order to make full use of the short pulses. Since precise timing is needed with a jitter of less than 30 fs we suggest to combine the proposed fs soft X-ray FEL with UV optical pulses generated in an additional undulator using the same electron beam as outlined in ref. [6].

Time resolved experiments with 30 fs resolution will open new scientific opportunities in chemistry, molecular physics, solid state physics and surface science. The use of pump-probe techniques will allow the study of vibrational and bond breaking and dissociation in complex molecules with element selectivity. Thanks to the local excitation it will be possible to distinguish the vibrational motion of non-equivalent atoms, e.g. the central and the terminal nitrogen atom in N_2O . Moreover, time resolved photoemission (XPS) can be used to ascertain decay rates and vibrational periods in well-defined subgroups in large molecules, since the chemical shift in the XPS spectrum is a fingerprint of chemical bonds.

In a similar way, research on clusters and nanocrystals will benefit from the proposed FEL. As a result of their small size a large fraction of atoms are located at the surface. Time resolved studies (pump-probe) will allow the investigation of surface and bulk states separately. Furthermore, photon induced reactions, phase transitions and electron transfer processes can be studied on a time scale of a few ten fs. Photoelectron, ion and fluorescence signals as well as combinations (electron ion: PEPICO, ion-ion, PIPICO, for the study of fragmentation and dissociation) can be used as a monitor. Metal, semiconductor and covalently bound systems, and complexes that play an important role in atmospheric processes are great interest in this context.

The element specific excitation of soft X-rays will allow the study of photodynamical processes of individual atoms and molecules on surfaces. Time resolved EXAFS/XANES or photoelectron diffraction making use of two colour pump- and probe techniques will give information on the motion (vibration dissociation) on well characterized surfaces in real time. The reaction dynamics of adsorbates is of major importance for the understanding of chemical processes at surfaces and an important issue in this context. Catalytic reactions of metal and semiconductor interfaces are of particular interest. UV light can induce a chemical reaction like oxidation, which can be studied by looking at reaction products on a fs time scale. The high photon density of the FEL beam - especially when focussed into a small spot - will result in efficient photodesorption and plasma formation. Many processes occurring in laser induced plasma going on in the plume are not well understood. Detailed information can be obtained using two-colour pump probe experiments and detecting photoelectrons and ions ejected from the plasma plume. Photoreactions and phase transition in bulk samples can be investigated with time resolved X-ray emission spectroscopy. The mean free path length of soft X-rays is much larger than the internuclear separations in solids. Thus, time resolved studies of bulk properties, the dynamics of atoms doped into solids and photoinduced reactions at buried interfaces become feasible.

All applications outlined above are based on 30 fs long soft X-ray pulses. One can expect that first successful experiments in this field will stimulate further applications.

3 Description of femtosecond X-ray FEL at the TESLA Test Facility

Present design assumes to use project parameters of the TESLA Test Facility accelerator [2]. Facility for production of femtosecond SASE X-ray pulses consists of a two-stage seeding system operating at the wavelength of 523 nm. Figure 1 shows a schematic diagram of a seed system for the femtosecond soft X-ray SASE FEL at the TESLA Test Facility. The scheme consists of seed quantum laser, two undulators and optical pulse shaping system located between them. The first undulator operates in a linear regime and produces short light pulse (of about 300 fs duration) synchronized with the electron bunch. After the exit of the first undulator the electrons are guided through a bypass and the radiation enters the shaping system. A zero area light pulse with peak power of about 10 kW is generated by pulse shaping system. This radiation pulse is amplified up to the saturation level in the second undulator. At the exit of the second undulator the most fraction of the electron bunch has large energy spread due to the FEL process except of a small region in the center of zero pulse area. This of the essence of the energy spread shaping technique. The process of amplification of radiation in the X-ray undulator develops in the same way as in conventional SASE FEL: fluctuations of the electron beam current density serve as the input signal. The seeding radiation (523 nm wavelength) does not interact with the electron beam in the X-ray undulator and is

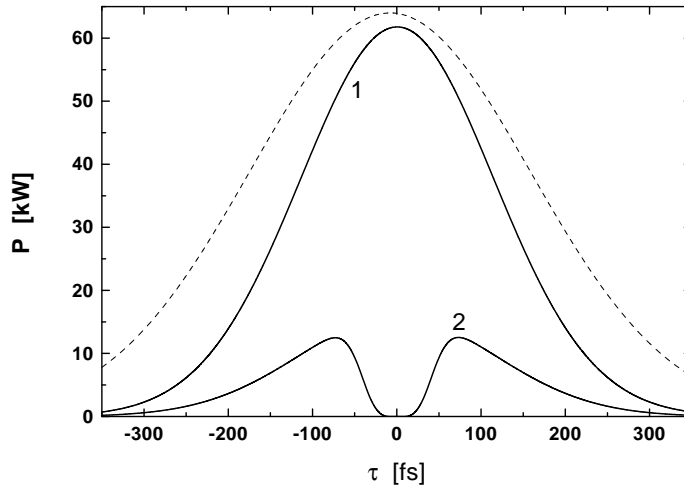


Fig. 3. Temporal profile of the radiation pulse at the exit of the first stage of 523 nm FEL amplifier (curve 1). Curve 2 present temporal profile of the radiation pulse after optical pulse shaping system. Dotted line denotes current profile of the electron bunch.

diffracted out of the electron beam. Since the gain of the FEL amplifier is very sensitive to the energy spread, only this small part of the electron bunch produces the radiation, thus providing short pulse duration (see Fig. 2). For ultrashort zero area of seed optical field, the slippage of radiation with respect to the electron bunch in the 523 nm high-gain FEL amplifier can be an essential mechanism for shortening the SASE radiation pulse. Starting with zero area of optical field of 60 fs duration (FWHM) we can obtain 30 fs (FWHM) pulses at the wavelength of 6 nm.

An attractive feature of this scheme is the absence of no apparent limitations which would prevent operation at even SASE pulse with duration close to coherence time (about 2 fs in our case). For example close to end of 523 nm FEL operation (i.e. close to saturation) we can use a magnetic delay to position the 523 nm radiation near the tail end of undisturbed part of the bunch. An experimenter can easily control the duration of "zero" area by tuning the magnetic field in the shifter (a three-dipole chicane). In this technique we use zero are of seed optical field that is much longer than the produced soft X-ray SASE pulse.

The function of the first stage of 523 nm FEL amplifier is to prepare short optical pulse strictly synchronized with the electron bunch. The amplifier is seeded by the laser pulse of 10 ps pulse duration and 30 kW peak power. The duration of the seeding pulse is much larger than the electron pulse time jitter of ± 1 ps, so it can be easily synchronized with the electron bunch. After the first stage the electron and the light beam are separated. The electron beam is guided through a nonisochronous bypass and the radiation enters the optical pulse shaping system. Details of the first stage FEL amplifier and the optical pulse shaping system are presented in [9]

The required level of the energy spread in the second FEL amplifier is induced only in the nonlinear stage of the FEL amplifier operation when the electrons be-

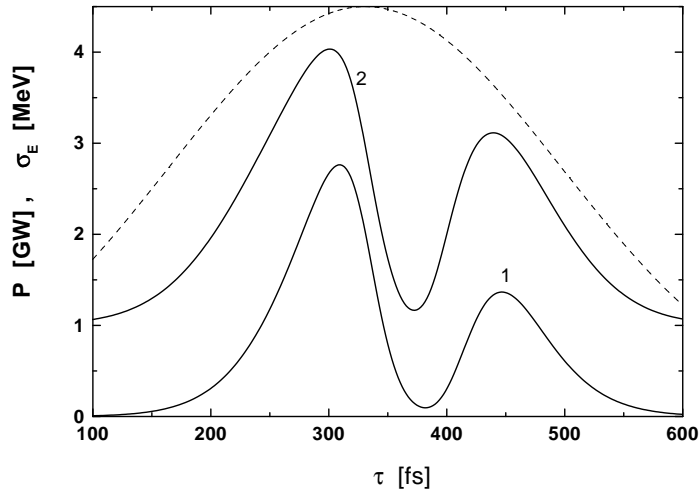


Fig. 4. Temporal profile of the output radiation (curve 1) and energy spread in the electron bunch (curve 2) at the exit of 523 nm FEL. Dashed line denotes current profile of the electron bunch.

come to lose visible fraction of their energy. In order to reach nonlinear stage, the undulator should be sufficiently long. Optimized length of the undulator is equal to 8.3 m, i.e. 110 undulator periods. Slippage effect at this distance play visible role in formation of the radiation, despite kinematic slippage (of about 60 microns) is visibly suppressed, by a factor of four, due to decrease of the group velocity of the radiation interacting with the electron beam [8]. This effect explains significant difference between the shape of the seeding pulse (see Figs. 3 and 4) and radiation profile and induced energy spread in the electron beam at the undulator exit.

A dispersion section is installed at the exit of the second stage of 523 nm FEL amplifier in order to provide more homogeneous distribution of the electrons in the phase at the entrance to the X-ray undulator. A simple chicane consisting of three dipoles with $R_{56} = 0.5$ mm is sufficient for this purpose.

X-ray undulator follows immediately after the second stage of the two-stage 523 nm FEL amplifier (see Fig. 2). Parameters of the femtosecond X-ray FEL amplifier are presented in Table 1. The only difference in parameters from the main option of the TTF FEL [2] is that the FWHM pulse duration is reduced down to the value of 30 fs. Figure 5 represents temporal structure of the radiation pulse at the exit of the X-ray FEL at the undulator length 26 m. Optimization of the parameters of the femtosecond foft X-ray facility at TTF has been performed with 3-D, time-dependent FEL simulation code FAST [7].

The electron bypass has to deflect the electron beam out of the straight flight pass to make room for the optical elements. In addition the microbunching introduced in the electron bunch in the first undulator has to be removed without increasing the overall length of the bunch significantly. The electron optical functions at the exit of 1st undulator and the entrance of the 2nd undulator are determined by the undulators and have to be matched by the bypass electron optics. The basic

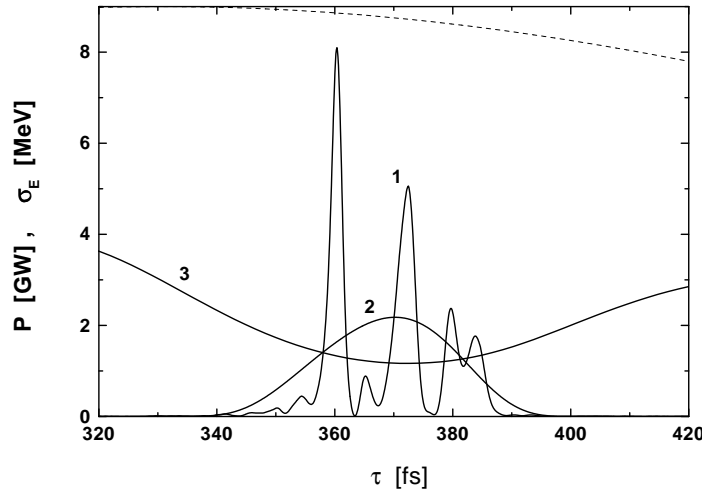


Fig. 5. Temporal structure of the output radiation from femtosecond X-ray FEL. Curve 1 corresponds to the single shot, and curve 2 is the averaged value. Curve 3 represent the energy spread along the electron bunch at the undulator entrance. Dashed line denotes current profile of the electron bunch.

Table 1

Parameters of femtosecond X-ray FEL at the TESLA Test Facility at DESY

<u>Undulator</u>	
Type	Planar
Period	2.73 cm
Peak magnetic field	0.497 T
External β -function	300 cm
Length of undulator	26 m
<u>Radiation</u>	
Wavelength	6.4 nm
Bandwidth, $\Delta\lambda/\lambda$	0.5%
rms angular divergence	15 μ rad
rms spot size at the undulator exit	90 μ m
Pulse duration (FWHM)	30 fs
Power average over pulse	2 GW
Flash energy	50 μ J
Average power	4 W
Peak spectral brilliance	3×10^{30} Phot./($\text{sec} \times \text{mrad}^2 \times \text{mm}^2 \times 0.1\% \text{ bandw.}$)

elements of the adopted symmetric bypass design are four dipole magnets. The first is located 1.3 m behind the first stage of 523 nm FEL amplifier and deflects the beam back in the direction parallel to the straight beam path at the distance of about 24 cm, which is sufficient for the installation of the optical elements. The total elongation of the electron beam path is approximately 12 mm. The layout of the bypass is shown in Fig. 6. In the middle of the bypass one finds a second mini-bypass, which serves for tuning the electron path length by up to 0.5 mm, i.e.

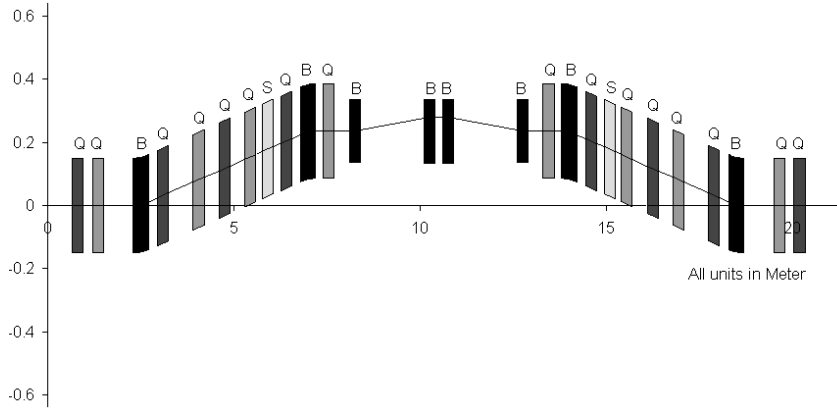


Fig. 6. Layout of the electron bypass. Here letters Q, S and B denote quadrupole, sextupole, and bending magnet, respectively.

Table 2

Parameters of the electron bypass

<u>Main bypass</u>	
Length	21 m
Extra path length	12.4 mm
Max. distance to the straight path	23.6 cm
Dipole bending angle	52.4 mrad
Extra path length for electrons with 0.1% energy deviation	0.73 μm
<u>Tuning bypass</u>	
Length of tuning bypass	4.8 m
Tunability of path length	0-0.952 mm
Max. distance to large bypass	43.6 mm
Tuning dipole bending angle	21.8 mrad
Extra path length for electrons with 0.1% energy deviation	0-1.86 μm

approximately 10 times of the bunch length. The additional focusing and defocusing quadrupole magnets are needed to adopt the bypass electron optics to that in the undulator, for decoupling of the beam path elongation from the electron energy and for keeping the transverse beam cross section small enough. The bypass parameter list is presented in Table 2. The transverse dimensions of the dipole and quadrupole magnets have been chosen such that they jut out in the direction of the straight beam path by no more than 15 cm. Preliminary optimization gives the length of the dipole and quadrupole magnets to be 20 cm and 30 cm, respectively. The final dimensions depend on the design of vacuum system.

For very short bunches, coherent synchrotron radiation (CSR) can dilute the horizontal emittance by similarly generated energy spread in the dipoles. Calculations of the CSR induced emittance dilution have been made using the DESY TRAFIC4 code [10] which includes field transients, bend-to-bend radiation, and radial forces. These results show that the dilution of the slice emittance in the

bypass is about 10% .

Acknowledgments

We thank J.R. Schneider and D. Trines for interest in this work

References

- [1] R. W. Schoenlein et al., *Science* 287(2000)2237
- [2] J. Rossbach, *Nucl. Instrum. and Methods A* 375(1996)269
- [3] L. Lehr et al., *Science* 284(1999)635
- [4] R. Tatchyn et al., *Nucl. Instrum. and Methods A* 375(1996)274
- [5] J. Andruszkow et al., *Phys. Rev. Lett.* 85(2000)3825
- [6] B. Faatz et al., DESY-print 00-94(2000)
- [7] E. L. Saldin, E. A. Schneidmiller, and M. V. Yurkov, *Nucl. Instrum. and Methods A* 429(1999)233
- [8] E. L. Saldin, E. A. Schneidmiller, and M. V. Yurkov, "The Physics of Free Electron Laser" (Springer, Berlin, 1999)
- [9] W. Brefeld et al., DESY Print TESLA-FEL 2001-02, Hamburg 2001
- [10] M. Dohlus, A. Kabel, and T. Limberg, *Nucl. Instrum. and Methods A* 445(2000)84

LINAC-Based Synchrotron Radiation Facility with Femtosecond Soft X-ray Pulses

W. Brefeld^a W. B. Faatz^a, J. Feldhaus^a, K. Floettmann^a,
M. Körfer^a, J. Krzywinski^b, T. Limberg^a, T. Möller^a, J. Pflueger^a,
J. Rossbach^a, E.L. Saldin^a, E.A. Schneidmiller^a, S. Schreiber^a and
M.V. Yurkov^c

^a*Deutsches Elektronen-Synchrotron (DESY), Notkestrasse 85, D-22607 Hamburg, Germany*

^b*Institute of Physics of the Polish Academy of Sciences, 02688 Warszawa, Poland*

^c*Joint Institute for Nuclear Research, Dubna, 141980 Moscow Region, Russia*

Abstract

In this paper we perform design consideration of a femtosecond linac-based synchrotron radiation facility. Proposed technique is based on the generation of energy chirped short electron bunches that would subsequently spontaneously radiate frequency chirped soft X-ray pulses in an undulator. These pulses are then spectrally dispersed using grazing incident grating. The spectrum is propagated through exit slit (spectral window) which filters the pulses of femtosecond duration. The shortest temporal structures (about 10 fs) are limited by the energy chirp and longitudinal emittance of the electron bunch, number of undulator periods, and resolution of monochromator. In this paper we analyze potential of the TESLA Test Facility (TTF) at DESY for construction of such a femtosecond X-ray facility.

1 Introduction

Phase transitions, surface processes, and chemical reactions are ultimately driven by the motion of atoms on the time scale of one vibration period ($\simeq 100$ fs). The pulse length of existing synchrotron sources is too long for resolving atomic motion on the 100 femtosecond time scale. Recent efforts at applying 300 fs X-rays pulses to probe structural dynamics have used a synchrotron radiation source combined with a femtosecond optical quantum laser [1]. The same technique can be used to generate in the future 100 fs X-ray pulses with an average brilliance of 10^{11} photons $\text{s}^{-1}\text{mrad}^{-2}\text{mm}^{-2}$ per 0.1 % BW at the photon energy of 2 keV [1].

New proposal of femtosecond soft X-ray facility, which is described in this paper, is based on frequency chirping of the undulator spontaneous radiation pulse.

Using spatial and spectral filtering we can reduce the duration of the synchrotron radiation pulse to about 10 fs. A correlated frequency distribution along the radiation pulse can be obtained by changing the electron energy along the electron bunch, i.e. chirping the electron bunch energy before it enters the undulator. The main ingredients of a femtosecond X-ray facility are a high energy electron beam with small longitudinal emittance. A small (close to diffraction limited) transverse emittance, is needed too.

In 1999 Pellegrini analyzed the possibility of producing femtosecond long pulses by chirping and compressing (in grating compressor) the output X-ray SASE FEL radiation [2]. In this paper we extend this approach for generation of short pulses of spontaneous radiation. This becomes possible due to application of an angular filter and use of grating monochromator.

In this paper we analyze a possibility for integration of femtosecond synchrotron radiation source into the TESLA Test Facility (TTF) being under construction at DESY. A 1 GeV superconducting linear accelerator at the TTF is capable to produce electron beam with high average and peak power, low energy spread and emittance. The main practical application of this accelerator is to use it for driving the soft X-ray SASE FEL [3]. TTF linac would be able to deliver up 500-700 MeV electron beam, prepared with properties to allow generation of fs soft X-ray pulse (with electron pulse duration 0.16 ps FWHM, energy chirp 1 %). The electron beam qualities required for fs facility operation (longitudinal emittance 10π keV-mm, normalized transverse emittance 2π mm-mrad, charge 0.1 nC) can be met with laser-driven rf-gun. After the exit of the undulator (number of periods $N_w \simeq 250$) the spontaneous undulator radiation enters the angular filter, which select power radiated in the central cone. After filter the frequency chirped soft X-ray pulse enters the monochromator with resolution $\Delta\omega/\omega \simeq N_w^{-1} \simeq 4 \times 10^{-3}$. It will provide radiation pulses with 30 fs (FWHM) duration. On the basis of the TTF linac parameters it should be possible to achieve an average brilliance of 10^{14} photons $s^{-1}mrad^{-2}mm^{-2}$ per 0.1 % BW in the photon energy range 50-200 eV. The average number photons at the monochromator exit (at monochromator efficiency 10 %) can exceed 10^5 photons within 30 fs pulse duration. The pulse duration can be tuned from 30 to 160 fs by changing the resolution of monochromator.

Here it is relevant to compare the technical challenges of linac-based soft X-ray SASE FEL and soft X-ray femtosecond synchrotron radiation source. Based on the requirements for a femtosecond synchrotron source, the design goal of rf photocathode gun is a 6-ps-(rms)-long beam of 0.1 nC charge with a normalized transverse rms emittance of 2π mm-mrad and longitudinal emittance 10π KeV-mm. Design goal for soft X-ray SASE FEL is a beam of 1 nC charge with the same emittances. Comparing the beam parameters we can conclude that to make preservation of the emittances in the case of the SASE FEL parameters is more difficult, since in our case the charge is about an order of magnitude smaller. The SASE process starts from spontaneous emission and grows exponentially along the undulator until saturation. Usually this occurs after about 10 exponential field gain

length. As a result, the output power of SASE FEL decreases drastically at the bunch charge decrease, or at the emittance growth. If we consider the femtosecond synchrotron radiation source, we find that the number of photons per pulse and time resolution evolve slowly with charge and emittance. This is a result of spontaneous emission.

2 Principle of operation

Let us introduce the basic features of undulator radiation. Note that for radiation within the cone of half angle

$$\theta_{\text{cen}} = \frac{\sqrt{1 + K^2/2}}{\gamma\sqrt{N_w}},$$

the relative spectral FWHM bandwidth is $\Delta\omega/\omega = 0.88/N_w$, where N_w is the number of undulator periods, K is undulator marameter, γ is relativistic factor. The photon flux within the central cone is given by

$$\frac{d N_{\text{cen}}}{d t} \simeq \frac{\pi\alpha A_{\text{JJ}}^2 K^2 N_e f}{1 + K^2/2},$$

Here $\alpha \simeq 1/137$ is fine-structure constant, N_e is the number of electrons in a bunch, f is the bunch repetition rate, $A_{\text{JJ}} = [J_0(Q) - J_1(Q)]$, where J_n is the Bessel function of n th order, and $Q = K^2/(4 + 2K^2)$.

Beyond the natural broadening, due to the finite number N_w of oscillations, further spectral broadening can be incurred with the passage of many electrons through the undulator in a bunch of finite size, divergence, and energy spread [4]. In what follows we use the following assumption:

$$4 \frac{\Delta E}{E} \ll \frac{1}{N_w}, \quad (\sigma')^2 \ll \frac{1 + K^2/2}{\gamma^2 N_w}, \quad (1)$$

where $\Delta\gamma/\gamma$ and σ' are the rms electron energy spread and rms angular divergence within the bunch, respectively. When these conditions are satisfied, the energy spread and angular divergence cause a spectral broadening less than $1/N_w$ and central cone will be rather well defined in terms of both its angular definition and spectrum.

The quality of the radiation source is described usually by the spectral brightness B defined as the density of photons in the six-dimensional phase space volume. Expression for B in terms of photon flux within the central cone is [4]:

$$B = \frac{(d N_{\text{cen}}/d t)(N_w/1000)}{4\pi^2(\sigma_{\text{tot}})_x(\sigma_{\text{tot}})_y(\sigma'_{\text{tot}})_x(\sigma'_{\text{tot}})_y} \frac{\text{photons/s}}{\text{mm}^2\text{mrad}^2(0.1\% \text{BW})}.$$

where $(\sigma_{\text{tot}})_{x,y}$ and $(\sigma'_{\text{tot}})_{x,y}$ are the (horizontal and vertical) photon beam Gaussian $(1/\sqrt{e})$ radius and Gaussian half angle respectively. Taking into account contribution of diffraction effects, we may write the following expressions for the size and angular divergence of the photon beam:

$$(\sigma_{\text{tot}})_{x,y}^2 = (\sigma_e)_{x,y}^2 + \sigma_d^2, \quad (\sigma'_{\text{tot}})_{x,y}^2 = (\sigma'_e)_{x,y}^2 + (\sigma'_d)^2,$$

where $\sigma_d = \sqrt{\lambda L_w / (4\pi)}$ is the diffraction limited radiation beam size, $\sigma'_d = \sqrt{\lambda / (4\pi L_w)}$ is the diffraction limited radiation beam divergence, and L_w is the undulator length. The particle beam parameters are

$$(\sigma_e)_{x,y}^2 = (\epsilon_e)_{x,y} \beta_{x,y}, \quad (\sigma'_e)_{x,y}^2 = (\epsilon_e)_{x,y} / \beta_{x,y},$$

where $\beta_{x,y}$ is the betatron function in the undulator, $\epsilon_{x,y}$ is the horizontal and vertical electron beam emittance, respectively.

The limiting condition of spatially coherent radiation is a space-angle product $d \cdot \theta = \lambda / (2\pi)$, where d is a Gaussian $1/\sqrt{e}$ diameter and θ is the Gaussian half angle [4]. In general case the phase space volume of photons in central radiation cone is larger than the limiting condition required for spatial coherence. Thus, for experiments that require spatial coherence, a pinhole and angular acceptance aperture are to be introduced. This pinhole spatial filter is used to narrow, or filter, the phase space of transmitted radiation. Filtering to $d \cdot \theta = \lambda / (2\pi)$ requires to use of both a small pinhole (d), and some limitation on θ , such that the product is equal to $\lambda / (2\pi)$.

Radiation is transversely coherent when

$$(\sigma_e)_{x,y} (\sigma'_e)_{xy} \ll \lambda / (4\pi), \quad \beta \simeq L_w.$$

Under this conditions, one has $(\sigma_{x,y})^2 \ll (\sigma_d)^2$ and $(\sigma'_{x,y})^2 \ll (\sigma'_d)^2$ and spectral-angular dependence of the radiation emitted by an electron beam can be approximated as spectral-angular dependence of the radiation emitted by a single electron. This limit corresponds to maximum of brilliance.

When the electron beam emittance is large, $(\sigma_e)_{x,y} (\sigma'_e)_{xy} \gg \lambda / (4\pi)$, the radiation is partially coherent. One can find that the influence of electron beam divergence on the properties of the undulator radiation can be neglected when the beta-function is large enough. In the region of parameters when $(\sigma'_{x,y})^2 < (\sigma'_d)^2$, a downstream diaphragm of aperture $d = 2\sigma_d$ is used for selection of the transversely coherent fraction of undulator radiation. Finally, in this limit, the flux of transversely coherent photons into the bandwidth $\Delta\omega/\omega = 0.1\%$ can be estimated simply as $d N_{\text{ph}} / dt \simeq \lambda^2 B / 4$.

The layout of the soft X-ray femtosecond facility is presented in Fig. 1. Soft X-ray pulse shortening is achieved in a two-step process sketched in Fig. 2. In the first step a frequency chirping is impressed on the radiation pulse which can be

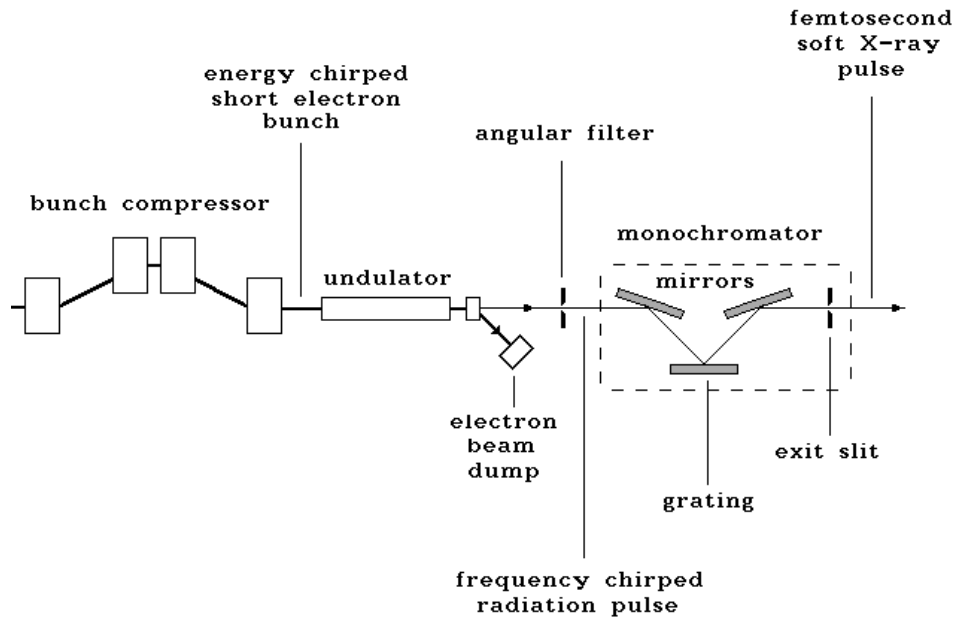


Fig. 1. Basic scheme of the soft X-ray femtosecond facility

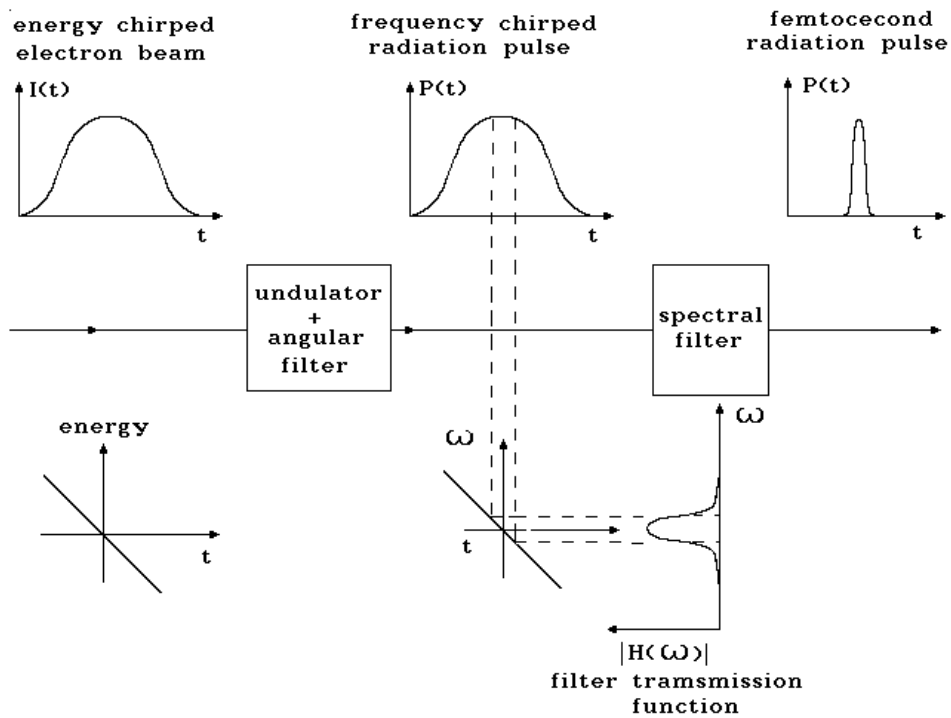


Fig. 2. Sketch of femtosecond soft X-ray pulse synthesis through frequency chirping and spectral filtering

obtained by changing the electron energy along the electron bunch, i.e. chirping the electron bunch energy before it enters the undulator. Optimum undulator performances obtained with small electron beam divergence and local energy spread (conditions (1) are fulfilled). The angular acceptance aperture is used for selection of the fraction of undulator radiation within the central cone. When this radiation is

partially coherent a downstream diaphragm is used for selection of the transversely coherent fraction of undulator radiation which is directed to the monochromator. The second step is the shortening (or shaping) through spectral filtering. This technique consists of manipulating the pulse spectrum. The pulse to be shortened is spectrally dispersed using grating. The spectrum is propagated through an exit slit which spectrally filters the pulse. The resolution of the monochromator is equal to $\Delta\omega_m$, the central frequency is equal to ω_0 and $\Delta\omega/\omega_0 < 1/N_w$. The shortest pulse durations $\Delta\tau$ that can be obtained are determined (at fixed number of undulator periods and under condition (1)) by the finite duration of the input pulse τ_0 (FWHM) and bunch energy chirp $\pm\delta E/E$: $\Delta\tau \simeq \tau_0/(4N_w\delta E/E)$. If there is an rms local energy spread ΔE within the bunch, the shortest pulse duration can be approximated by

$$\Delta\tau \simeq \tau_0 \sqrt{E^2/(4N_w\delta E)^2 + (\Delta E/\delta E)^2}. \quad (2)$$

3 Numerical example

The operation of linac-based femtosecond synchrotron radiation facility is illustrated for the TESLA Test Facility. Table 1 lists some of the basic parameters of the electron beam, undulator, monochromator, and output radiation. The radiation wavelength can be changed either by changing the electron beam energy and additionally by changing the undulator magnet gap. Fig. 1 illustrates how the technique is used to obtain spatially coherent radiation from the undulator. Only the angular acceptance aperture is introduced. The design value of the transverse emittance of the electron bunch in the TTF accelerator is small, so the spontaneous radiation within the central cone is transversely coherent at the wavelength 10 nm and longer and there is no need in an addition diaphragm. For undulator with 250 periods, a monochromator and beamline optics, with an overall efficiency η of 10 % (30 % grating efficiency and five glancing incidence mirrors at 0.8 reflectivity each) are used to obtain $\Delta\omega/\omega \simeq 4 \times 10^{-3}$. In this case we have $\delta E/E \simeq 1\%$ and $\Delta E/E \simeq 0.1\%$ and, according to (2), the minimum soft X-ray pulse duration reaches a value about 30 fs (FWHM). The average number of photons at the monochromator exit can exceed 10^5 photons per 30-fs duration pulse. An average brilliance would be about 10^{14} photons $s^{-1}mrad^{-2}mm^{-2}$ per 0.1 % BW. The femtosecond facility at TTF is designed to be tunable in the photon energy range 50-200 eV, corresponding to the 500-700 MeV electron energy and 0.2-0.5 T undulator field. Note that monochromator provides spatially and spectrally filtered radiation pulse.

The proposed phase bunching system is sketched in Fig. 3. Compressing the bunch will be done in stages to avoid space charge and coherent synchrotron radiation (CSR) and other wakefield effects limiting the achievable bunch length and transverse emittance. The first compression is from 1.6 mm to 400 μm (rms). It consists of a 150 MeV accelerating module followed by the first TTF magnetic chicane

Table 1

Parameters of the TTF linac-based femtosecond facility

<u>Electron beam</u>	
bunch energy, MeV	500 - 700
bunch charge, pC	100
rms local energy spread, %	0.1
rms incoming energy spread, %	1
final rms bunch length, μm	20
normalized emittance, π mm-mrad	2
number of bunches per train	7200
bunch spacing, ns	111
repetition rate, Hz	10
<u>Undulator</u>	
Type	planar
number of periods	250
period, cm	2.7
min. gap, mm	12
max. peak field, T	0.5
external beta-function, m	10
<u>Grating monochromator</u>	
resolution, %	0.4
efficiency, %	10
photon energy, nm	50 - 200
<u>Output radiation</u>	
photon energy, nm	50 - 200
min. pulse duration, fs (FWHM)	30
number of photons per pulse	10^5
spectrum width, % (FWHM)	0.4

generating R_{56} needed for bunch compression [5]. Calculations show that induced energy spread and emittance dilution should not be a serious limitation in BC1 at 100 pC bunch charge. After leaving the first bunch compressor the electron bunch of 400 μm length is accelerated in the next part of the TTF linac with an on-crest phase from 150 MeV to 500 MeV. For the second compression the required large correlated energy spread in the bunch of 5 MeV is induced by passing the last part of accelerating structure at 90° crossing phase. Our analysis shows that adequate solution for the BC2 design is a double chicane. The requirements for the magnetic bunch compressor in our case are very close to those for the magnetic bunch compressor BC2 in the Linac Coherent Light Source (LCLS) project [6]. Each chicane is twelve meters long and contains for a C-type bending magnets. Four quadrupoles are placed between the chicanes in locations where the dispersion passes through zero. Since the energy spread generated by CSR is correlated along the bunch, its effect on the transverse emittance can be compensated in a double chicane with optical symmetry to cancel the longitudinal-transverse coupling [6]. Calculations show a net BC2 emittance dilution of 2 % with CSR induced energy spread of 0.03 % (at 100 pC charge per bunch). Table 2 summarizes the proposed design parameters for BC2 providing bunch compression from 400 to 20 μm (rms).

Table 2
Parameters of the 2nd bunch compressor double chicane

Parameters	Symbol	Unit	Value
bunch energy	E	MeV	500
bunch charge	Q	pC	100
initial rms bunch length	σ_z	μm	400
final rms bunch length	σ_z	μm	20
rms incoming energy spread	$\delta E/E$	%	1
net momentum compaction	R_{56}	mm	34
total system length	L_{tot}	m	35
length of each dipole magnet	L_B	m	1.5
drift between 1st two (last two) dipoles	ΔL	m	3.4
drift between center two dipoles	ΔL_c	m	0.5
bend angle for each of 1st four dipoles	θ_{B1}	deg	3.4
bend angle for each of last four dipoles	θ_{B2}	deg	1.3
magnetic field for each of 1st four dipoles	H_1	G	660
magnetic field for each of last four dipoles	H_2	G	250
emittance dilution due to CSR	$\Delta\epsilon/\epsilon$	%	1.5
rms CSR energy spread	$\Delta E_{\text{CSR}}/E$	%	0.03

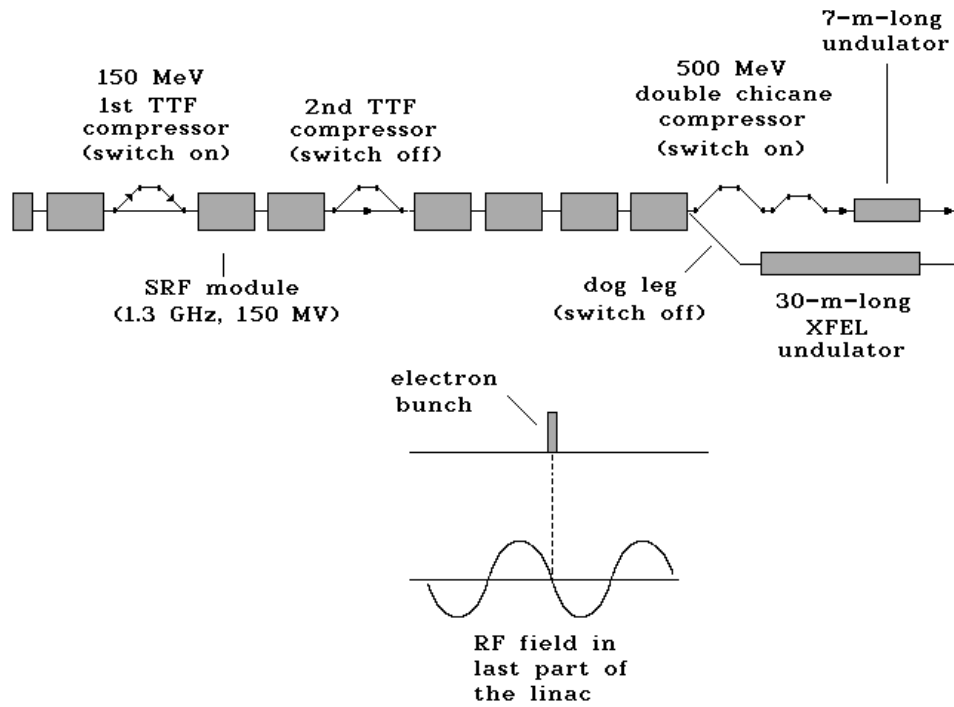


Fig. 3. TTF femtosecond facility compression and acceleration schematic

Acknowledgments

We thank J.R. Schneider and D. Trines for interest in this work.

References

- [1] R. W. Schoenlein et al., *Science* 287(2000)2237
- [2] C. Pellegrini, *Nucl. Instrum. and Methods A* 445(2000)124
- [3] J. Rossbach, *Nucl. Instrum. and Methods A* 375(1996)269
- [4] D. Attwood, "Soft X-ray and Extreme Ultraviolet Radiation" (Cambridge University Press, 1999)
- [5] M. Dohlus, A. Kabel, and T. Limberg, *Nucl. Instrum. and Methods A* 445(2000)84
- [6] The Linac Coherent Light Source (LCLS) Design Study Report, SLAC-R-521, 1998

Generation of High Power Femtosecond Pulses by Sideband-Seeded X-ray FEL

W. Brefeld^a, B. Faatz^a, J. Feldhaus^a, M. Körfer^a, J. Krzywinski^b,
T. Möller^a, J. Pflueger^a, J. Rossbach^a, E.L. Saldin^a,
E.A. Schneidmiller^a, S. Schreiber^a, and M.V. Yurkov^c

^a*Deutsches Elektronen-Synchrotron (DESY), Hamburg, Germany*

^b*Institute of Physics of the Polish Academy of Sciences, 02688 Warszawa, Poland*

^c*Joint Institute for Nuclear Research, Dubna, 141980 Moscow Region, Russia*

Abstract

New proposal of a fs X-ray facility, which is described in this paper, is based on the use of X-ray SASE FEL combined with a fs quantum laser. An ultrashort laser pulse is used for modulation of the energy and density of the electrons within a slice of the electron bunch at a frequency ω_{opt} . The density modulation exiting the modulator (energy-modulation undulator and dispersion section) is about 10%. Following the modulator the beam enters an X-ray SASE FEL undulator, and is bunched at a frequency ω_0 . This leads to an amplitude modulation of the beam density at the sidebands $\omega_0 \pm \omega_{\text{opt}}$. The sideband density modulation takes place at the part of the electron pulse defined by the duration of the seed laser pulse that is much shorter than the electron pulse. Following the SASE FEL undulator the beam and SASE radiation enter undulator section (radiator) which is resonant at the frequency $\omega_0 - \omega_{\text{opt}}$. Because the beam has a large component of bunching at the sideband, coherent emission is copiously produced within fs slice of the electron bunch. Separation of the sideband frequency from the central frequency by a monochromator is used to distinguish the fs pulses from the sub-ps intense SASE pulses.

1 Introduction

In this paper we propose sideband seeded X-ray SASE FEL capable to produce femtosecond pulses (see Figs. 1, 2). An ultrashort laser pulse is used to modulate the density of electrons within a femtosecond slice of the electron bunch at a frequency ω_{opt} . We begin the FEL operation by positioning the interaction region on the electron bunch. The seed laser pulse will be timed to overlap with central area of the electron bunch. This ultrashort laser pulse serves as a seed for modulator which consists of an uniform (energy-modulation) undulator and a dispersion section. The

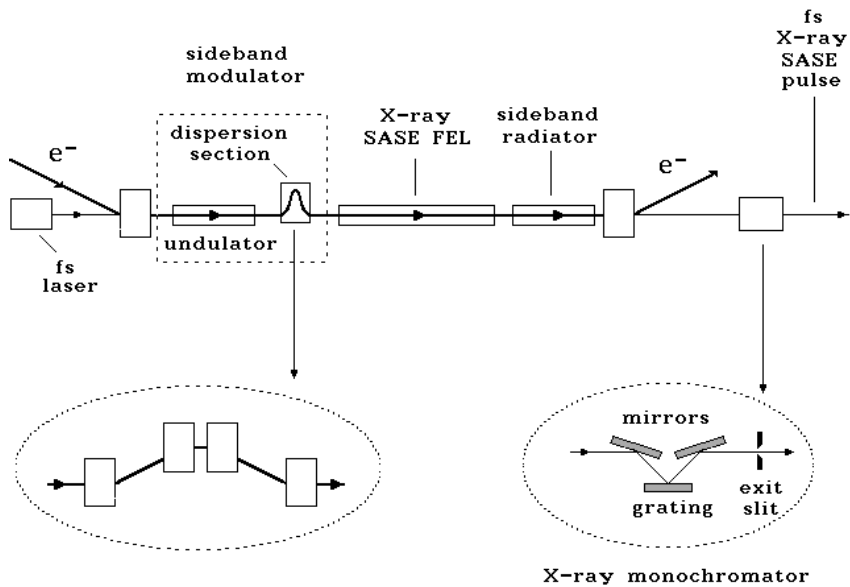


Fig. 1. Basic scheme of a sideband seeded SASE FEL

density modulation has the form

$$A_0 [1 + M \cos(\omega_{opt}t + c)] \cos(\omega_0t + d)$$

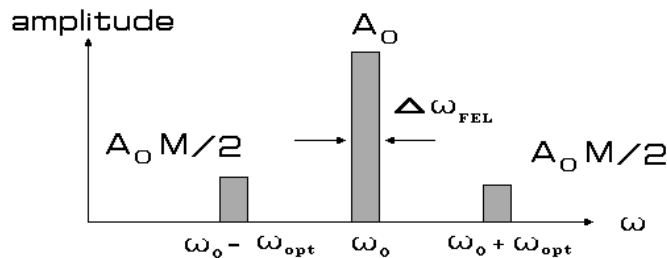
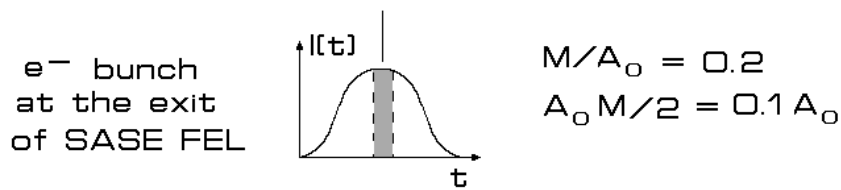


Fig. 2. Description of the sideband generation for the case of the density modulation as initial conditions.

interaction of seed pulse with the electron beam produces an energy modulation at ω_{opt} .

This energy modulation is converted into a spatial bunching in the dispersion section. Density modulation at the modulator exit is about 10%. The energy modulation, introduced by the modulator, is smaller than the initial energy spread. Following the modulator the beam and seed radiation enter SASE undulator which is

resonant with X-ray radiation at frequency ω_0 . The process of amplification of the radiation in the X-ray undulator develops in the same way as in the conventional SASE FEL: fluctuations of the electron beam current density serve as the input signal. The seeding optical radiation does not interact with the electron beam in the X-ray undulator and is diffracted out of the electron beam. By the time the beam is bunched in the SASE FEL undulator at frequency ω_0 , the X-ray radiation power has reached saturation. This leads to amplitude modulation of density at the sidebands ($\omega_0 \pm \omega_{\text{opt}}$). The sideband density modulation takes place only at that part of the electron bunch defined by the length of the seed laser pulse that is much shorter than the electron bunch. Following the SASE FEL undulator the beam and X-ray radiation enter undulator section (radiator) which is resonant with the $\omega_0 - \omega_{\text{opt}}$ radiation. Because the beam has a relatively large component of bunching at the long wavelength sideband, coherent emission at $\omega_0 - \omega_{\text{opt}}$ is copiously produced within femtosecond slice of electron bunch. After leaving the radiator the electron beam is deflected onto a beam dump, while the photon beam enters the monochromator, which selects fs soft X-ray pulse.

In this paper we analyze a possibility for integration of proposed femtosecond facility into the soft X-ray SASE FEL being under construction at the TESLA Test Facility at DESY [1]. On the basis of the parameters of TTF SASE FEL and laser pulses of 25 fs duration and 6 μJ energy at a repetition rate of 10 kHz (from a Ti:sapphire laser system), it should be possible to achieve an average brilliance of 10^{22} photons $\text{s}^{-1}\text{mrad}^{-2}\text{mm}^{-2}$ per 0.1 % BW in the photon energy range 25-100 eV. The femtosecond SASE FEL will provide soft X-ray pulses with 30 fs (FWHM) duration. The number of photons at the monochromator exit (at monochromator efficiency 10%) can exceed 10^{11} per pulse which is by three orders of magnitude above the background. This creates perfect conditions for experiments. It is important to notice that the proposed femtosecond option of SASE FEL at the TTF is an additional to a fully functioning SASE FEL improving the output radiation beam properties considerably and thus extending the range of possible applications.

2 General description of femtosecond X-ray FEL option at TTF

The main goal of the present study has been to design a femtosecond soft X-ray facility which is compatible with the layout of the TTF and the soft X-ray FEL being under construction at DESY. Figures 3 illustrate how the proposed femtosecond facility fits the TTF FEL layout. This design makes use of the spent electron beam leaving the SASE FEL. An additional facility to be installed is a sideband modulator and sideband radiator. The sideband modulator is located in front of main undulator and consists of 0.4 m long undulator (magnetic period length $\lambda_w = 7.5$ cm, the maximum value of magnetic field is $H_w = 0.7$ T) and 0.5 m long dispersion section (chicane consisting of permanent magnets). The sideband radiator is located after the main undulator and consists of one or two 4.5 m standard TTF undulator modules ($\lambda_w = 2.73$ cm, $H_w = 0.51$ T) tuned to the sideband frequency. In this con-

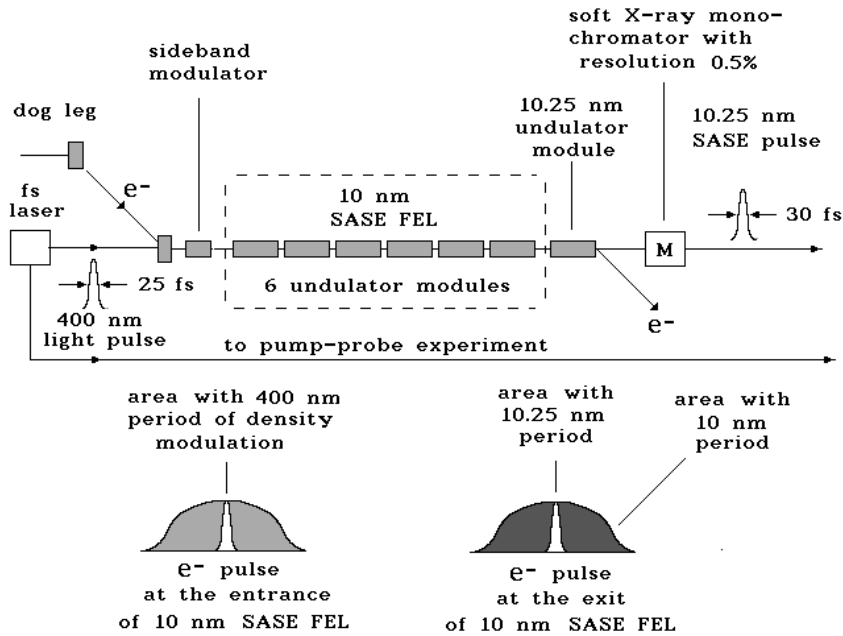


Fig. 3. Schematic layout of the femtosecond pump-probe facility which fits with soft X-ray SASE FEL

ceptual design we assume to use a Ti:sapphire laser system as a seed laser, which provides at 400 nm wavelength (the 800 nm pulses will be doubled to 400 nm in a frequency conversion crystal) a train of 30 fs pulses with $6 \mu\text{J}$ optical energy per pulse, at 10 kHz repetition rate. The installation of the femtosecond seeding system is greatly facilitated by the fact that present design of the SASE FEL at TTF provides required free space for the input optical elements and sideband modulator.

The sideband seeded SASE FEL operates as follows (to be specific, we consider the case of 10 nm SASE FEL). The seed laser pulse is timed to overlap with central area of electron bunch. This ultrashort laser pulse interacts with the electron beam in the short modulator undulator, which is tuned to be resonant to 400 nm. The resulting energy modulation (about 0.5 MeV) is then converted to spatial bunching while the electron beam traverses a dispersion section (a three-dipole chicane). Density modulation at the chicane exit is about 20%. Following the modulator the beam and seed radiation enter SASE undulator which is resonant with X-ray radiation at 10 nm. The process of amplification of the radiation in the 10 nm undulator develops in the same way as in the conventional SASE FEL: fluctuations of the electron beam current density serve as the input signal. The 400 nm seeding optical radiation does not interact with the electron beam in the 10 nm undulator and is diffracted out of the electron beam. By the time the beam is bunched in the SASE FEL undulator at 10 nm, the X-ray radiation power has reached GW level. This leads to amplitude modulation of density at the sidebands $10 \pm 0.25 \text{ nm}$ (see Fig 2). The sideband density modulation takes place at the 30 fs part of the electron pulse, defined by the duration of the seed laser pulse that is much shorter than electron pulse (400 fs FWHM). When this coherently bunched beam enters the sideband radiator undulator there is a rapid coherent generation of 10.25 nm radiation. For

Table 1

Parameters of the sideband modulator

<u>Undulator</u>	
Type	planar
number of periods	5
period, cm	7.5
peak field, T	0.7
external beta-function, m	1.7
<u>Seed laser</u>	
wavelength, nm	400
min. pulse duration, fs (FWHM)	25
energy per pulse, μ J	6
spectrum width	transform limited
rep. rate, kHz	10

an optical wavelength 400 nm, the peak-to-sideband separation has a value of 2.5% . Monochromator with resolution 0.5% located at the end of beamline provides a means for selecting radiation originating from different frequency regions of radiation spectrum. Because the SASE FEL bandwidth (about 0.5 % FWHM) is much less than the separation of the sidebands from the main peak, we obtain clean fs pulse after the monochromator.

The wavelength of femtosecond soft X-ray pulses can be tuned continuously in a wide range. At fixed gaps of the modulator undulator and the sideband radiator undulator the tunability of the output radiation is provided by changing simultaneously the electron energy and the wavelength of the seed laser. In this case the sideband radiator undulator is a version of the standard TTF FEL undulator module with the peak magnetic field on axis a few per cent larger comparing with the main undulator. An additional possibility of variable gap modulator undulator and radiator undulator would allow to increase further the tunability of output radiation from the sideband seeded SASE FEL. Application of both methods (variable gap modulator and radiator undulator and tunable seed laser) would allow to cover the wavelength range of the sideband seeded SASE FEL at TTF from 40 to down 10 nm.

The synchronization of the optical laser with the electron pulses to within 200 fs is the most challenging task of this proposal. The main problem is the time jitter (± 1 ps) of electron and seed laser pulses. The jitter of electron pulses originates in the photoinjector laser system (laser pulse jitter) and in the magnetic bunch compressors (from predicted $\pm 0.1\%$ electron bunch energy jitter). Due to this uncertainty not every femtosecond optical pulse will produce femtosecond X-ray pulse. The predicted probability of positioning the interaction region on the electron bunch is about 10% only. Random production of femtosecond soft X-ray pulses needs to be controlled. Separation of the sideband frequency from the central frequency can be used to distinguish the 30-fs pulses from the intense 200-fs SASE pulses. I.e.,

Table 2

Parameters of the sideband-seeded X-ray SASE FEL

<u>Radiator undulator</u>	
Type	planar
number of periods	150
period, cm	2.73
peak field, T	0.51
external beta-function, m	1.7
<u>Output radiation after monochromator</u>	
wavelength, nm	10-40
min. pulse duration, fs (FWHM)	30
number of photons per pulse	10^{11}
spectrum width, % (FWHM)	0.5

appearing of X-ray pulse at the sideband frequency will indicate that the seed optical pulse is overlapped with the central part of the electron bunch. Moreover, this also indicates that the seed optical pulse and output fs X-ray pulse are synchronized with an accuracy better than 30 fs.

Pump probe techniques which are commonly used with optical lasers, are highly desirable in order to make full use of the femtosecond soft X-ray pulses. Since in this case precise timing is needed with a jitter of less than 30 fs, we suggest to combine the femtosecond soft X-ray pulses with optical pulses generated in the seed laser system. It should be emphasized that in proposed scheme femtosecond X-ray pulse is naturally synchronized with his femtosecond optical pulse and cancel jitter.

Tables 1–2 list some of the basic parameters of the undulators, seed laser system, monochromator and output radiation. For fs facility at TTF, a monochromator and beamline optics, with an overall efficiency of 10 % (30 % grating efficiency and five glancing incidence mirrors at 0.8 reflectivity each) can be used to obtain resolution $\Delta\omega/\omega = 0.5\%$. The femtosecond SASE FEL will provide soft X-ray pulses with 30 fs (FWHM) duration. The average number photons at the monochromator exit can exceed 10^{11} photon/pulse. The femtosecond facility at TTF is designed to be tunable in the photon energy range 25-100 eV. Analysis of the practical limit for the achievable pulse duration has shown that the output X-ray pulse duration is limited by the optical pulse duration. A practical limit for achievable pulse duration of Ti:sapphire laser system is about 10 fs.

3 FEL Physics and Simulations

From the very beginning of this section we combine all the conditions sufficient for the effective operation of a fs SASE FEL. During the passage through a long main SASE undulator the electron density modulation at optical wavelength can be suppressed by energy spread in the electron beam. For effective operation of

the fs FEL energy spread suppression factor should be close to unity. This leads to following condition:

$$\langle (\Delta\mathcal{E})^2 \rangle L_{(2)}^2 \omega_{\text{opt}}^2 / (2c^2 \gamma_l^4 \mathcal{E}_0^2) \ll 1 .$$

where $\sqrt{\langle (\Delta\mathcal{E})^2 \rangle}$ is the standard energy deviation, $\gamma_l = \gamma / (1 + K_{(2)}^2 / 2)^{1/2}$ is the longitudinal relativistic factor, $K_{(2)}$ and $L_{(2)}$ is the undulator parameter and undulator length, respectively, the subscript (2) refers to the main undulator. The chosen parameters for the SASE FEL and the seed laser system satisfy this condition, and to make preservation of the beam density modulation in the case of the TTF SASE

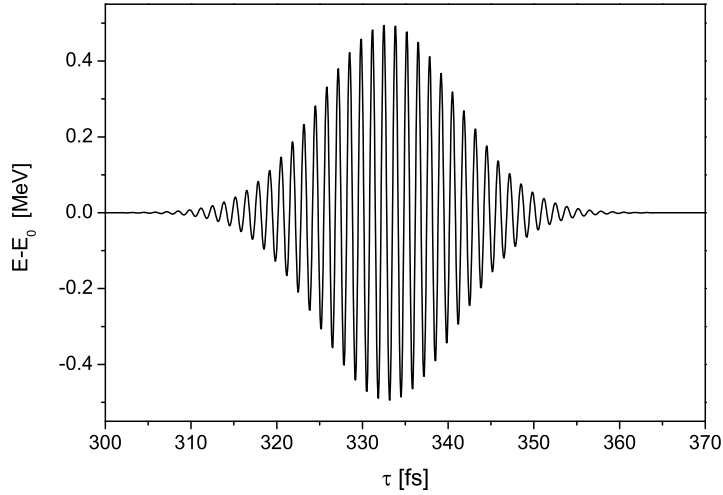


Fig. 4. Energy modulation of the electron beam at the exit of the modulator undulator.

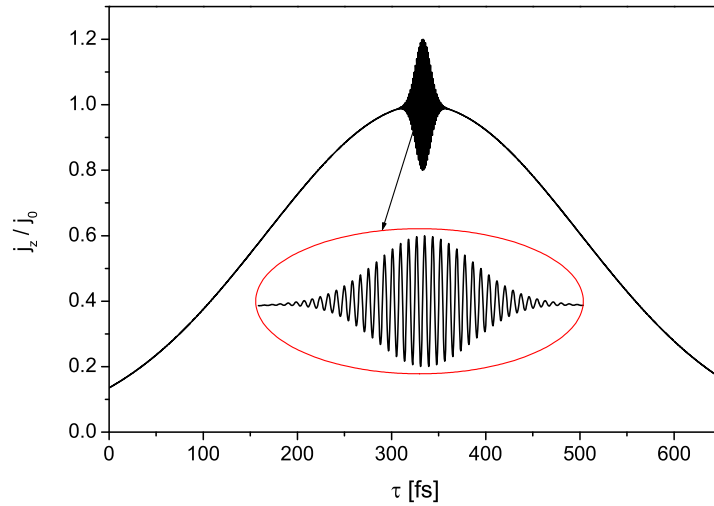


Fig. 5. Density modulation of the electron beam at the exit of the dispersion section.

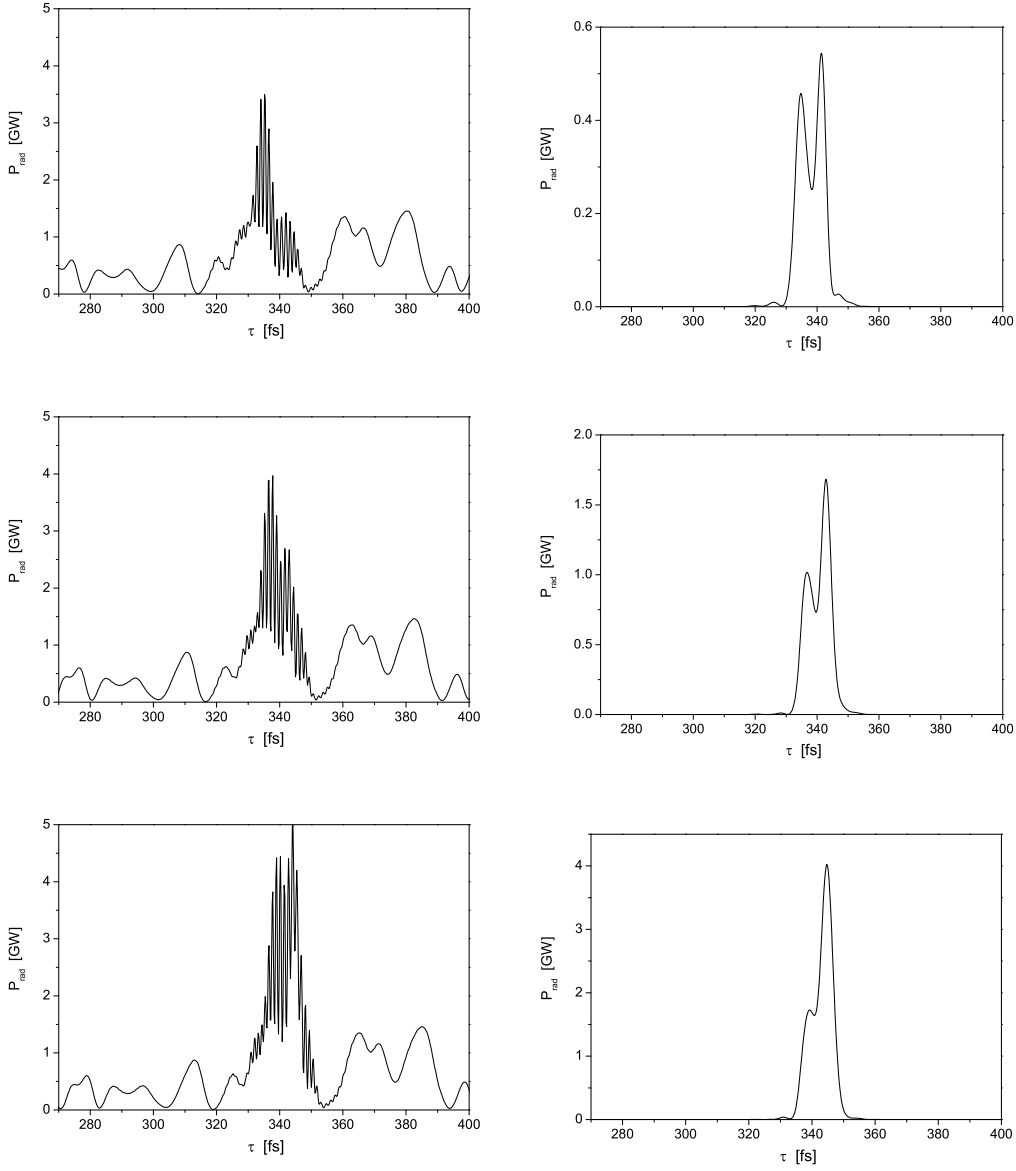


Fig. 6. Evolution of the radiation pulse in the radiator undulator. In the left plots we present total pulse, and in the right plots – spectrally filtered at the sideband. The length of the radiator undulator is equal to 3, 4 and 5 m for upper, middle and lower plots, respectively.

FEL parameters is possible.

In what follows we use the following assumptions: $\omega_0 \gg \omega_{\text{opt}} \gg \Delta\omega_{\text{SASE}}$. We also assume that $\Delta\omega_{\text{SASE}} \gg 1/\tau_{\text{opt}} \gg 1/\tau_e$. Here τ_{opt} and τ_e is the seed optical pulse and electron pulse duration, respectively. Such assumptions do not reduce significantly the practical applicability of the result obtained. Let us consider the first condition. It is obvious that the parameter $\omega_{\text{opt}}/\omega_0$ is much less than unity for X-ray SASE FEL. We also assume that the SASE bandwidth is much less than the separation of the sidebands from the main peak. This requirement is of a critical

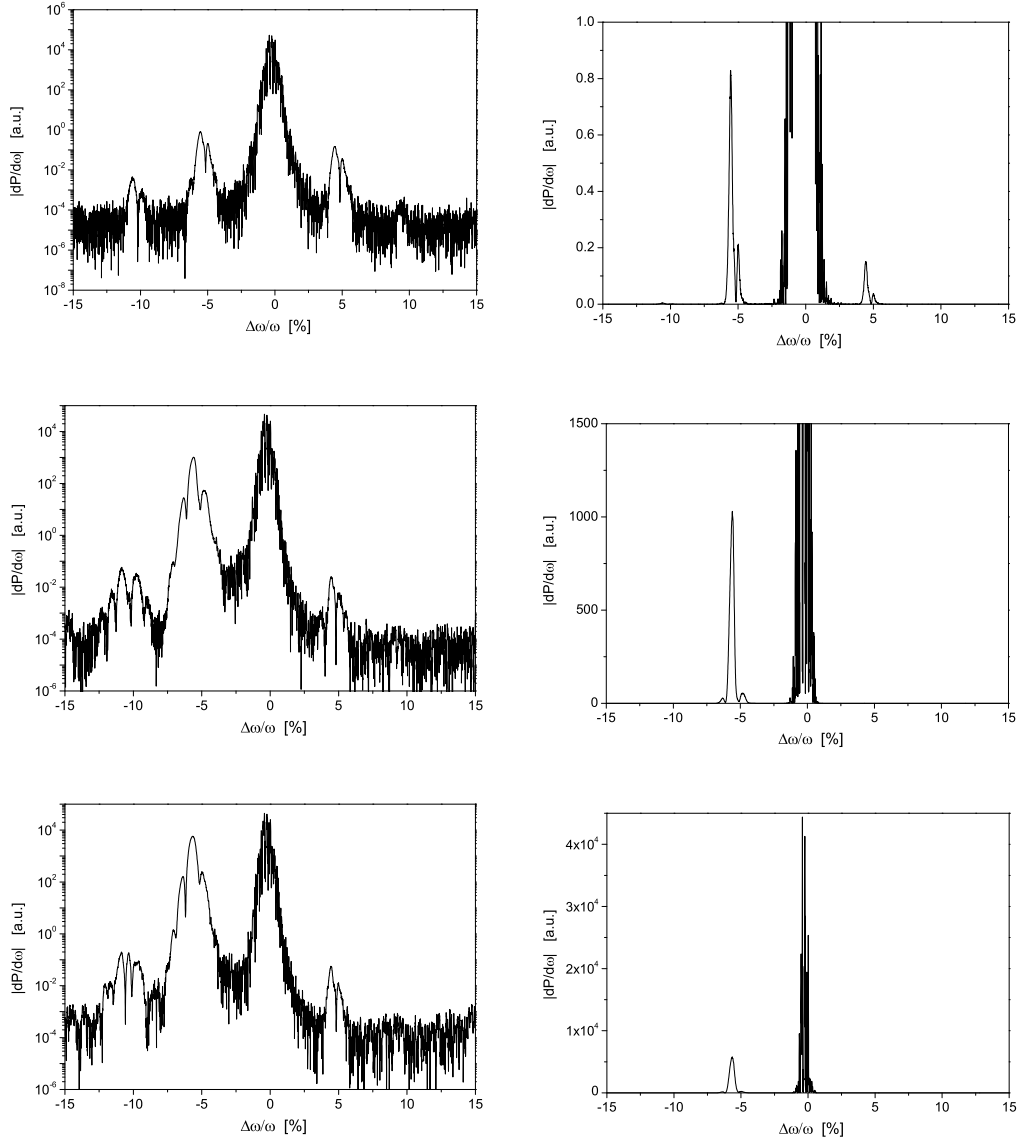


Fig. 7. Evolution of the spectral distribution of the output radiation power in the radiator undulator. In the left plots we present spectrum in logarithmic scale, and in the right plots – in the linear scale. The length of the radiator undulator is equal to 0, 3 and 5 m for upper, middle and lower plots, respectively.

importance to the overall performance of the fs SASE FEL. In this case, monochromator can be used to distinguish the fs pulses from the intense SASE pulses. The present study assumes wavelength of seed light to be very long compared to the SASE radiation wavelength. Under this limitation we neglect the gradient of density and energy within the SASE radiation wavelength at the entrance of main undulator. Due to this reason it is also convenient to describe effect of the energy and density modulation not by energy-phase distribution function, but by periodical bunch profile and periodically correlated energy spread. The physical interpretation of approximation $\Delta\omega_{\text{SASE}}/\omega_{\text{opt}} \ll 1$ is that the slippage of the radiation with

respect to the electrons per gain length (in the SASE FEL) is much longer than the seed laser wavelength. Let us consider the second condition. It is obvious that the fs FEL has advantage over conventional SASE FEL only when electron bunch is much longer than the seed laser pulse. The physical interpretation of condition $\Delta\omega_{\text{SASE}} \gg 1/\tau_{\text{opt}}$ is that the optical pulse is much longer than the slippage of the radiation with respect to the electrons at one gain length.

We illustrate operation of a fs option of FEL for parameters of the TTF FEL operating at the wavelength of 20 nm. Parameters of the optical laser are: wavelength 400 nm, energy in the laser pulse 6 μJ , and FWHM pulse duration 25 fs. The laser beam is focused onto the electron beam in a short (five periods) undulator resonant at the optical wavelength of 400 nm. Optimal conditions of focusing correspond to the positioning of the laser beam waist in the center of the undulator. The size of the laser beam waist is twice as large than the electron beam size. Due to the resonant interaction of the electron beam with optical field in the undulator the electron beam is modulated in the energy as it is shown in Fig. 4. Upon leaving the modulator the electron beam passes the dispersion section, is modulated additionally in the density (see Fig. 5), and is directed to an X-ray undulator.

Parameter optimization have been preformed with three-dimensional, time-dependent code FAST [2] taking into account all physical effects influencing the FEL amplifier operation (diffraction effects, energy spread, emittance, slippage effect, etc). In [3] we discussed the modification of code FAST required to carry out the calculations of the sideband generation. The results of optimized configuration of 20 nm sideband-seeded option of SASE FEL at the TESLA Test Facility are summarized in Table 3. Initial conditions for the seeded sideband have been fixed with general case, i.e. the slice of the electron bunch is modulated in energy and in density at the entrance to the X-ray undulator (see Figs.. 4 and 5). Optimal length of the main undulator is given by the condition of maximum spectral purity of the sideband. In the case under study optimal length of the main undulator should is equal to 10 m. Figures 6 and 7 show the evolution of the fs radiation pulse and the spectral distribution of the output radiation power in the sideband radiator. Analysis of the spikes of the complete radiation pulse (plots in the left column of Fig. 6) shows that the radiation, produced in the main undulator, does not interact with the electron beam. Only that slice of the electron bunch, seeded by the sideband, produces the radiation. Cut structure of the spikes of the central part of the beam is due to the interference of the radiation from the main undulator with frequency ω and from the sideband radiator with frequency $\omega - \omega_{\text{opt}}$. After 5 m long sideband radiator the radiation power in fs pulse rapidly reaches the level of a few GW, and the energy in the fs pulse reaches the value of about 30 μJ . Total undulator length of the sideband seeded SASE FEL is about 15 meters.

In conclusion to this section we should note that calculations of the radiation power have been performed for the case of an ideal monochromator. In the wavelength range of 10–40 nm the monochromator efficiency is about 10 per cent only, so the radiation power available for user experiments is roughly by one order of

magnitude less than that shown in Figs. 6 and 7.

Acknowledgments

We thank J.R. Schneider and D. Trines for their interest in this work.

References

- [1] J. Rossbach, Nucl. Instrum. and Methods A 375(1996)269
- [2] E. L. Saldin, E. A. Schneidmiller and M. V. Yurkov, Nucl. Instrum. and Methods A 429(1999)233
- [3] W. Brefeld et al., DESY-print 01-63(2001)

Electro–optic experiments at the TESLA Test Facility

M. Brunken^{a *}, H. Genz^a, C. Heßler^a, M. Hüning^b, H. Loos^{a†}, A. Richter^a, P. Schmüser^b, S. Simrock^b, M. Tonutti^c and D. Türke^c

^aInstitute of Nuclear Physics, Darmstadt University of Technology, Schlossgartenstr. 9, D-64289 Darmstadt, Germany

^bDESY, Notkestr. 85, D-22607, Hamburg, Germany

^cIII. Department of Physics, RWTH Aachen, D-52056 Aachen, Germany

Several experiments are planned at the TESLA Test Facility using electro-optic sampling for determining the temporal profile of the electron bunches with a resolution in the 100 fs regime. In the first step coherent transition radiation in the THz range will be utilized to compare the direct (time-domain) determination of the longitudinal bunch structure with the interferometric (frequency domain) method. In the next step the electro–optic sensor will be mounted inside the beam vacuum chamber for probing the Coulomb field carried by the bunch. A 15 fs Ti:Sa laser will be used to probe the bunch field by differential optical gating. The high bandwidth (60 nm) of the laser permits also single bunch measurements by using linearly chirped laser pulses. The experimental setup is described and first results are presented on the synchronization of the Ti:Sa laser, running at 81 MHz repetition rate, to the 1300 MHz RF frequency of the linac.

1. INTRODUCTION

The TTF Free Electron Laser currently achieves wave lengths below 100 nm and will soon be extended into the soft X ray regime. To achieve the high peak currents needed in the SASE process the electron bunches must be compressed to sub-picosecond length, hence an ultrafast diagnostics is needed. The technique of electro–optic sampling (EOS) [1] offers this possibility: the time profile of picosecond THz radiation pulses can be determined by passing them through a non-linear optical crystal like ZnTe where they induce a birefringence proportional to the electric field. This birefringence is then sampled with a polarized femtosecond laser pulse. In an electron linac the THz pulse can come either from coherent transition radiation or from the Coulomb field co-moving with the relativistic bunch [2]. Non-destructive bunch length measurements are possible by using a diffraction radiation screen with a central slit for beam passage or by placing the ZnTe crystal directly into the beam pipe at a few mm dis-

tance from the axis. The synchronization between the bunches and the ultrashort laser pulses is a challenge which can be greatly relieved by applying a linear chirp of 5 – 10 ps to the probe laser pulse. The resulting time–frequency correlation allows to encode the time-varying electric field of the relativistic bunch into the frequency-dependent elliptical polarization of the chirped laser pulse which can be recovered by a diffraction grating and a CCD camera. It has been recently demonstrated at the FELIX that this method allows single shot measurements of high resolution [3].

2. EXPERIMENTAL SETUP

The experimental setup used for the first tests is located behind the TTF undulator. Coherent diffraction radiation (0.1 – 1 THz) from an aluminized screen with a central slit is passed through a wire grid splitting it into two polarization components. One of these enters a Martin–Puplett interferometer while the other is focused onto a 0.1 mm thick $\langle 110 \rangle$ ZnTe crystal. The pulses from a 15 fs Ti:Sa laser [4] are guided through the ZnTe crystal parallel to the THz pulse. The remaining part of the experiment resembles closely the standard setup for electro–optic sam-

*Supported by the Graduiertenkolleg 'Physik und Technik von Beschleunigern' (DFG GRK 410/2) and DESY, Hamburg

†Present address: Brookhaven National Laboratory, Upton, N.Y 11973

pling in THz spectroscopy [1] and will not be described in this short note.

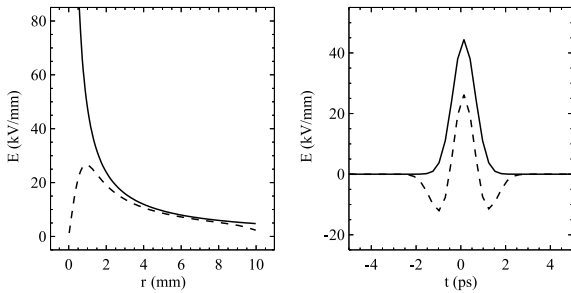


Figure 1. Radial electric field strengths of transition radiation and from the relativistic Coulomb field. The transverse distribution is shown in the left part and the temporal one in the right part for 1 mm distance to the symmetry axis.

For an estimation of the electro-optic effect in ZnTe the strength of the electric fields must be known. The radial fields, computed for an electron energy of 230 MeV, a bunch charge of 1 nC, and an rms bunch length of 0.5 ps, are plotted in fig. 2. The peak electric field amounts to 24 kV/mm for transition radiation in the image plane of the transport telescope and to 8 kV/mm for the Coulomb field at 10 mm distance to the electron beam. The resulting phase difference between the ordinary and extraordinary laser ray for a 100 μ m long ZnTe crystal is 0.3 rad and 0.1 rad, respectively.

The laser is mounted on an vibration-damped optical table outside the accelerator building. The optical transport is actively stabilized with a piezo-controlled mirror and restricts the positional jitter of the laser beam on the ZnTe-crystal to less than 10% of the beam diameter.

Due to the low repetition rate of the electron bunches in TTF (1 MHz) the synchronization with the Ti:Sa pulses (81 MHz) is a demanding task. In a first step the 16th harmonic of the laser repetition frequency is synchronized to the 1.3 GHz frequency of the linac by means of a phase locked loop. The measured phase jitter is plotted in fig. 2. The rms time jitter derived from this measurement amounts to 0.75 ps. This value is sufficiently small to provide a good temporal overlap between a chirped laser pulse

and the THz signal from the bunched electron beam. It may even allow to apply the principle of differential optical gating [5].

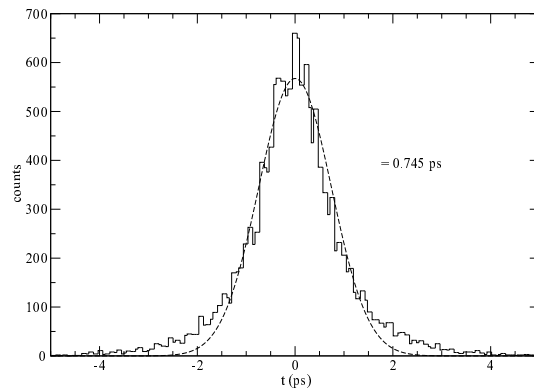


Figure 2. Measured phase jitter of Ti:Sa laser with respect to 1.3 GHz linac frequency.

The authors wish to thank G.M.H. Knippels, D. Oepts and I. Wilke for valuable advice.

REFERENCES

1. Q. Wu, X.-C. Zhang, Appl. Phys. Lett. 70 (1997) 1784.
2. X. Yan, A.M. MacLeod, W.A. Gillespie, G.H.M. Knippels, D. Oepts, A.F.G. van der Meer, W. Seidel, Phys. Rev. Lett. 85 (2000) 3404.
3. I. Wilke, A.M. McLeod, W.A. Gillespie, G. Berden, G. H. M. Knippels, A. F. G. van der Meer, these proceedings
4. Femtosource Compact 20, manufactured by Femtolasers, Vienna. Pumplaser: Coherent Verdi 5W
5. C.W. Rella, G.M.H. Knippels, D.V. Palanker, H. A. Schwettman, Opt. Comm. 157 (1998) 335.

Use of micro-channel plate for nondestructive measurement of VUV radiation from the SASE FEL at the TESLA Test Facility

B. Faatz^a, A.A. Fateev^b, J. Feldhaus^a, C. Gerth^a, U. Hahn^a,
U. Jastrow^a, M. Jurek^c, J. Krzywinski,^c N.I. Lebedev^b,
M. Meschkat^a, V.A. Petrov^b, T.V. Rukoyatkina^b, E.L. Saldin^a,
E.A. Schneidmiller^a, S.N. Sedykh^b, V.S. Shvetsov^b, W. Sobala^d,
K.P. Sytchev^b, V.V. Tarasov^b, K. Tiedtke^a, R. Treusch,^a
M.V. Yurkov^b

^a*Deutsches Elektronen Synchrotron (DESY), 22607 Hamburg, Germany*

^b*Joint Institute for Nuclear Research, Dubna, 141980 Moscow Region, Russia*

^c*IP PAS, Warszawa, Poland*

^d*Institute of Nuclear Physics, Cracow, Poland*

Abstract

In this paper we describe the radiation detector for a nondestructive measurement of VUV radiation. Detector consists of a thin gold wire scattering tiny fraction of the SASE FEL radiation onto a micro-channel plate (MCP). Such a simple system meets all the requirements for the VUV radiation detector. Its dynamic range for intensity measurements covers up to eight orders of magnitude which ideally fits the operating range of a SASE FEL. The described detector is used in the RAFEL experiment being under preparation at the TESLA Test Facility at DESY.

1 Introduction

The Regenerative FEL Amplifier (RAFEL) project [1,2] is under development at the DESY TESLA Test Facility. Realization of this project will allow to increase the brilliance of the output radiation by two orders of magnitude with respect to single-pass scheme and obtain the light source with laser-like characteristics. This becomes possible due to installation of narrow-band optical feedback system in the high-gain FEL amplifier. The base of the optical feedback system at TTF is equal to 66.5 m (half the distance between two electron bunches when the accelerator is operated in a 2.25 MHz multibunch mode). Layout of RAFEL at TTF is shown

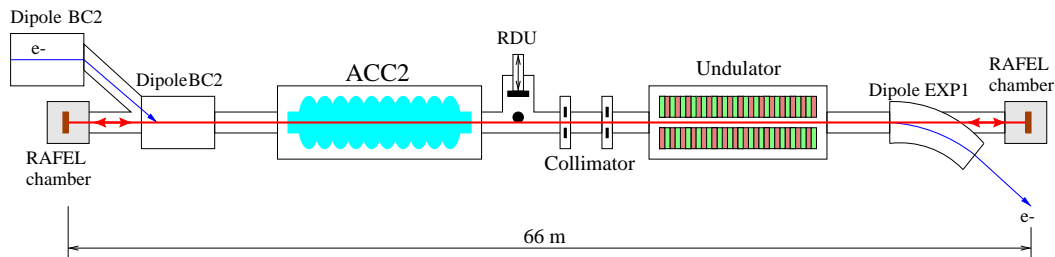


Fig. 1. Layout of the regenerative FEL amplifier at the TESLA Test Facility

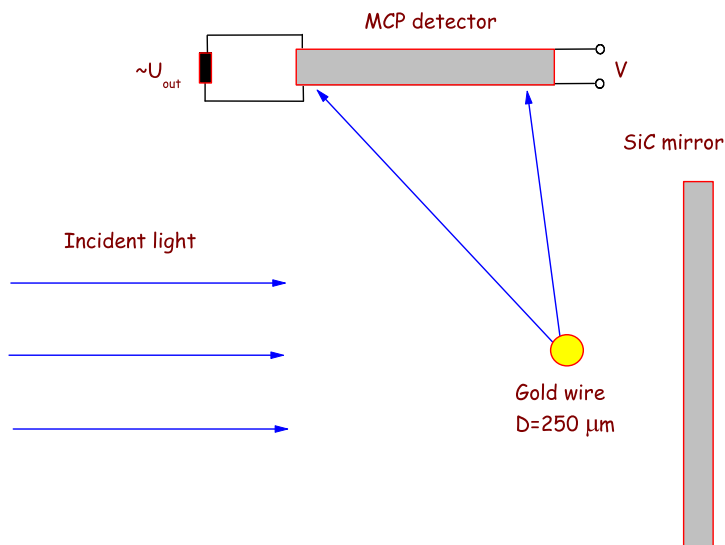


Fig. 2. Scheme of non-destructive radiation detector

in Fig. 1. The RAFEL operates as follows. The first bunch in a train of up to 1800 bunches amplifies shot noise and produces intense, but wide-band radiation. A fraction of the radiation is back-reflected by a mirror. The spherical grating in Littrow mounting which is installed in a straight section in the electron bunch compression area between the first and the second accelerator module, disperses the light and focuses a narrow band of radiation back on the entrance of the undulator to seed next electron pulse. After several round-trips output radiation spectrum approaches transform-limited width and output power reaches saturation level.

Specific features of the TTF FEL do not allow us to use its photon diagnostic system for monitoring an optical beam at operation in the RAFEL mode which forced us to develop compact, nondestructive diagnostics of VUV radiation. At the moment such diagnostics has been developed and successfully tested at TTF FEL.

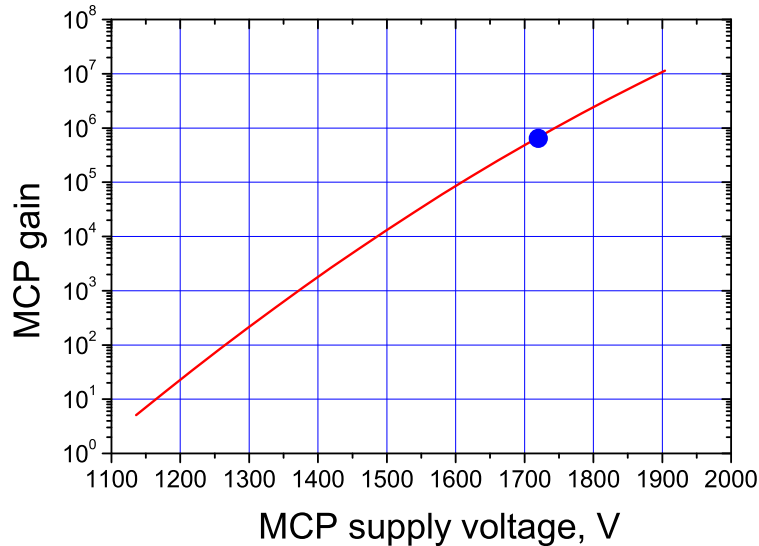


Fig. 3. MCP gain versus applied voltage. The circle is a reference point corresponding to intensity of spontaneous radiation from TTF FEL undulator at 1 nC and energy of 230 MeV

2 Principle of operation

Principle of nondestructive optical beam monitoring is illustrated in Fig. 2. A thin (0.25 mm in diameter) gold wire is installed in front of each optical element (mirror or grating). A tiny fraction of the incident radiation is reflected in transverse direction and detected by a micro-channel plate (MCP). The MCP consists of a large number of thin conductive glass capillaries which work as an independent secondary-electron multipliers and form a two-dimensional secondary-electron multiplier as a whole. We use the MCP of F4655-type manufactured by the Hamamatsu Corporation. These device is directly sensitive to UV/VUV radiation with high detection efficiency. The MCP amplification coefficient can be easily tuned in a wide range by changing power supply voltage which is applied to MCP assembly. These features make an MCP a perfect detector for monitoring VUV radiation generated by TTF FEL.

Specific feature of MCP is nonlinear dependence of the gain on the voltage applied, so special efforts have been directed for calibration procedure (manufacturer of MCP does not provide the calibration characteristics with required accuracy). Calibration of MCP gain has been performed directly at the TTF with VUV incoherent radiation from the TTF FEL undulator. The stability of this source is mainly given by fluctuations of the bunch charge and was about 5% rms during calibration run. Time duration of one radiation pulse is about one picosecond. The intensity of radiation was changed by means of changing the bunch charge and inserting of diaphragms with different aperture between the TTF FEL undulator and diagnostic chamber. Local gain characteristics were measured at different levels of radiation

intensities and then general gain curve was reconstructed in a wide range of MCP power supply voltages. An absolute setting of MCP gain was performed in the regime of single photon detection. In the region of lower power supply voltages these data were supplemented with similar measurements performed by means of Xe flash lamp. The gain curve outside calibrated region was extrapolated from experimental points. General gain characteristic of MCP-based detector is shown in Fig. 3. It is seen that detector is capable to monitor the radiation in the whole range of SASE FEL operation up to saturation level (between six and seven orders of magnitude with respect to the level of spontaneous emission). The circle at the gain curve in Fig. 3 is a reference point corresponding to the energy of the radiation pulse of spontaneous radiation from TTF FEL undulator (about 1 nJ within coherent angle) at the bunch charge of 1 nC and energy of 230 MeV. Such absolute calibration gives us the possibility for absolute measurements of the radiation energy in the radiation pulses.

3 Experimental results

The MCP-based photon detectors are installed in both RAFEL chambers and are in operation at the TTF FEL during one year. Our experience shows that at normal operating regime of the accelerator the background (electron beam and dark current losses) almost does not disturb signal which allows us to monitor very low levels of VUV radiation intensities. For example, we can detect simultaneously the

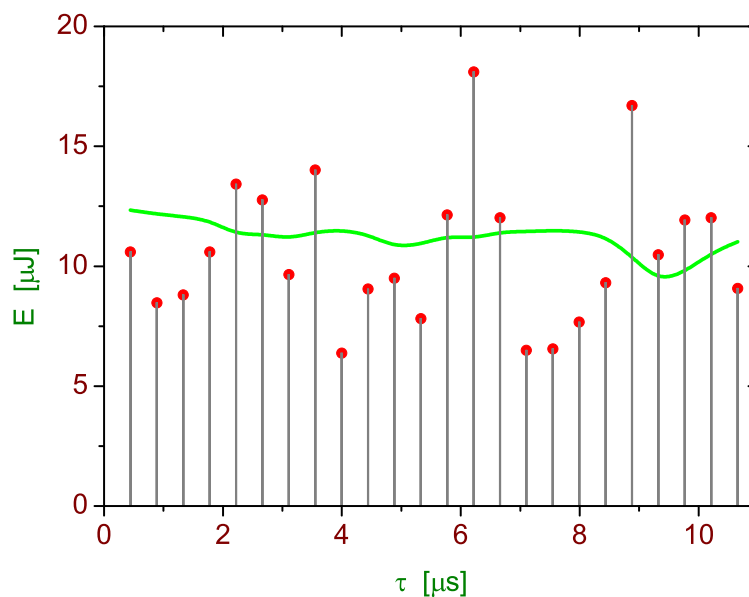


Fig. 4. On-line monitoring of the radiation at TTF FEL. The circles represent a train of radiation pulses produced by TTF FEL. Solid curve is average over many macropulses.



Fig. 5. Photo of radiation detector unit installed at the TTF accelerator

direct SASE radiation pulse from undulator and the same pulse passed complete round-trip in the optical feedback system of the RAFEL [2]. This is very effective tool for final alignment of optical elements of the RAFEL. Our experience also shows that use of MCP-based detector significantly simplifies tuning the SASE regime, since it detects reliably very small increase of the radiation intensity at a level of a few per cent at normalization of the signal to the bunch charge.

At the moment MCP-based detector installed downstream the undulator is routinely used for on-line monitoring of SASE FEL radiation and allows one to measure the energy of individual radiation pulses. Figure 4 illustrates typical macropulse of the TTF FEL operation at 2.25 MHz. The relative accuracy of these measurements is better than 5%. One should not wonder that large fluctuations of the bunch-to-bunch radiation energy occur. These is intrinsic property of the single-pass FEL amplifier starting from shot noise. The use of such a precise tool as MCP-based radiation detector gave us the possibility to perform precise study of statistical properties of the SASE FEL radiation [3].

During last shutdown we installed an additional radiation detector unit (RDU) in front of the undulator (see Fig. 5). The purpose of this detector is alignment and monitoring the seeding radiation pulse at the undulator entrance. This unit also uses thin reflecting wire and MCP detector. The wire is placed horizontally and is movable in vertical direction within ± 20 mm with respect to the axis of the accelerator. With this device we can measure simultaneously signals corresponding to the electron beam pulse, radiation pulse propagating from the mirror at the undulator exit to the grating, and the seeding pulse reflected from grating. This becomes possible be-

cause all these pulses are separated in time. Scanning with a wire gives us averaged spot size and positions of the electron beam and the radiation pulses. Background conditions at the location of RDU are quite moderate for performing precise measurements. One of the results is first experimental verification of the fundamental feature of the SASE FEL radiation: fluctuations of the radiation intensity after the narrow-band monochromator follows negative exponential distribution [3].

Acknowledgments

From the side of JINR and IP the work has been funded by the grant program of the special purpose use of the Polish contribution to JINR. We thank I.N. Meshkov, J.R. Schneider, D. Trines and A. Wagner for interest in this work and support. We thank all staff of the TESLA Test Facility for fruitful collaboration and help in solving technical problems.

References

- [1] B. Faatz et al., Nucl. Instrum. and Methods **A429**(1999)424
- [2] B. Faatz et al., "Alignment of the optical feedback system of VUV Regenerative FEL Amplifier at the TESLA Test Facility at DESY", Presentation at FEL2001 Conference
- [3] M.V. Yurkov for TTF FEL Team, "Statistical properties of SASE FEL radiation: experimental results from VUV FEL at the TESLA Test Facility at DESY", Presentation at FEL2001 Conference

Alignment of the optical feedback system of VUV Regenerative FEL Amplifier at the TESLA Test Facility at DESY

B. Faatz^a, A.A. Fateev^b, J. Feldhaus^a, C. Gerth^a, U. Hahn^a,
U. Jastrow^a, J. Krzywinski^c, N.I. Lebedev^b, J. Lewellen^d,
L. Malkinski^c, M. Meschkat^a, V.A. Petrov^b, J. Rossbach^a,
T.V. Rukoyatkina^b, E.L. Saldin^a, E.A. Schneidmiller^a,
S. Schreiber^a, S.N. Sedykh^b, V.S. Shvetsov^b, R. Sobierajski^c,
K.P. Sytchev^b, V.V. Tarasov^b, K. Tiedtke^a, R. Treusch^a,
M.V. Yurkov^b

^a*Deutsches Elektronen-Synchrotron (DESY), Hamburg, Germany*

^b*Joint Institute for Nuclear Research, Dubna, 141980 Moscow Region, Russia*

^c*Institute of Physics PAS, Warszawa, Poland*

^d*Argonne National Laboratory, USA*

Abstract

In this paper we describe optical feedback system of VUV Regenerative FEL Amplifier (RAFEL) at the TESLA Test Facility at DESY. The aim of the RAFEL experiment is to construct fully coherent, tunable VUV radiation source by means of applying narrow-band optical feedback in the VUV SASE FEL operating currently at DESY. One of the problem of the realization of the RAFEL is severe requirements for the angular stability of the optical elements (about few microradians). This problem has been solved by means of installation of active alignment system with reference laser. Another problem is alignment of optical elements separated by 65 meters within complicated experimental conditions connected with aperture limitations (down to 6 mm). This problem has been solved in two steps. Preliminary alignment with an accuracy of about 80 microradians has been performed with laser alignment system and OTR screens used at the TTF accelerator for electron beam diagnostics. Final alignment has been performed with VUV SASE FEL radiation. Measured feedback coefficient is about 1 per cent and is in agreement with designed value.

1 Introduction

A VUV/soft X-ray SASE FEL (self amplified spontaneous emission free electron laser) is being under construction at the TESLA Test Facility at DESY [1,2]. At the moment Phase I of the TTF FEL facility is in operation continuously covering wavelength range between 80 and 180 nm [3,4]. Despite SASE FEL is capable to provide much higher peak brilliance than synchrotron radiation sources, it still possesses a high potential for its further increase. Mainly brilliance of the output radiation from the SASE FEL is limited by poor longitudinal coherence of the radiation: it consists of a large number of statistically independent wavepackets. This is natural consequence of the start-up from shot noise of the FEL amplification process. An improvement of the longitudinal coherence is possible only when coherent radiation from external source is fed to the undulator entrance. The power of the seed radiation must exceed significantly effective power of shot noise in the electron beam in order to obtain fully coherent radiation at the exit of the FEL amplifier. One of the solutions of the seeding problem exploits an approach of regenerative FEL amplifier [5] with narrow band optical feedback [6]. Our previous studies have shown that RAFEL might be an ideal source of powerful, tunable, fully coherent UV/VUV radiation with laser-like characteristics. Expected parameters of RAFEL option of RAFEL at the TESLA Test Facility at DESY are presented in Table 1.

Table 1
VUV Regenerative FEL amplifier at DESY

<u>Electron beam</u>	
Energy	180-260 MeV
Charge per bunch	1 nC
Peak current	500 A
Bunch separation	444 ns
<u>Undulator</u>	
Period	2.73 cm
Peak magnetic field	0.497 T
<u>Feedback system</u>	
Distance between mirrors	66.4 m
Monochromator resolution	5×10^{-5}
Total transmission	5×10^{-4}
<u>Radiation</u>	
Wavelength	80-140 nm
Micropulse duration (RMS)	500 fs
Peak output power	300 MW
Average power	up to 25 W

2 Facility description

General layout of RAFEL option at the TESLA Test Facility is shown in Fig. 1. The installation of the feedback is greatly facilitated by the fact that there is free space available for the optical components at exactly half the distance between two electron bunches when the accelerator is operated in a 2.25 MHz multibunch mode. The optical system consists of a mirror and a grating. Because one can use optical components with good reflectivity near normal incidence, SiC appears to be particularly well suited for the energy range of the Phase I facility. This material has excellent thermal properties such that surface distortions by the average absorbed power are negligible. A simple, far too pessimistic estimate shows that the high peak power should also

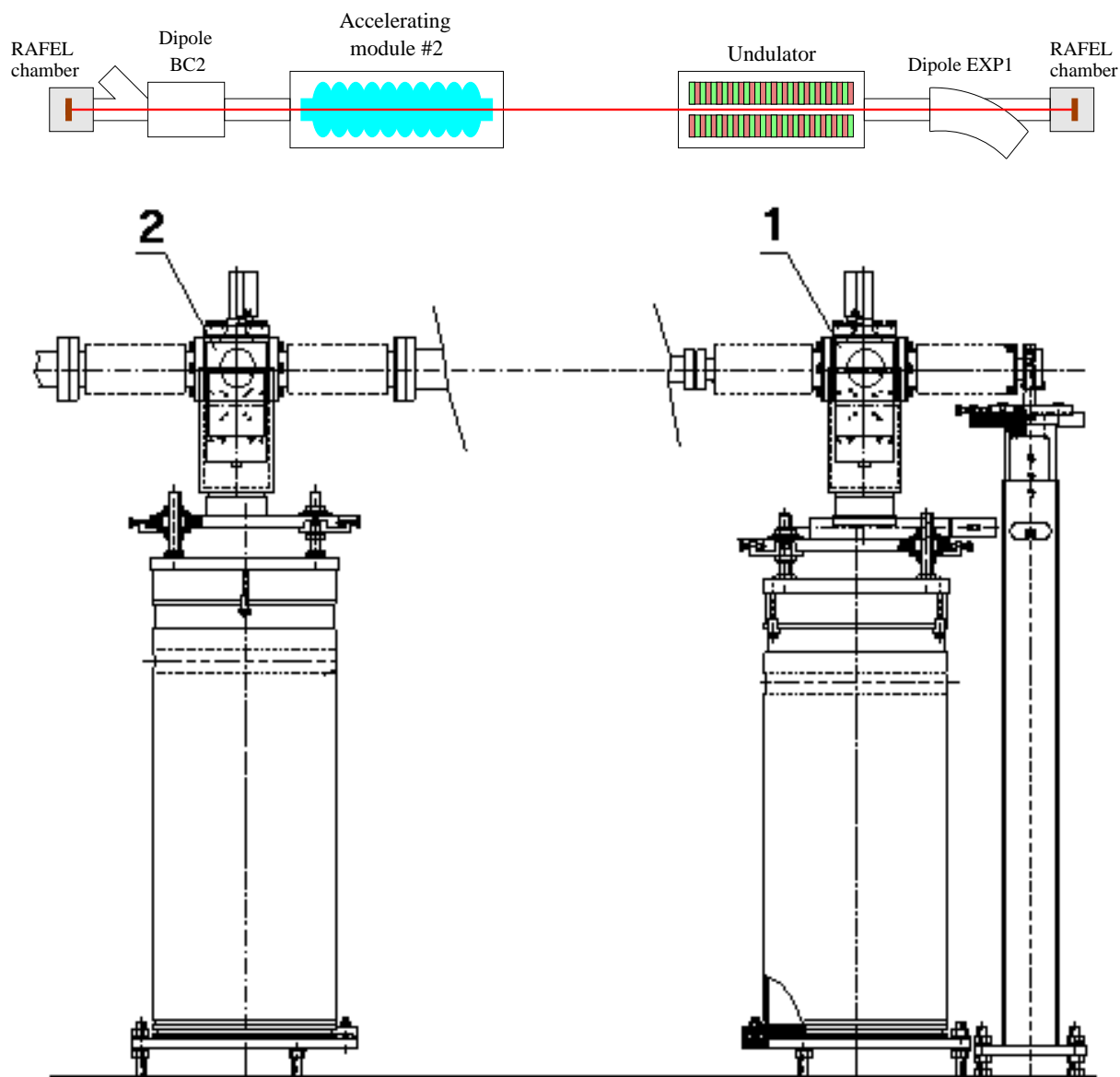


Fig. 1. General layout of regenerative FEL amplifier at the TESLA Test Facility. Here 1 is mirror assembly, and 2 is grating assembly

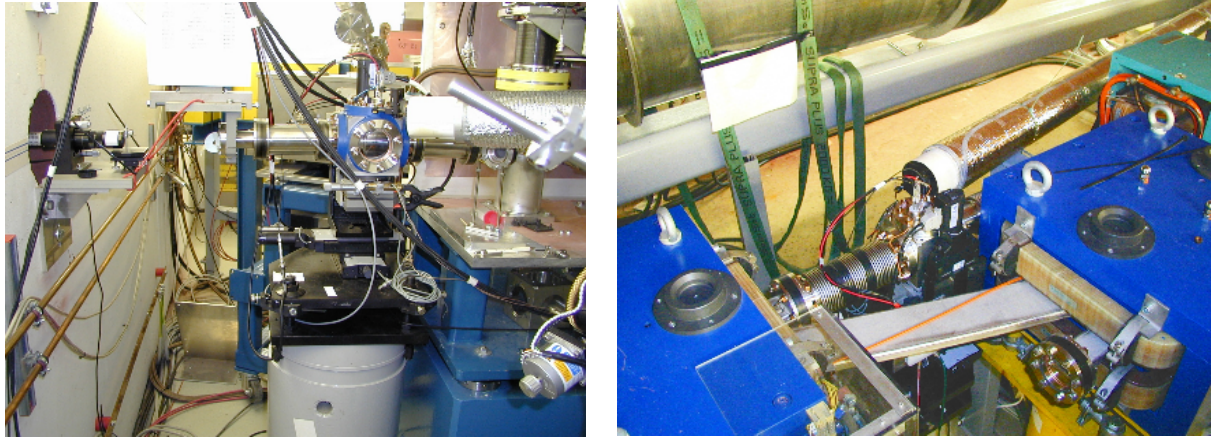


Fig. 2. Mirror (left) and grating (right) assembly mounted at the TTF accelerator

not pose a serious problem. If the energy absorbed per pulse were transformed into heat within the same absorption volume, the temperature would increase by about 1000 K — far too little to cause laser ablation.

The RAFEL at the TESLA Test Facility operates as follows. The first bunch in a train of up to 1800 bunches amplifies shot noise and produces intense, but wide-band radiation. A fraction of the radiation is back-reflected by a plane SiC mirror. The spherical grating in Littrow mounting which is installed in a straight section in the electron bunch compression area between the first and the second accelerator module, disperses the light and focuses a narrow band of radiation back on the entrance of the undulator.

At present all RAFEL equipment is installed at the TTF accelerator. It consists of three elements: mirror assembly (installed 14 meters downstream the undulator), grating assembly (installed in the bunch compressor area, 35 meters upstream the undulator), and radiation detector unit (installed 6 meters upstream the undulator). Figures 1 and 2 show the mirror and the grating assembly at TTF accelerator. Each assembly consists of a vacuum chamber, a set of translators and a rigid support. The optical elements (mirrors and gratings) are fixed firmly inside the vacuum chambers. The tuning of the optical elements is provided by means of translation of the whole vacuum chamber. The chambers are installed on the translators having sufficient number of degrees of freedom.

The vacuum chambers have similar design. A plane SiC mirror and radiation detectors (MCP and photodiode) are mounted inside the vacuum chamber of the mirror assembly. Tiny fraction of radiation is scattered to the detectors by a thin gold wire or wire grid, thus providing the possibility of non-destructive monitoring. The following elements are mounted inside the vacuum chamber of the grating assembly: a curved SiC mirror, curved grating, an optical prism, and radiation detectors. The design of the grating vacuum chamber allows one to move all the elements out of the beam axis, thus providing sufficient aperture for the electron beam transport in the mode of the TTF Linac operation without bunch compressor 2 (BC2). Each vacuum chamber has a viewport for laser pre-alignment of the optical elements. During recent shutdown we installed additionally non-destructive monitor of the radiation in front of the undulator [7] which allows us to detect position of the light beam and to measure the spectrum of

the radiation.

In order to minimize effort and risk, the optical system has been simplified as much as possible, particularly in order to facilitate the alignment and stability of the system at a distance of 66.4 m between mirror and grating. Each assembly is equipped with an active laser alignment system for stabilization of angular position of the vacuum chambers similar to that used at Duke University [8]. The active alignment system provides accuracy of measurements of angle deviations of a fraction of microradians. Special efforts were directed to avoid mechanical resonances in order to keep oscillation amplitudes around a microradian level (see Fig. 3).

3 Alignment of the RAFEL components

3.1 Suppression of angular oscillations

One of the problems for RAFEL design was that of tight requirements for stability of optical elements. The distance from the grating assembly to the undulator entrance is of about 35 meters. The spot size of the radiation at the undulator entrance is of about 1 mm, and the transverse size of the electron beam is of about 0.1-0.2 mm. Transverse space jitter of the electron bunches and transverse walk of the optical pulse position at the undulator entrance will lead to the reduction of their overlap and degradation of RAFEL operation. Tolerance for the off-axis walk of the optical pulse is of about 0.2 mm, or about 5 microradians for angular stability of optical elements. Angular motion of the optical elements consists of two contributions. The first one are broad-band and relatively fast oscillations excited by industrial noise in the tunnel. Figure 3 shows the time structure and probability distribution of fast oscillations. It is seen that they are within tolerable limit. Long-term observations have shown that fast oscillations occur on the top of slow variation of average angular position with typical time scale of few hours. Slow angular deviations are caused mainly by temperature variations inside the tunnel and ground motion,

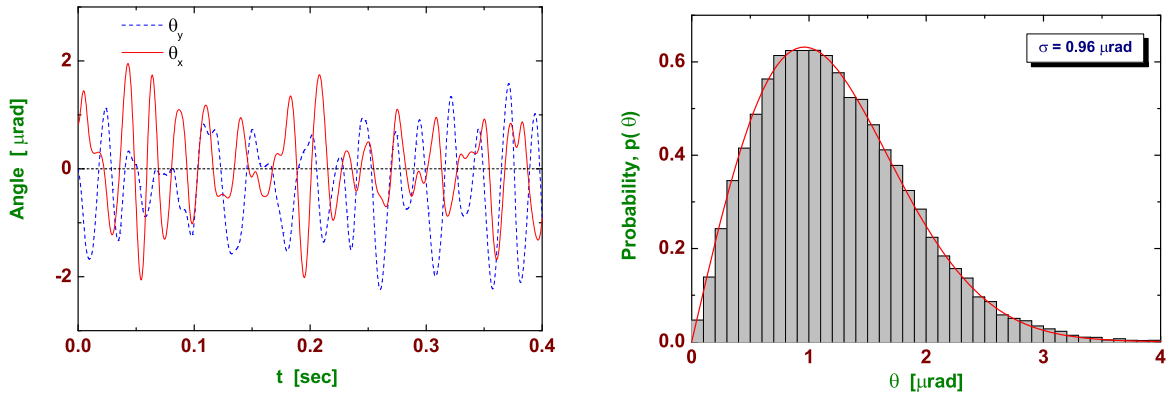


Fig. 3. Angular oscillations of the grating chamber (left) and probability distribution of the angle deviation (right). Solid line on the right plot presents Rayleigh probability distribution with $\sigma = 0.96 \mu\text{rad}$

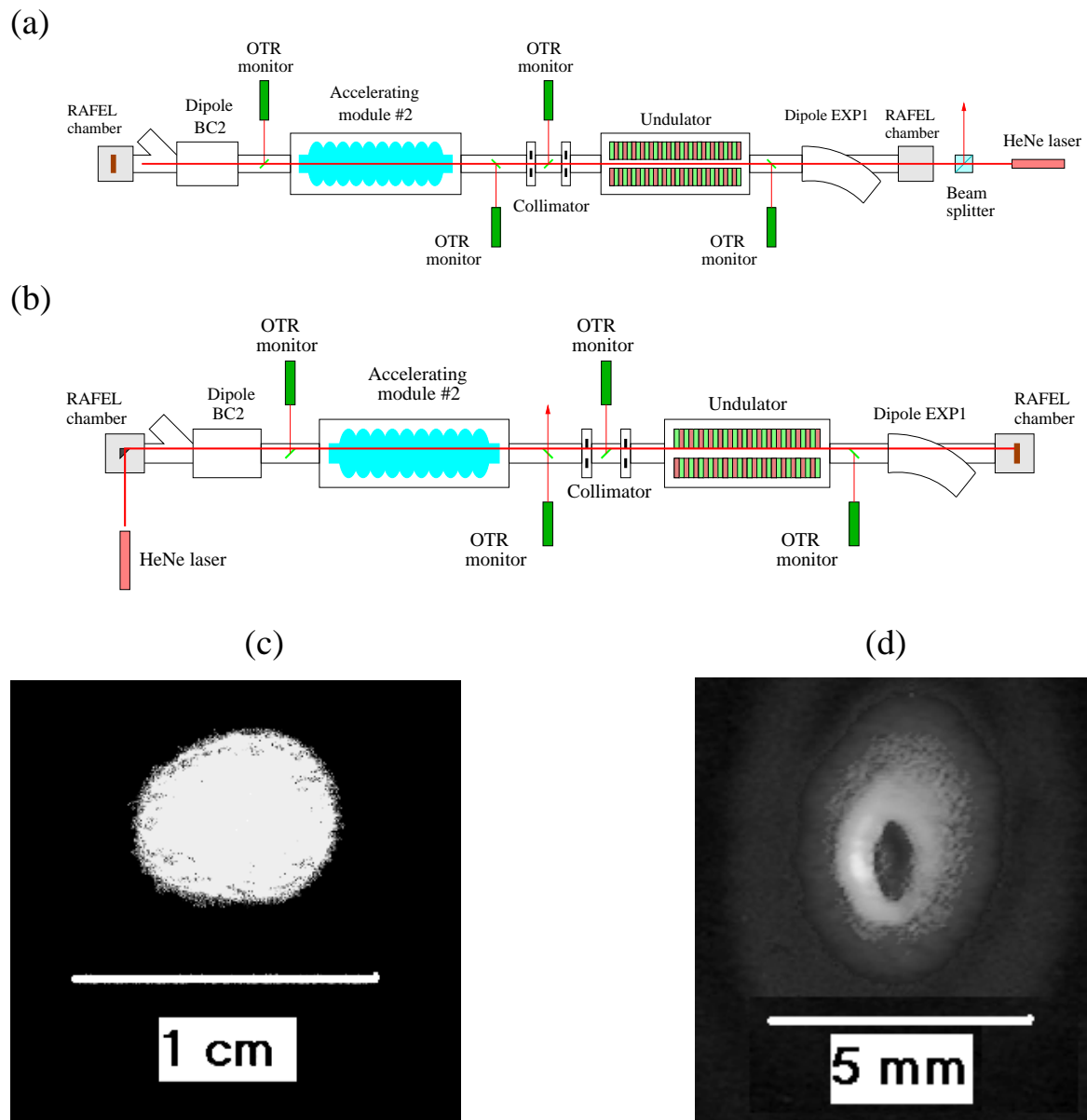


Fig. 4. Laser pre-alignment of RAFEL optical elements. Plots (a) and (c) refer to alignment of elements in the grating assembly, and plots (b) and (d) illustrate alignment procedure of elements in the mirror assembly

and may reach the value of about few tens of microradians. This slow walk is suppressed by the active laser alignment system mentioned above. As a result, RAFEL elements are kept stabilized with an accuracy better than 5 microradians.

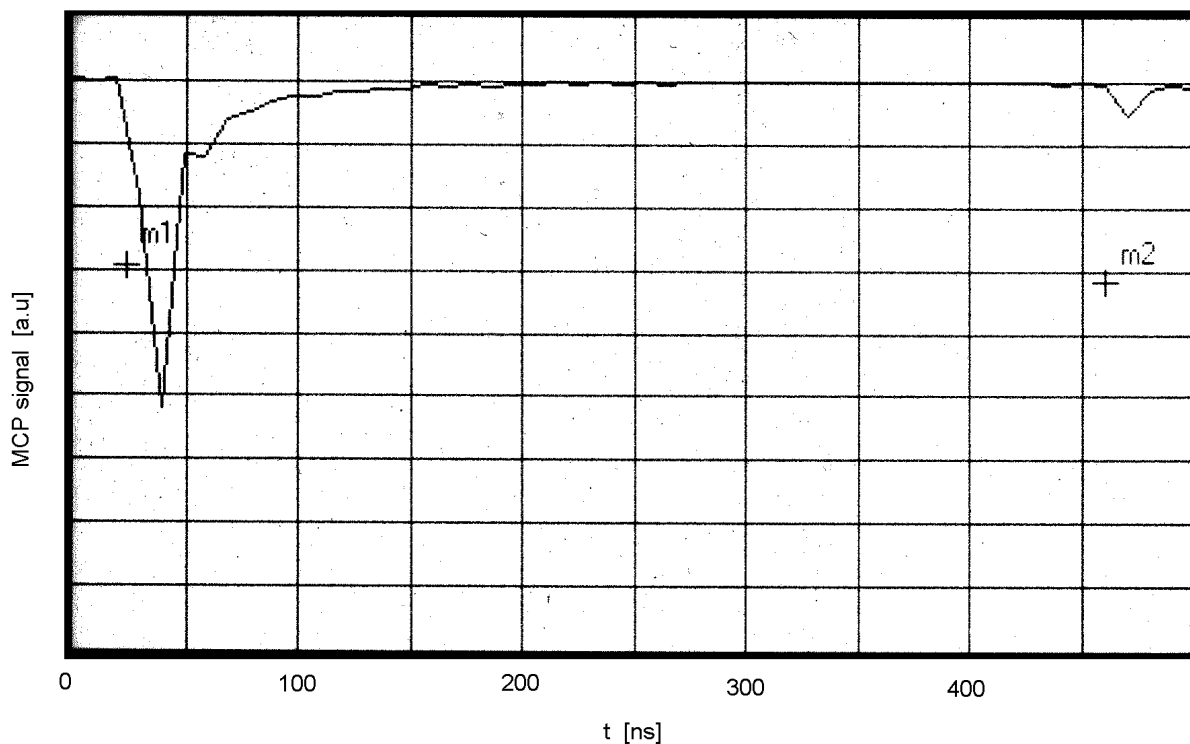


Fig. 5. MCP signal in the mirror chamber. First peak is SASE pulse. Second peak is the same SASE pulse after complete round-trip in the optical feedback system. Pulse separation is 444 ns

3.2 Alignment procedure

Specific problems of pre-alignment of optical elements of the RAFEL at TTF are connected with long base of optical feedback (66.4 m) and aperture limitations of vacuum chamber: 9 mm in the undulator and 6 mm in the collimator at the undulator entrance. Under these conditions the optical elements must be pre-aligned with an accuracy better than 80 microradians. Due to space limitation problem in the TTF tunnel, pre-alignment procedure has been performed with laser beams propagating in the vacuum chamber. Two alignment lasers have been installed at each assembly (see Fig. 4). Helpful factor for visual tracing the laser beam in the narrow vacuum chamber was the presence of optical transition monitor screens used at the TTF for observation of electron beam. These screens are manufactured of a thin captan film covered by an Al layer, and are semi-transparent for laser light. Alignment procedure have been performed in two steps. First, we aligned the mirror in BC2 area (see drawing (a) in Fig. 4). The beam passed through the whole distance between mirrors, reflected back from the mirror in the grating assembly, and is detected after the beam splitter (see photo (c) in Fig. 4). This technique guarantees obtaining of required pre-alignment accuracy due to long base passed by reference beam (130 m) with aperture limitation of 6 mm. At the second stage plane mirror in the mirror assembly have been aligned using reference laser beam from the laser installed in the grating assembly (see drawing (b) in Fig. 4). At this alignment stage we made the use of autocollimation technique with small aperture installed at the path of the laser beam 5 m in front of the mirror. Photo (d) in Fig. 4

shows the final view of back-reflected light on the rear surface of the aperture for alignment accuracy of the plane mirror of about 80 microradians.

Final alignment of the mirrors has been performed with SASE FEL radiation (see Fig. 5). VUV radiation, generated in the undulator reaches plane mirror in the mirror assembly. A non destructive radiation monitor [7] detects the radiation (left pulse in the oscillogram). Then re-reflected radiation propagates to the mirror installed in the grating assembly, reflected back, and is detected again in the mirror assembly (second pulse in the oscillogram). Measurement of the efficiency of the optical feedback gives the value of about 1%.

4 Present status

At the moment we finished transverse alignment of the optical elements. RAFEL experiment is in the progress. The main problem which is solved now is alignment of the longitudinal base and tuning the accelerator to reduce time and transverse space jitter of the electron bunches.

Acknowledgments

From the side of JINR and IP the work has been funded by the grant program of the special purpose use of the Polish contribution to JINR. We thank I.N. Meshkov, J.R. Schneider, D. Trines and A. Wagner for interest in this work and support. We thank all staff of the TESLA Test Facility for fruitful collaboration and help in solving technical problems.

References

- [1] T. Åberg, et al., A VUV FEL at the TESLA Test Facility at DESY, Conceptual Design Report, DESY Print TESLA-FEL 95-03 (1995)
- [2] J. Rossbach, Nucl. Instr. and Meth. **A 375**, 269 (1996)
- [3] J. Andruszkow et al., Phys. Rev. Lett. **85**(2000)3825
- [4] J. Rossbach et al., Presentation at FEL2000 Conference
- [5] J. Goldstein, D. Nguyen and R. Sheffield, Nucl. Instrum. and Methods **A393**(1997)137.
- [6] B. Faatz et al., Nucl. Instrum. and Methods **A429**(1999)424
- [7] B. Faatz et al, "Use of micro-channel plate for nondestructive measurement of VUV radiation from SASE FEL at the TESLA Test Facility", Presentation at FEL2001 Conference
- [8] I. Pinayev et al., Proceedings of the 1999 Particle Accelerator Conference, New York, 1999, p. 2468

A concept of a 150 nm FEL oscillator driven by rf linear accelerator with a thermionic gun

B. Faatz^a, A.A. Fateev^b, V.I. Kobets^b, I.N. Meshkov^b, S. Reiche^c,
E.L. Saldin^a, E.A. Schneidmiller^a, M.V. Yurkov^b

^a*Deutsches Elektronen-Synchrotron (DESY), Hamburg, Germany*

^b*Joint Institute for Nuclear Research, Dubna, 141980 Moscow Region, Russia*

^c*University of California, Los Angeles, USA*

Abstract

RF linear accelerator with a thermionic gun and a subharmonic buncher is proven to be reliable driver for FEL oscillators operating in a wide wavelength range, from far infrared down to 278 nm (FELI, Osaka). However, relatively large value of the normalized emittance, $\epsilon_n \sim 20 - 30\pi$ mm-mrad, prevents to reach shorter wavelength due to sharp drop of the net gain. In this paper we describe a concept of an UV FEL oscillator operating at an ultimately short wavelength, down to 150 nm. Driving beam is produced by rf linear accelerator with thermionic gun and conventional subharmonic buncher (peak current 50-60 A, rms pulse length 2.4 mm, rms energy spread 150 keV, rms normalized emittance 30π mm-mrad). At the energy of about 100 MeV the driving beam is compressed in the magnetic bunch compressor, then accelerated further up to the energy of about 300 MeV and drives FEL oscillator. Increase of the net gain due to the high value of the peak current compensates gain degradation due to the energy spread and emittance effects. As a result, the net gain becomes to be about 40-50% at the wavelength of about 150 nm. This value of the gain is sufficient to achieve saturation within relatively short rf pulse duration, of about 5 microseconds.

1 Introduction

The project DELSY (Dubna ELeCtron Synchrotron) is being under development at the Joint Institute for Nuclear Research [1–3]. It is based on an accelerator facility donated to JINR by the Institute of Nuclear and High Energy Physics (NIKHEF, Amsterdam). Originally this facility has been designed and used for nuclear physics experiments [4]. The NIKHEF linear accelerator, called MEA (Medium Energy Accelerator), was designed by the Haimson Research Corporation (USA) in 1969-1974, built in 1975-1978, and commissioned in 1978. Design of the MEA accelerator is similar to that of SLAC linear accelerator at Stanford,

USA. The electron storage ring AmPS (the Amsterdam Pulse Stretcher) has been put in operation in the early 1990s, and served as a pulse stretcher for nuclear physics experiments. At present the most fraction of the NIKHEF facility has been transferred to Dubna. Thorough analysis of possibilities of available facility and of recent progress in accelerator techniques has shown that it would be possible to build in Dubna a universal light source consisting of the following components:

- (1) Complex of free electron lasers covering continuously the wavelength range from far infrared ($150 \mu\text{m}$) down to UV (150 nm) and far infrared coherent radiation source [5] capable to generate high power radiation (up to 100 MW peak and up to 50 W average) in the wavelength range from $150 \mu\text{m}$ up to 1 mm;
- (2) DELSY storage ring;
- (3) VUV/soft X-ray free electron laser with minimal wavelength down to 5 nm (SASE FEL - Self Amplified Spontaneous Emission Free Electron Laser).

In accordance with this concept the construction of the DELSY facility will proceed in three phases. An ultimate goal of the first stage is to construct a complex of coherent radiators covering continuously the wavelength range from 1 mm down to 150 nm. Table 1 presents general parameters of coherent radiators planned for the Phase 1. All the equipment and user facility will be placed inside existent building with total length of about 230 meters. The ground floor is occupied by the tunnel equipped with radiation shielding. Technical systems and user laboratories will be placed at the upper floor.

The generators of coherent radiation will be driven by the electron beam (1 nC bunch charge, 50 A peak current, 10 ps pulse duration, 30π mm-mrad normalized emittance) produced by the linear accelerator upgraded with by subharmonic rf buncher. These parameters of the beam are sufficient for driving the FEL oscillators of infrared and optical wavelength range. An important feature of the DELSY project is that it is aimed to produce the radiation with much shorter wavelength (down to 150 nm) with respect to the present world record (270 nm) for linac-driven FELs. This breakthrough is possible due to application of the bunch compression technique.

2 Parameter optimization

Optimization strategy for FEL oscillator involves joint optimization of the cavity and undulator parameters, energy of electrons and electron beam focusing. It is not a big problem to optimize an FEL oscillator operating at fixed wavelength (see, e.g., refs. [6,7]). The rules of optimization of a low-gain oscillator are simple. The optimum Rayleigh range of the cavity should be of about half of the undulator length. The electron beam should be focused in the center of the undulator in such a way, that the size of the electron beam and the optical beam spot size should be roughly equal. Optimization for maximal output power is performed by means

Table 1
FEL parameter list for DELSY project

	Units	G1	G2	G3	G4
<u>Electron beam</u>					
Energy	MeV	30-60	30-70	50-110	120-280
Bunch charge	nC			1	
Peak current	A		50-70		150-250
Bunch length (rms)	mm		2.4		0.5-0.8
Normalized emittance (rms)	mm-mrad			30	
Energy spread (rms)	keV	150	150	150	450-750
Micropulse repetition rate	MHz		19.8/39.7/59.5		
Macropulse duration	μ s		5-10		
Repetition rate	Hz		1-100		
<u>Undulator</u>					
Type			Hybrid, planar		
Period	cm	8	5.5	4	3.2
Number of periods	#	35	40	60	80
Beta-function	m	2-3	1.6-2.5	1.6-2.5	1.6-2.5
<u>Cavity</u>					
Length	cm		756.3		
Rayleigh length	cm		140-150		
Total cavity loss	%	3.5-6.5	3.2-7	3.2-6.5	2.5-3
<u>Radiation</u>					
Radiation wavelength	μ m	20-150	5-30	1-6	0.15-1.2
Net gain		0.9-1.7	0.5-0.9	0.5-0.9	0.5-0.8
Peak output power	MW	1-5	1-5	3-15	10-20
Micropulse energy	μ J	50-200	25-100	25-100	50-100
Micropulse duration (FWHM)	ps	10-30	10	10	3-5
Spectrum bandwidth (FWHM)	%	0.2-0.4	0.6	0.6	0.6
Average output power (max.)	W		0.2-1		

of an optimal choice of ratios between cavity loss, outcoupling efficiency of mirrors, and FEL efficiency [8,9]. In order to avoid gain degradation due to the energy spread and emittance, the following conditions must be fulfilled: $\Delta\gamma/\gamma < 1(2N_w)$, and $\epsilon_n/\gamma < \lambda/4\pi$ [8,10–12]. The energy spread falls linearly when the energy is increased, so this effect is more important for long wavelength FELs. Situation with the emittance contribution is an opposite one: FEL wavelength drops quadratically with energy, while the geometrical emittance falls only linearly. It should be noticed that despite the above mentioned limitations are not very strict (in some limits situation may be corrected by increase of the gain), they show a clear idea that with given parameters of the electron beam there is a limit on the minimal achievable

wavelength at reasonable parameters of the undulator (i.e., peak field and period).

Simple optimization strategy described above gives only a rough idea about the region of FEL parameters, since a lot of additional restrictions (mainly of technical nature) should be taken into account. Final optimization of the parameters of FEL oscillators (see Table 1) has been performed with numerical simulations. The net gain has been optimized using three-dimensional, steady-state code FS2R [13] taking into account diffraction of the radiation, energy spread, and emittance effects. Final optimization has been performed with one-dimensional version of time-dependent FEL simulation code FAST [14] adopted for calculation of FEL oscillator. The code takes into account slippage effects, finite pulse duration and start-up from shot noise. The value of effective energy spread, obtained from simulations with FS2R code, has been used to take into account energy spread and emittance effects in the code FAST.

An ultimate goal of designed facility is to cover continuously the wavelength range from far infrared down to 150 nm with minimal number of FEL oscillators. We adopted well-proven approach when the wavelength of each FEL oscillator changes by a factor of 5-7 [15,16]. Fast change of the operating wavelength by a factor of 2-3 will be provided by the change of the undulator gap. Change of the electron beam energy will extend the tunability range additionally by a factor of two. With given parameters of the electron beam there is a wide range of opportunities for optimization of infrared facilities G1 and G2, since the required energy of the electron beam is still low which allows to maintain high net gain. The net gain degradation due to the energy spread and emittance remains in tolerable limits in the whole range of operation. Also, the slippage effect does not reduce the net gain significantly. However, operation of near-infrared facility G3 becomes critical to the value of the emittance when approaching to 1 μm wavelength. Thorough analysis shows that direct use of the driving beam from the subharmonic buncher (peak current 50-60 A, rms pulse length 2.4 mm, rms energy spread 150 keV, rms normalized emittance 30 $\pi\text{mm-mrad}$) would not allow to go significantly beyond 1 μm wavelength within our constrain of a high net gain of about 50 %. A record value of the linac-based FEL oscillator at the wavelength of 278 nm was obtained at the FELI facility (Osaka, Japan) with driving beam parameters close to ours [17]. Despite the latter facility has been completely optimized, the net gain was only of about 5-8 %, and saturation level has been reached in the end of 24 μs long rf pulse [18]. Main obstacle to reach short wavelength is connected with the emittance limitation. Reduction of the small-signal gain due to longitudinal velocity spread is given by [19]:

$$g \simeq \frac{5.6g_s}{5.6 + \hat{\Lambda}_T^2}, \quad (1)$$

where $\hat{\Lambda}_T^2 = [(\Delta\mathcal{E})^2/(\mathcal{E}_0^2) + \gamma_z^4 \epsilon^2/\beta^2](4\pi N_w)^2$ is the longitudinal velocity spread

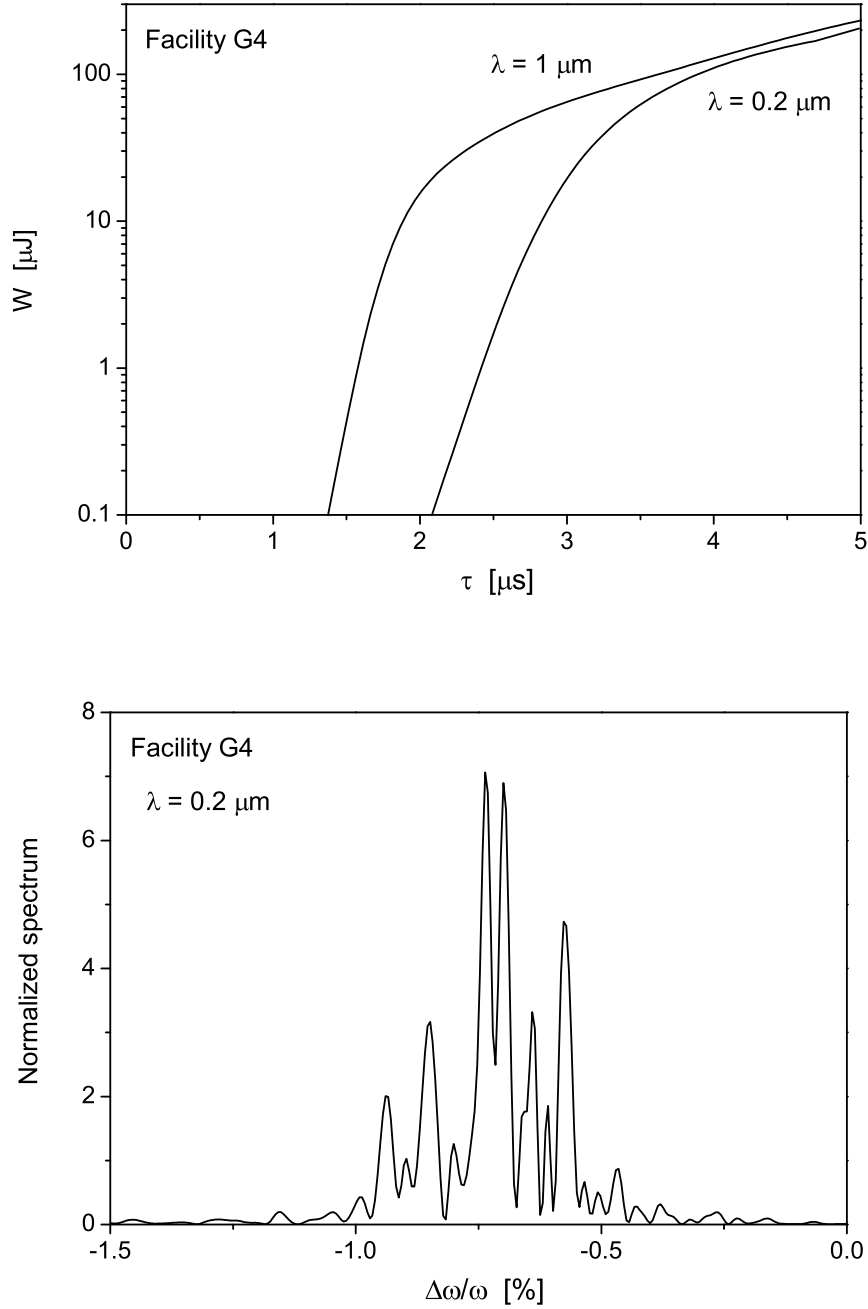


Fig. 1. Characteristics for visible/ultraviolet facility G4. Upper plot: evolution of the energy in the radiation pulse as function of time. Lower plot: radiation spectrum averaged over full rf pulse

parameter, β is focusing beta function. Factor g_s is given by (see, e.g. [6]):

$$g_s = 0.135\tau, \quad \tau = \pi\omega\theta_s^2 j_0 l_w^3 A_{JJ}^2 (c\gamma_z^2 \gamma I_A)^{-1}, \quad (2)$$

where τ is gain parameter, l_w^3 is undulator length, $\omega = 2\pi c/\lambda$, $j_0 = I/\Sigma$, I is beam current, Σ is combined transverse area of the optical mode and electron beam, $A_{JJ} = [J_0(Q) - J_1(Q)]$, $Q = K^2/(4 + K^2)$, and J_0 and J_1 are Bessel functions. In our case minimum achievable wavelength is defined by the emittance contribution to the longitudinal velocity spread parameter. This contribution increases drastically with the energy increase needed to achieve lasing at shorter wavelength. On the other hand, contribution of energy spread is relatively small and reduces further at the energy increase. Analysis of this situation leads to an idea how to overcome the problem of the gain reduction. Namely, at all parameters fixed, there is the only way to increase the gain parameter τ by means of the peak current increase. In our case this can be done with bunch compression scheme at the energy of about 100 MeV. Such an approach has been proven to be extremely effective for production of intensive driving beams for VUV and X-ray SASE FELs [20–23]. The electron bunch is accelerated in off-crest phase in order to induce correlated energy dispersion along the bunch. This energy dispersion forces the beam to compress in the bunch-compressor. At the bunch compression exit the peak current is increased, but at the same the energy spread increases proportionally. However, our calculations show that increase of the gain due to the growth of the peak current is higher than its degradation due to energy spread increase. Also, the increase of the gain compensates the gain degradation due to emittance. This allows us to have desirable value of the net gain of about 50 % in a wide wavelength range down to 150 nm and reach FEL saturation within 5 μ s rf pulse duration (see Fig. 1).

In conclusion to this section we note again that features of our FEL design are strongly influenced by short rf pulse duration. Natural consequence of a short rf pulse is a need for a high value of the net gain. A harmful consequence of a high net gain is possible growth of the sidebands in the nonlinear regime leading to the widening of the spectrum [24,25]. Our simulations shows that this effect takes place in our short wavelength FELs. In practice, it can be suppressed by an appropriate choice of cavity detuning [26,27]. Another trick would be adjusting the gain in such a way that saturation level is reached in the end of rf pulse. The price for narrow spectrum is reduction of radiation pulse energy and average power. A technique of intracavity dispersive elements for sideband suppression can be also used [28]. At this conceptual design stage we can state only that practical steps for sideband suppression will strongly depend on user demands. In the future upgrade of the facility the rf pulse duration will be increased up to 10 μ s which would allow to operate at a lower net gain, thus relaxing sideband problem.

References

- [1] V.A. Arkhipov et al., "Project of the Dubna electron synchrotron, Nucl. Instrum. and Methods A, in press
- [2] I. N. Meshkov et al, "Perspective of DELSY for the fourth generation SR facility", Proc. EPAC-2000

- [3] "DUBna Electron Synchrotron: Technical Project". Available at JINR by request only
- [4] G. Luickx et al., The Amsterdam Pulse Stretcher Project (AmPS), PAC, Chicago, 1989, NIKHEF/AmPS/89/03
- [5] B. Faatz et al., Preprint DESY 00-95, DESY, Hamburg, 2000
- [6] C.A. Brau, *Free electron Lasers* (Academic Press, Inc., New York, 1990)
- [7] S. Benson, Nucl. Instrum. and Methods, A **304**(1991)773
- [8] *An Infrared Free Electron Laser for the Chemical Dynamics Laboratory: Design Report*, Preprint LBL PUB-5335, April 1992
- [9] E.L. Saldin, E.A. Schneidmiller and M.V. Yurkov, Opt. Commun. **102**(1993)360
- [10] P. Sprangle et al., Nucl. Instrum. and Methods, A **331**(1993)6
- [11] C.W. Roberson and B. Hafizi, Nucl. Instrum. and Methods, A **331**(1993)331
- [12] J.B. Murphy and C. Pellegrini, *Laser Handbook, Vol. 6* (North Holland, Amsterdam, 1990), p.9
- [13] E.L. Saldin, E.A. Schneidmiller and M.V. Yurkov, Opt. Commun. **95**(1993)141
- [14] E.L. Saldin, E.A. Schneidmiller and M.V. Yurkov, Nucl. Instrum. and Methods **A429**(1999)233
- [15] A.F.G. van der Meer et al., Nucl. Instrum. and Methods, A **331**(1993)282
- [16] T. Tomimasu et al., Nucl. Instrum. and Methods, A **407**(1998)494
- [17] K. Saeki et al., Nucl. Instrum. and Methods, A **375**(1996)10
- [18] T. Tomimasu et al., Nucl. Instrum. and Methods, A **393**(1997)230
- [19] E.L. Saldin, E.A. Schneidmiller and M.V. Yurkov, *The Physics of Free Electron Lasers* (Springer-Verlag, Berlin, 2000)
- [20] T. Aberg et al., *A VUV free electron laser at the TESLA Test Facility at DESY. Conceptual Design Report*, DESY Print June 1995, TESLA-FEL 95-03, Hamburg, DESY, 1995
- [21] J. Rossbach, Nucl. Instrum. and Methods, A **375**(1997)269
- [22] T. Limber et al., Nucl. Instrum. and Methods, A **375**(1997)322
- [23] J. Andruszkov et al., Phys. Rev. Lett. **85**(2000)3825
- [24] N.M. Kroll, P. Morton and M.N. Rosenbluth, IEEE J. Quantum Electron. **QE-17**(1981)1436
- [25] J.C. Goldstein, Proc. SPIE **453**(1984)2
- [26] R.W. Warren, J.C. Glodstein and B.E. Newnam, Nucl. Instrum. and Methods, A **250**(1986)19
- [27] R.W. Warren and J.C. Glodstein, Nucl. Instrum. and Methods, A **272**(1988)155
- [28] P.G. O'Shea et al., Nucl. Instrum. and Methods, A **331**(1993)62

Magnetic Characterization of the Hybrid Undulator U27 for the ELBE-Project

P. Gippner^a, E. Grosse^{a*}, J. Pflüger^b, A. Schamlott^a, W. Seidel^a, U. Wolf^a, R. Wünsch^a

^aForschungszentrum Rossendorf, Postfach 51 01 19, D-01314 Dresden, Germany

^bDESY Hamburg, Notkestr. 85, D-22603 Hamburg

At the Dresden Radiation Source ELBE an intense IR beam in the 3–30 μm range will be produced in the undulator U27. It consists of two 34-pole sections, allowing to insert a magnetic chicane in between [1]. The undulator structure has a period of $\lambda_u=27.3$ mm and consists of NdFeB permanent magnets and poles of decarborized iron, mounted on two carriages [delivered by DANFYSIK] such that the distance between the two sections is adjustable for phase-matching. The gaps of both sections can be varied independently to eventually produce two IR-colours at the same electron energy. For high-gain lasing one can introduce a tapering of the field.

Both sections were scanned and adjusted using a calibrated Hall probe setup [2]. After installation at the beam line the field distribution was checked using the pulsed wire method.

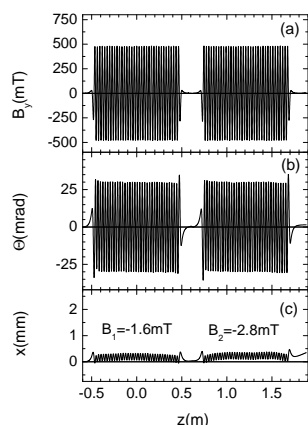


Fig. 1: Measured vertical field component B_y on the axis of the two undulator sections (a), and the 1st (b) and 2nd (c) field integrals for a gap width $g = 12$ mm calculated for a reference electron at 20 MeV.

The measured field and the resulting field integrals are displayed in fig. 1. Auxiliary coils were inserted to get a minimum electron displacement at the exit sides of

*also at TU Dresden

both sections. Only weak magnetic fields $B_{1,2}$ as generated by these coils are necessary to keep the electrons within the optical beam. This can be seen from fig. 2, where the effect of the correction coils on the 2nd field integrals is illustrated by results of pulsed wire measurements.

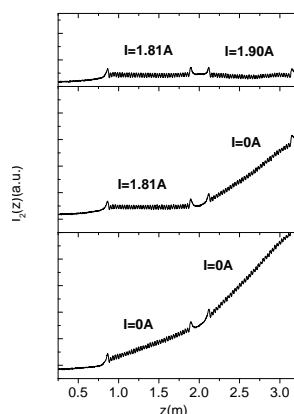


Fig. 2: 2nd field integrals as measured by the pulsed-wire method. The effect of correction coils with 100 windings and the corresponding current values are indicated.

The horizontal field distributions (as measured at different gaps, cf fig. 3) are constant over the x -range covered by the beam. As the field inhomogeneities remaining after tuning the poles influence the lasing process, we determined them for various gap widths. For $g = 14$ mm the minima and maxima B_i of the field relative to their average values are shown in fig. 4. The standard deviation σ_B contributes to the inhomogeneous line broadening of the emitted light according to

$$\frac{\delta_B \lambda}{\lambda} = \frac{2 K_{\text{rms}}^2}{1 + K_{\text{rms}}^2} \frac{\sigma_B}{B_{\text{av}}} \quad (1)$$

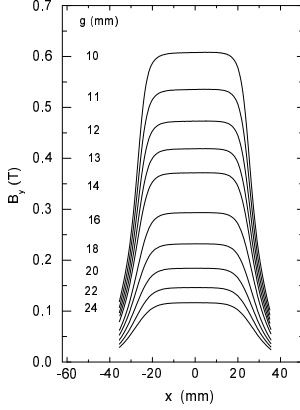


Fig. 3: The magnetic field $B_y(x, 0, z_5)$ in the horizontal plane perpendicular to the electron beam at different gaps g where z_5 is the z -coordinate of the 5th pole.

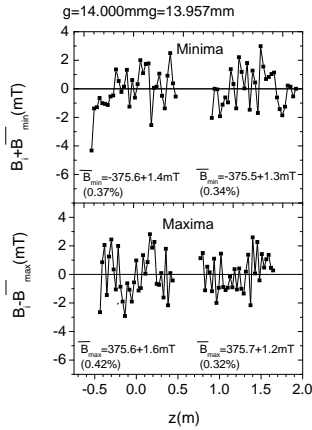


Fig. 4: Maxima and minima of the magnetic field $B_y(z)$ in the middle plane of the undulator. For both sections also the average values, their standard deviations σ_B and (in brackets) the relative field roughness are given.

If the FEL works with sufficient laser power the Lorentz factor γ of the electrons decreases by $\delta\gamma \approx \gamma/2N_u$ (for the first harmonic) along the electron path due to the interaction of the electron beam with the electromagnetic field. The electron energy changes continuously leading to a resonance wavelength $\lambda(z)$ which depends on the coordinate z .

Within a certain interval of λ this effect can be corrected by field tapering. To compensate the energy loss $\delta\gamma$ by a reduction δB of the magnetic field one has to ensure

$$\frac{\delta B}{B} = \frac{1 + K_{\text{rms}}^2}{K_{\text{rms}}^2} \frac{\delta\gamma}{\gamma}. \quad (2)$$

Figure 5 shows the effect of field tapering in both sections of the undulator U27, which would be applied in a situation typical for high intensity lasing.

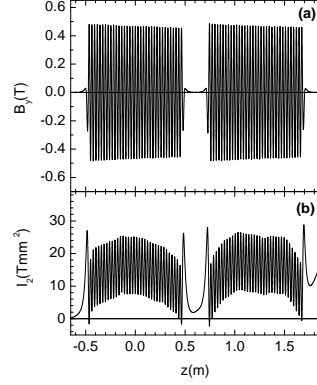


Fig. 5a: Measured field distribution $B_y(z)$ on the undulator axis for a gap width $g = 12$ mm and a tapering of 0.3 mm in both undulator sections.

b: Second field integral $I_2(z)$. The corresponding x coordinate of the electron can be obtained by $x(\mu\text{m}) \approx 300I_2(T \cdot \text{mm}^2)/E(\text{MeV})$

The optical phase along the undulator axis z can be expressed by

$$\Psi(z) = \frac{2\pi}{\lambda} \left[\frac{z}{2\gamma^2} + \frac{\int^z dz' \Theta^2(z')}{2} \right]. \quad (3)$$

Here λ , γ , Θ are the radiation wavelength, the Lorentz factor and the electron deflection angle.

Using eq. (3) the phase can be determined experimentally by measuring $B_y(z)$ along the axis and calculating the deflection angle Θ . Phase matching is achieved when the phase (3) is the same in both sections. This has to be done by properly choosing the drift space d between the two sections. Phase matching is obtained periodically after an increase of d by $\Delta d = (1 + K_{\text{rms}}^2)\lambda_u$. A measured phase is shown in fig. 6.

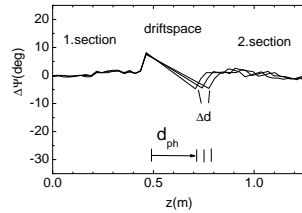


Fig. 6: Phase deviation $\Delta\Psi(z)$ for a gap $g = 17$ mm and $K_{\text{rms}} = 0.47$. Three phasing distances d_{ph} are shown.

REFERENCES

1. R. Wunsch et al., contribution to this conference (We-P-24)
2. B. Faatz, J. Pflüger and Y.M. Nikitina, Nucl. Instr. Meth. A 375 (1996) 618

Experimental investigation of wake fields excited by a rough surface

M. Hüning¹

RWTH Aachen and DESY, Notkestrasse 85, D-22607 Hamburg, Germany

P. Schmüser

Universität Hamburg and DESY, Notkestrasse 85, D-22607 Hamburg, Germany

Abstract

An experiment has been carried out at the TESLA Test Facility (TTF) linac to investigate the wake fields generated by picosecond electron bunches in narrow beam pipes with artificially roughened inner surface. Two methods were employed: (a) the energy structure imposed on the bunches by the wake fields was analysed with a magnetic spectrometer, and (b) the generated THz radiation was directly recorded in an interferometer equipped with Golay cell detectors. Both methods indicate the presence of strong wake field effects as expected from simulations in which the rough surface is modelled by a dielectric layer. Preliminary results are presented which demonstrate very clearly the existence of surface roughness wake fields.

Key words: wake fields, surface roughness

PACS numbers: 41.60.m, 41.60.Cr

1. Introduction

The small gap in the TTF FEL undulator magnets restricts the beam pipe diameter to less than 10 mm. The wake potential generated by the short electron bunches of high charge density is expected to be dominated [1] by the residual surface roughness of the undulator vacuum chamber which has been measured to be in the 0.8 μm range [2]. Since these wake fields have been predicted to have a

significant impact on the beam quality in present and future free electron lasers [3] an experimental verification of the simulation model prediction appeared highly desirable. For this purpose a special vacuum chamber has been built containing six beam pipes with various diameters and different surface preparations each of which can be placed into the beam line under remote control.

¹ Corresp. Author E-mail: markus.huening@desy.de

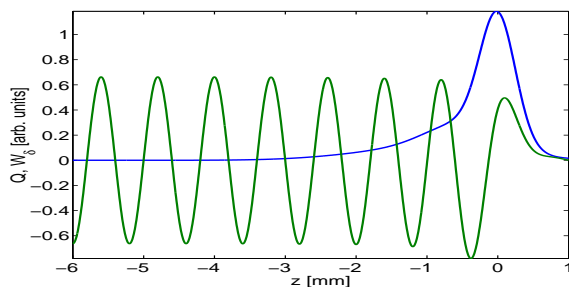


Fig. 1. Longitudinal charge distribution in the bunch and the wake potential created by a dielectric surface layer.

2. The Wake Fields

In the dielectric layer model one single mode is excited propagating synchronously with the beam. Its wave number in a circular tube with radius r and roughness depth δ reads

$$k_0 = \sqrt{\frac{2\varepsilon_{eff}}{(\varepsilon_{eff} - 1)r\delta}}. \quad (1)$$

All the details of the roughness are summarized in the effective dielectric constant ε_{eff} . The wake function is harmonic in the longitudinal coordinate s

$$w_0^{\parallel}(s) = \widehat{W}_c \cos(k_0 s), \quad (2)$$

with $\widehat{W}_c = Z_0 c / (\pi a^2)$ (see fig. 1). See [4][5] for further details.

In the limit of vanishing surface roughness one gets $\lambda_0 \ll \sigma_z$. Then the energy loss vanishes and the impedance becomes inductive, as discussed in ref. [6].

3. Layout of the experiment

The experiment was carried out at the linear electron accelerator of the TESLA Test Facility (TTF). The main components of the linac are: a radio frequency photocathode delivering electron bunches of 5 ps rms length, 1 to 8 nC charge and an energy of 4 MeV, a superconducting (sc) booster cavity raising the energy to 16 MeV, two acceleration sections each containing 8 nine-cell

sc cavities, raising the energy to 230 MeV, a magnetic bunch compressor in between the two sections, and three undulator magnets with a total length of 13.5 m for the production of FEL radiation in the 100 nm regime. A collimator with a 6 mm bore protects the neodym iron boride permanent magnets of the undulator from radiation damage. For optimum bunch length compression by about a factor of 5, such as needed for the production of FEL radiation, the bunches are accelerated 14° off-crest in the first acceleration section to impress a position-energy correlation onto the bunch, the leading electrons having lower energy than the trailing ones. In the magnetic chicane the tail electrons move on a shorter path and thereby catch up with the head electrons. The acceleration in the second section is then done on-crest.

In the present experiment a more moderate bunch compression turned out to be advantageous for the observation of wake field effects: a 6° off-crest acceleration was used in both sections. The main component of the experiment was a special ultrahigh vacuum chamber, containing six 80 cm long test pipes of diameters between 6 and 15 mm and with different surface preparations (smooth, sandblasted, grooved), which was mounted behind the undulator. By remote control any of the pipes could be moved into the electron beam and centered with an accuracy of 0.1 mm. The pipes are composed of half cylinders machined into two flat aluminum plates. This way a controlled surface preparation by sandblasting or grooving was possible. The surface roughness has been measured with a tracer type surface roughness measuring machine featuring a resolution of $0.02 \mu\text{m}$. A tube with smooth surface and 8 mm diameter served as a reference; according to model calculations the surface roughness wakefields in this tube should be negligible. The parameters of the 6 pipes are listed in table 1.

Having traversed the selected test tube the electron bunches pass a diffraction radiation screen located 1 m downstream. This screen is made of two polished silicon wavers coated with aluminum. Between the two wavers a slit is left open for beam passage. The screen is oriented at 45° with respect to the beam axis deflecting far infrared radiation horizontally into a Martin-Puplett inter-

preparation	diameter	rms roughness, δ	r_a	f (interf)	ε_{eff}	f (energy)	ε_{eff}
reference	8 mm	$1.4 \mu m$	$2.3 \mu m$	-	-	-	-
sandblasted	10 mm	$8.3 \mu m$	$6.2 \mu m$	500 ± 40 GHz	1.78	490 ± 40 GHz	1.8
sandblasted	8 mm	$8.3 \mu m$	$6.2 \mu m$	550 ± 40 GHz	1.82	540 ± 40 GHz	1.9
sandblasted	6 mm	$8.3 \mu m$	$6.2 \mu m$	620 ± 40 GHz	1.91	610 ± 40 GHz	1.8
grooves	10 mm	$60 \mu m$	$19.7 \mu m$	177 ± 10 GHz	1.94		
grooves	8 mm	$60 \mu m$	$19.7 \mu m$	200 ± 10 GHz	1.90		

Table 1

Parameters of the beam tubes. The frequencies f have been determined from interferometric measurements and from the energy distribution of the electron bunches. The parameter δ is the rms depth of the roughness, r_a the so called roughness parameter.

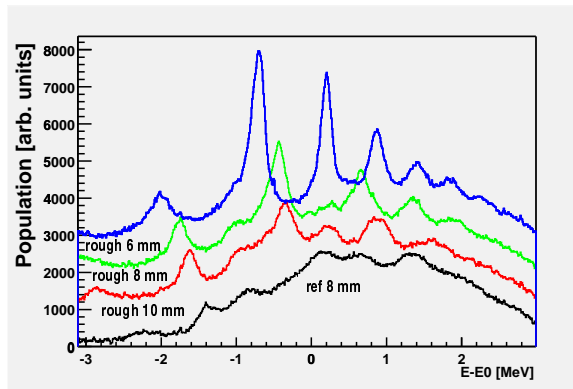


Fig. 2. Energy profiles with different beam tubes. The profiles have been shifted vertically for visual separation.

ferometer [7]. The electron beam is then deflected by 20° in a spectrometer dipole behind which a transition radiation screen with vertical deflection is mounted. Optical transition radiation produced at this screen is imaged by a CCD camera. The horizontal dispersion at the position of the screen amounts to 1 m while the horizontal β -function is small (0.25 m). Therefore the width of horizontal particle distribution on the screen is predominantly given by the dispersion, with a negligible widening caused by the horizontal emittance of the incoming beam ($\varepsilon_N \approx 6 \cdot 10^{-6}$ m). The momentum resolution of the magnetic spectrometer is better than $5 \cdot 10^{-4}$.

4. Experimental results

Some measured energy profiles of the moderately compressed bunches are shown in figure 2. The bottom curve shows the energy distribution

obtained when the beam has traversed the smooth reference pipe of 8 mm diameter. A wide distribution is observed, created by the off-crest acceleration, which is superimposed with a slight structure. The structure can possibly be attributed to surface roughness wake fields in the upstream collimator and undulator beam pipes. The next three curves show the energy profiles obtained for the test tubes which were roughened by sandblasting. A clear structure is observed which becomes very pronounced at the smallest pipe diameter of 6 mm. This regular structure can be assigned to a harmonic wake potential, where the distance between the peaks can be related to the wavelength of the potential by the given time to energy correlation. A comparison of the energy distributions shows that the wavelength of the wake is scaling with $1/\sqrt{r}$ where r is the beam pipe radius. Simulations show reasonable agreement to a frequency close to 500 GHz for the 8 mm sandblasted beam pipe. For the 6 mm beam pipe this then corresponds to 600 GHz.

In the energy distribution of the 6 mm beam pipe the peaks reach their minimal width. Under these special conditions the amplitude of the wake potential can be derived from the distance of two peaks yielding 560 kV/m. For the other beam pipes the point of maximum contrast of the peaks is reached at different acceleration phases. Accelerating at these different phases one finds 550 kV/m for the 8 mm beam pipe and 750 kV/m for the 10 mm pipe. For a quantitative understanding of these preliminary results it is necessary to take into account the $1/r^2$ behaviour of the impedance and the nonlinear increase of the exciting spectrum towards lower frequencies. In

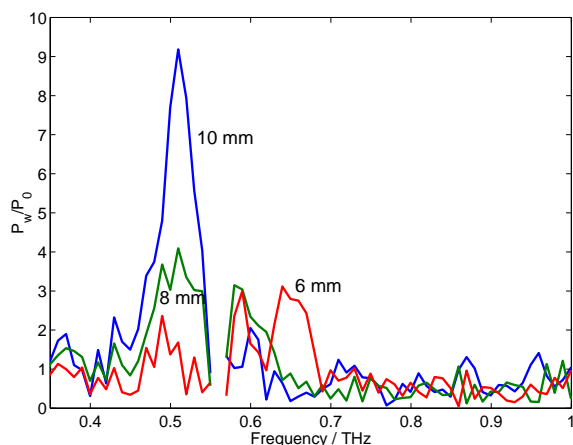


Fig. 3. Spectra of the roughened beam pipes normalized to the spectrum of the bunch.

all cases the bunch charge was 1 nC, the bunch compression was not complete by setting an off-crest phase of 6° in the first acceleration module. Hence the front part of the bunch contains only a fraction of 1 nC.

A complementary measurement is shown in figure 3. Here the far infrared radiation pulse produced at the diffraction radiator next to the test tubes has been analyzed by measuring its auto-correlation function. The depicted curves already show the ratio of the frequency spectra measured with the sandblasted beam pipes divided by the spectrum measured with the reference pipe. Each measurement shows a peak at a characteristic frequency (see table 1). Unfortunately these spectra are strongly distorted by water vapour absorption inside the interferometer. The gaps in the spectra can be identified with known water absorption lines [8]. The measurements with the interferometer were done at maximum compression of the bunches.

5. Conclusion and Outlook

An experiment has been conducted to study wake fields excited by a rough surface of the beam pipe. Evidence is found for a harmonic wake potential. Within the measurement errors the observed wavelengths scale with the square root of the beam pipe radius. The preliminary analysis

yields wake potentials of a few hundred kV/m at bunch charges of less than 1 nC. A more detailed analysis including a longitudinal phase space tomography is in progress.

References

- [1] S. Reiche, H. Schlarb, Simulation of Time-Dependent Energy Modulation by Wake Fields and its Impact on Gain in the VUV Free Electron Laser of the TESLA Test Facility, FEL 99, NIMA 445 (2000) 155-159
- [2] U. Hahn, J. Pflueger, M. Rueter, P.K. Den Hartog, M. Erdmann, E.M. Trakhtenberg, G. Wiemerslage, S. Xu, The Vacuum Chambers for the VUV SASE FEL at the TESLA Test Facility (TTF FEL) at DESY, PAC 99, New York, March 1999
- [3] A. Novokhatski, M. Timm, T. Weiland, H. Schlarb, A Proposal for the Surface Roughness Wake Field Measurement at the TESLA Test Facility, PAC 99, New York, March 1999
- [4] A. Novokhatski, M. Timm, T. Weiland, The Surface Roughness Wakefield Effect, EPAC 98, Stockholm, May 1998
- [5] M. B. Timm, Wake Fields of Short Ultra-Relativistic Electron Bunches, PhD thesis Univ. Darmstadt, Der Andere Verlag (2001), ISBN 3-935316-11-9
- [6] G. Stupakov, R.E. Thomson, D. Walz, R. Carr, Effects of Beam-Tube Roughness on X-Ray Free Electron Laser Performance, Phys. Rev. ST Accel. Beams, 2(6),060701-1,1999
- [7] M. Geitz, Bunch Length Measurements, DIPAC 99, Chester, May 1999
- [8] J.R. Pardo, E. Serabyn, J. Cernicharo, Submillimeter atmospheric transmission measurements on Mauna Kea during extremely dry El Niño conditions: Implications for broadband opacity contributions, Journal of Quantitative Spectroscopy & Radiative Transfer 68(2001)419-433

The TTF-FEL Status and its Future as a Soft X-ray User Facility

M. Körfer, DESY, Germany, for the TTF FEL Group ¹⁾
Deutsches Elektronen Synchrotron, Notkestr. 85, 22607 Hamburg

Abstract

This paper presents the progress of the SASE and RAFEL experiments at the TESLA Test Facility (TTF). In the second part the layout of the soft X-ray user facility TTF2 and the status of construction work is described.

- 1) Members of the TTF FEL Group: V. Ayvazyan, N. Baboi, I. Bohnet, R. Brinkmann, M. Castellano, P. Castro, M. Dohlus, H.T. Edwards, B. Faatz, A. Fateev, J. Feldhaus, K. Flöttmann, A. Gamp, T. Garvey, C. Gerth, V. Gretchko, U. Hahn, C. Hessler, K. Honkavaara, M. Hüning, R. Ischebeck, M. Jablonka, T. Kamps, M. Körfer, M. Krassilnikov, J. Krzywinski, J. Lewellen, M. Liepe, A. Liero, T. Limberg, H. Loos, C. Magne, J. Menzel, P. Michelato, M. Minty, A. Mosnier, D. Nölle, A. Novokhatski, C. Pagani, F. Peters, J. Pflüger, P. Piot, L. Plucinski, K. Rehlich, A. Richter, J. Rossbach, E.L. Saldin, W. Sandner, H. Schlarb, G. Schmidt, P. Schmüser, J.R. Schneider, E.A. Schneidmiller, H.J. Schreiber, S. Schreiber, D. Sertore, S. Setzer, S. Simrock, R. Sobierajski, B. Steeg, F. Stephan, K. Sytchev, K. Tiedke, M. Tonutti, R. Treusch, D. Trines, D. Türke, V. Verzilov, R. Wanzenberg, T. Weiland, H. Weise, I. Will, K. Wittenburg, M.V. Yurkov, K. Zapfe

Introduction

High-gain single pass SASE FEL's require high peak current (kA-level), ultra short (100 μm -level) and low emittance (few mm mrad normalised) electron bunches. On the road towards a Self Amplified Spontaneous Emission (SASE) FEL user facility intermediate stages have to be taken for reaching the final target beam parameters. In the beginning of SASE FEL activities at DESY the Tesla Test Facility TTF1 was devoted to reach SASE in a proof of principle experiment and check the SASE FEL theory around 100 nm laser wavelength. The experimental results agree completely with theoretical predictions [1]. Based on the results and experience TTF will be upgraded to a SASE FEL user facility in two stages. First, the SASE FEL will be driven in a single pass modus starting from shot noise and lasing below 25 nm. In a second stage the accelerator runs with a seeding option to increase the signal to noise ratio of SASE FEL radiation by orders of magnitudes. In this scheme the short electron beam with high peak current and demodulated energy spread overlaps with its own irradiated light pulse.

1 TTF FEL Status

The Tesla Test Facility (TTF) is a linear accelerator mainly devoted to the test and development of components for future X-ray FELs and Linear Colliders. TTF is presently equipped with a photo-injector gun, two regular superconducting TESLA accelerator modules, a bunch compressor and a 15m long permanent magnet undulator. A wide range of studies is being performed at TTF related to FEL and beam physics.

1.1 SASE FEL performance

Since first lasing of SASE FEL at DESY (February 2000) [1] there were two dedicated SASE runs in the year 2000 (of about four months in total). The present SASE run started in June 2001 and will continue until early 2002. The radiation wavelength is continuously tunable in a wide range from 80 to 180 nm [2]. Permanent efforts are directed towards the improvement of facility performance. The linac operation in FEL mode has been sustained over a period of several months, demonstrating the stability and reproducibility of the linac components. The superconducting cavities, the RF control and the cryogenic system showed a good performance at moderate gradients of about 15 MV/m. Moreover, the linac operation for the lasing of the FEL

was recovered within only a few days of linac start up after the shutdown of April-May 2001. After the restart of SASE FEL operation in June 2001 the SASE FEL gain is routinely tuned to the value of about 10^6 (which corresponds to peak brilliance of radiation of about 10^{27} [Phot./((sec · mrad · mm² · 0.1% bandw.))]) in a long-pulse mode of operation at 2.25 MHz repetition rate (see Fig.1). This is a significant progress compared to the FEL gain of about 3×10^3 obtained last year [1]. Special efforts were devoted to the development of photon diagnostics which allows to measure radiation energy and spectrum of individual bunches in a train (see Fig.1). The radiation energy is measured by three different techniques (PtSi photodiodes, thermopile sensor and MCP detector) which guarantees the reliability of measurements [3,4]. Single-shot spectrums are detected by an intensified CCD camera installed after the monochromator [5]. At the moment pilot user experiments are being performed at the TTF FEL taking advantage of the high peak brilliance of the radiation.

1.2 Preparation of RAFEL experiment

Despite of the SASE FEL's capability to provide much higher peak brilliance than synchrotron radiation sources, it still possesses a high potential for further increases by means of improving the longitudinal coherence. This is possible only when coherent radiation from an external source is fed to the undulator entrance. One of the solutions of the seeding problem exploits the approach of a regenerative FEL amplifier [6] with a narrow band optical feedback (RAFEL) [7]. We believe that RAFEL might be an ideal source of powerful, tunable, fully coherent UV/VUV radiation with laser-like characteristics. The installation of the optical feedback at TTF FEL was greatly facilitated by the fact that there is free space available for the optical components at exactly half the distance (66.5 m) between two electron bunches when the accelerator is operated in a 2.25 MHz multibunch mode. The RAFEL operates as follows. The first bunch in a train of up to 1800 bunches amplifies shot noise and produces intense, but wide-band radiation. A fraction of the radiation is back-reflected by a mirror. The spherical grating in Littrow mounting is installed in a straight section in the electron bunch compression area between the first and the second accelerator module. It disperses the light and focuses a narrow band of radiation back on the entrance of the undulator to seed the next electron pulse. After several round-trips the output radiation spectrum approaches Fourier-transform-limited width and the output power reaches saturation level.

At present all RAFEL equipment is installed at the TTF accelerator. It consists of three elements: mirror assembly (installed 14~meters downstream the undulator), grating assembly (installed in the bunch compressor area, 35~meters upstream the undulator), and radiation detector unit (installed 6~meters upstream the undulator). The optical elements (mirrors and grating) are made of SiC having good reflectivity in the VUV band around 100 nm. At the moment the transverse alignment of the optical elements is finished and non-destructive photon beam diagnostics is successfully tested [4,7]. The main problem which is being solved now is the alignment of the longitudinal base and tuning the accelerator to reduce time and transverse position jitter of the electron bunches in order to provide successful multi-bunch amplification of the radiation [8].

1.3 Wakefield and energy profile

Wakefields of charged particles in accelerators interact with their direct surroundings. Depending on the bunch length and beam pipe the interaction may increase the energy spread of the beam. Simulations gave hints that also surface roughness plays a significant role on SASE FEL performance [9,10]. Several models were developed with rather different predictions. Therefore, an experiment was designed to check the model calculations. In a section of 80 cm length a series of beam pipes with various surface treatments has been installed. Figure 2 shows the effect on the energy distribution of the bunch. The roughened beam pipe generates a substructure in the energy profile of the bunch which can be explained by the dielectric layer model. Independently the emission of THz-radiation has been observed. The measured frequencies around 500 GHz fit well with the expectations from the model. The detailed analysis is going on.

2. TTF2 User Facility

To provide a SASE FEL for applied research TTF will be upgraded to a soft X-ray user facility operating at electron beam energies up to 1 GeV. A further bunch compression stage and a seeding monochromator will be installed. This section presents the final design and the status of construction work.

2.1 Accelerator design

The sketch for the accelerator part of the SASE FEL user facility at 6 nm wavelength is shown in Figure 3. The bunches are generated by an injector that incorporates a photon-emission rf-gun, a TESLA module (#1) and an rf-linearizer (3rd harmonic). At the injector exit the 2 mm (rms) long electron bunches are compressed by using a magnetic compressor (BC2) to yield 0.5 kA peak current at 130 MeV. The required peak current of 2.5 kA is

achieved by a second compressor (BC3) located at 450 MeV. After the exit of the accelerator module 6 the final energy is up to 1.0 GeV. The 20 m long collimator protects the permanent magnet undulator against the unacceptable dose deposition coming from beam halo, dark current or faulty operation of the accelerator. A fast orbit feedback system is installed in the collimator part. The seeding option downstream consists of three undulators followed by separated photon and electron beamlines. The monochromised photon beam and the incoherent electron beam will be synchronised at the entrance of the FEL amplifier. The FEL amplifier consists of six undulators. Additional undulator insertions can be installed in the drift space behind the FEL amplifier. At the end of the electron beam trajectory the SASE FEL radiation will be guided into the experimental hall downstream. The electron beam is dumped in an absorber system. The complete beamline covers 257m length. On the way to the final SASE FEL setup described above, an intermediate stage is foreseen. The 3rd harmonic cavity of the photo-injector might not be available during the first phase of accelerator commissioning. Nevertheless, the injector beam parameters allow first lasing at about 25 nm with gain saturation. The seeding system and the space for extra undulators will be substituted with beamlines. The temporary beamline in the seeding section offers a possibility for beam diagnostic. For instance, by using OTR screens for measuring the beam dimensions inside a FODO lattice the beam emittance can be determined.

2.1.1 Injector and Bunch Compressors

State of the art photo-injectors cannot simultaneously produce short bunches with sub-mm-mrad normalized transverse emittance. To reach the required target parameters for emittance and bunch length at the undulator entrance the upgrade of the TTF1 injector is planned [11]. The new injector will incorporate an axis-symmetric rf-gun that generates 2 mm (rms) bunches. The electron bunches are directly (after $\approx 1.3\text{m}$) injected in a TESLA module and accelerated up to 140 MeV. Because of the long incoming bunch length, the longitudinal phase space accumulates a curvature due to the cosine-like rf-wave and yields an increase of longitudinal emittance. This correlated distortion will be corrected with a 3rd harmonic section (composed of four TESLA cavities scaled to 3.9 GHz). Downstream of the injector, the longitudinal rms emittance is 50 mm-keV at an energy of ~ 130 MeV. The scheme allows to compensate non-linearities that might occur further down in the beam transport line (e.g. wake fields). The magnetic compressor BC2 consists of a four bend achromatic chicane. The section behind BC2 is equipped with a FODO channel to verify online the transverse emittance of the beam. The magnetic compressor section BC3 is embedded between accelerator modules three and four. Within the bunch compressor, where the bunch length is very short, coherent synchrotron radiation becomes significant and may induce unacceptable emittance growth. Several compression schemes are investigated to keep the emittance small while the beam is compressed. An asymmetric S-Type layout is proposed by CEA Saclay [12]. Within the energy range of 300–500 MeV a bunch length reduction down to 50 μm (rms) corresponding to 2.5 kA peak current at the nominal matrix element of $R_{56}=0.05$ m is achieved. Emittance growth coming from the magnetic multipole fields inside the chicane is negligible if the dipole field quality is $\Delta B/B=3\cdot 10^{-4}$.

2.1.2 Undulator Protection

The FEL permanent magnet undulator at TTF consists of radiation sensitive material (NdFeB). Since the requirements on the magnetic field integrals are tight, the tolerable accumulated dose for the SASE FEL operation will be 10^5 Gy.

The collimator has to collimate 5 dimensions of the electron beam phase space. The design has to consider the beam dynamics, the interaction of particles with collimator materials, as well as the survival of the material in case of an emergency and thermal heating during normal operation. Figure 4 shows the maximum collimator aperture that still protects the undulator as a function of energy deviation [13]. A minimum value of an aperture radius of about 2 mm allows to protect in the considered range of the energy deviation from -50% up to $+25\%$ and to stop all particles with $|\Delta E/E_0| > 3\%$ before the undulator entrance. For comparison, the aperture radius of 4.75 mm is related to the mechanical bore in the undulator chamber. Particles within $\pm 3\%$ energy deviation and with small amplitude betatron oscillations go safely through the undulator. Secondary particles are created by beam particles hitting collimator. The collimator efficiency can be estimated at 1×10^{-6} considering both the particles which are back-scattered into the beam line and the secondary particles.

Nevertheless, to obtain information on protection efficiency and radiation damage of the permanent magnet material the deposited dose will be recorded. Unfortunately, the gap between the magnet joke and vacuum chamber is a narrow slit, inaccessible for conventional online dosimeter systems. The TESLA collaboration started the development of optical fibre dosimeter systems for different applications along the accelerator [14,15]. A fibre optical powermeter was successfully tested, which allows to obtain the accumulated dose during operation.

2.1.3 FEL Section and Bypass

This part of the linear accelerator consists of the seeding section and the FEL amplifier. The undulator for TTF2 is similar to the existing TTF1 concept and totally nine units will be installed. In contrast to the TTF1 design, the beam focussing magnets are separated from the undulators. Electromagnetic quadrupoles located in between the undulators have several advantages for the TTF operation. A variable focussing system allows well matched twiss parameters independent of the beam energy. The elimination of integrated permanent quadrupoles reduces the number of orbit distortions along the undulator axis and thus the number of correctors. Consequently, the beam based alignment is easier to handle. The disadvantage is an increased length of the beamline section the undulators.

The bypass is a simple beam transport line in parallel to the SASE FEL and is needed for commissioning, temporary tests and optimisation of different accelerator sections.

3. Construction work

The experimental hall for the user facility as well as the tunnel for the linear accelerator were accomplished in spring 2000. The layout of the machine with respect to the position of magnets, collimators, fast feedback, diagnostic tools, power supplies, signal processing units and the cryogenic system is fixed. The construction of components starts in autumn 2001. The beginning of beamline installation in the tunnel will be in spring 2002. In spring 2003 the accelerator commissioning starts and the first user operation is planned in early 2004.

References

- [1] J. Andruszkow et al, First Observation of Self-Amplified Spontaneous Emission in a Free-Electron Laser at 109 nm Wavelength, Phys. Rev. Lett., Vol.85, Number 18
- [2] J. Rossbach et al., Observation of Self-Amplified Spontaneous Emission in the Wavelength Range from 80 nm to 180 nm at the TESLA Test Facility FEL at DESY, FEL2000 Conference
- [3] R. Treusch et al, Development of photon beam diagnostics for VUV radiation from a SASE FEL, Proceedings FEL99, Nucl. Instrum. And Meth., A445, p. 456-462 (2000)
- [4] B. Faatz et al, "Use of micro-channel plate for non-destructive measurement of VUV radiation from SASE FEL at the TESLA Test Facility", Presentation at FEL2001 Conference
- [5] Ch. Gerth et al, Diagnostics for the study of electron beam properties of VUV SASE FEL, Proceedings FEL2000, Durham, North Carolina, to be published in Nucl. Instrum. and Meth. A
- [6] J. Goldstein, D. Nguyen and R. Sheffield, Nucl. Instrum. and Methods A393(1997)137.
- [7] B. Faatz et al., Nucl. Instrum. and Methods A429(1999)424
- [8] B. Faatz et al, "Alignment of the optical feedback system of VUV Regenerative FEL Amplifier at the
- [9] M. Hüning, Recent Results from the TESLA TEST FACILITY (TTF), Proceedings PAC2001, Chicago
- [10] M. Hüning, P. Schmüser, Wakefields excited by a rough Surface, Presentation at FEL2001 Conference
- [11] P. Piot et al, Injector Upgrade for TTF User Facility: Design and Performance Analysis, to be published as TESLA-FEL report.
- [12] A. Loulergue, A. Mosnier, A Simple S-Chicane for the final bunch compressor of TTF/FEL, Proceedings EPAC2000, Vienna
- [13] V. Balandin, N. Golubeva and M. Körfer, Studies of beam optics in the collimator system for beam optics in the collimator system, Presentation at FEL2001 Conference
- [14] H. Henschel, M. Körfer, F.Wulf, Fibre Optic Radiation Sensing System for TESLA, DESY TESLA report 2000-26
- [15] E. Janata, M. Körfer, Radiation Detection by Cerenkov Emission in Optical Fibers at TTF, DESY TESLA report 2000-27

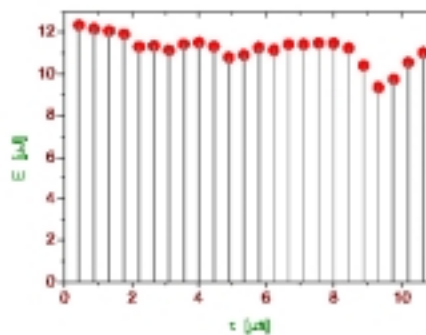
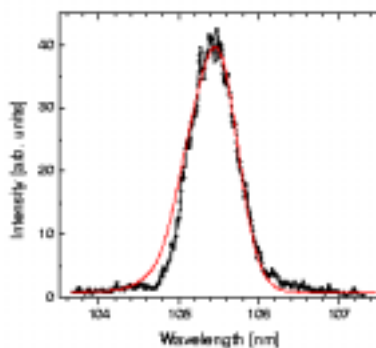


Figure1: Single-bunch radiation spectrum (left plot), and average radiation energy along a train from SASE FEL operating at 2.25 MHz repetition rate (right plot). Output radiation has full transverse coherence. Shot-to-shot statistical fluctuations of the radiation energy from single bunch are about 25% which corresponds to the number of longitudinal modes (spikes) of about 16.

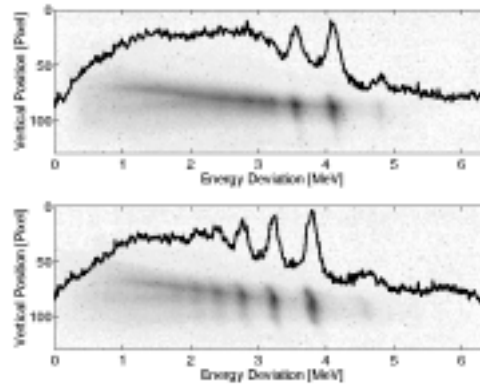


Figure2: Influence of surface roughness on the beam energy profile. Top: Accumulated wakefields from the upstream beamline generate a substructure in the energy profile of the bunch. Bottom: The beam fragmentation in energy is excited by a rough pipe.

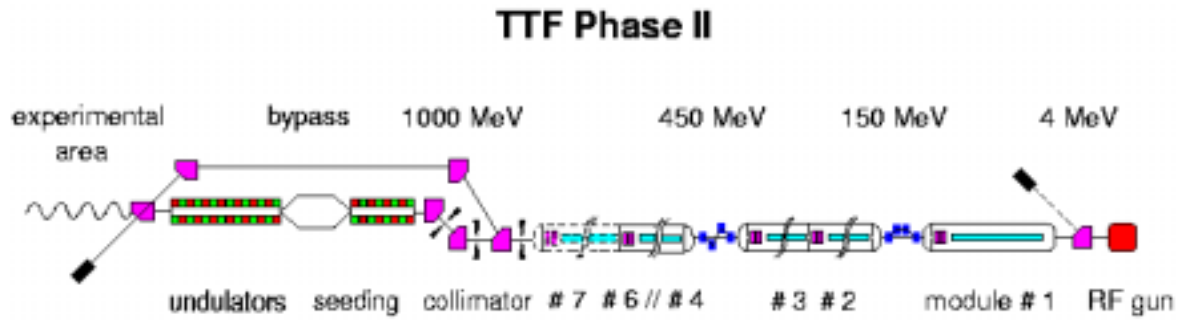


Figure3: Principle scheme of the TTF2 layout.

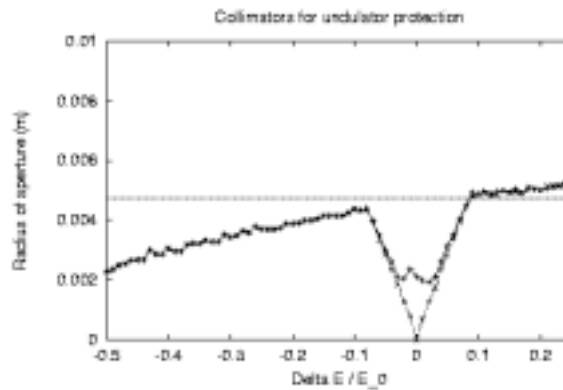


Figure4: Determination of the collimator aperture with respect to the beam energy acceptance.

Measurement of the longitudinal phase space for the photo injector test facility at DESY Zeuthen

D. Lipka^a, J. Bähr^a, I Bohnet^a, K. Flöttmann^b, D. Richter^c, F. Stephan^a, Q. Zhao^a

^aDESY Zeuthen, Platanenallee 6, 15738 Zeuthen, Germany

^bDESY Hamburg, Notkestr. 85, 22607 Hamburg, Germany

^cBESSY, Albert-Einstein-Str. 15, 12489 Berlin, Germany

A setup for measuring the longitudinal phase space of the photo injector test facility at DESY Zeuthen is described. This setup includes a YAG-screen and a Cherenkov detector which are used to convert the electron beam into a photon beam with the wavelength in the visible range. The momentum spread of the electron bunch can be measured with the YAG-screen. The Cherenkov radiation mechanism will be used to measure the bunch length with good time resolution. As radiators silica aerogels with very low refractive indices as well as a special shaped fused silica plate will be used. A streak camera system will measure the time dependent behavior of the photon bunch. The combination of bunch length measurement and momentum spread measurement gives the information about the whole longitudinal phase space. The design considerations of the radiators and their properties are discussed.

1. Introduction

A photo injector test facility at DESY Zeuthen (PITZ) for the development and operation of optimized photo injector for future free electron lasers and linear colliders will be commissioned in autumn 2001. The components of PITZ are described in [1–3].

The ability of beam diagnostics to investigate the properties of the electron bunch is the basic for a successful optimization and improvement of the performance of PITZ. In this contribution we focus on the design for measuring the longitudinal emittance. The diagnostics of the longitudinal phase space is expected to be done in a following way:

At first the momentum spread is measured using a dipole magnet and a YAG-screen. For this, the properties of a screen laminated with YAG-powder were studied and compared with an OTR-screen. Furthermore the error for measuring the momentum spread and the resolution of the momentum measurement are estimated.

The second step is to determine the bunch length. This will be done by using a radiation process, where the electrons produce light with the same time properties as the bunch has. Then a streak camera is used to observe the longitudinal pulse shape. A high number of photons and very good intrinsic time resolution become the main requirements to the radiator especially at low electron energies. Cherenkov radiation in aerogel and in special shaped quartz plates are discussed as possible options for photon production mechanism. The properties of aerogel material in vacuum will be shown.

Ideas to measure the bunch length and energy spread si-

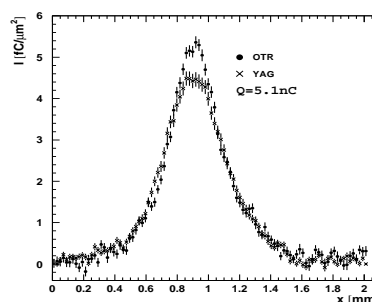


Figure 1. Beam profile of a 16 MeV 5.1 nC electron bunch

multaneously will be described as well.

2. Momentum spread measurement

The momentum of the electrons will be measured via deflection of about 60° caused by a magnetic field. The momentum is a linear function of the current in the dipole, while the momentum spread is a function of the spot size at the screen. The estimated energy spread is expected to be 2%. Therefore a screen with good resolution should be used.

The energy of the electrons at first will be up to 5 MeV. At these energies a small number of transition radiation photons with large angles would be produced if an OTR-radiator would be used. The number of scintillation photons in YAG-screens is much higher. On the other hand,

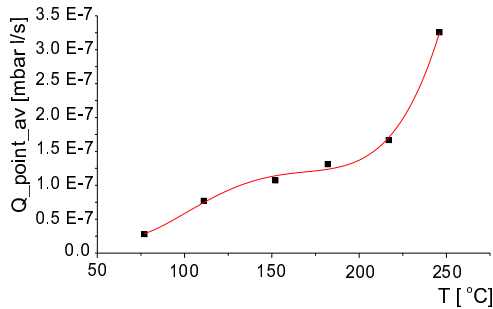


Figure 2. Average gas load after a certain aerogel temperature is reached

YAG-screens at high electron densities will reach saturation. The image of 16 MeV electron bunches was measured at the Tesla Test Facility with increasing charge densities by OTR- and YAG-screens (figure 1). The intensity of the outgoing light from the YAG-material increases up to an electron density of about $4fC/\mu m^2$, the maximum density achieved at this measurement. There was not seen a clear evidence of saturation. The intensity measured with the YAG-screen is lower at the maximum and shows a slightly wider distribution compared to the OTR-screen. The expected maximum electron density at the screen in the dispersive arm of PITZ is of the order of $1fC/\mu m^2$. Therefore no saturation is expected.

The momentum spread will be extracted from the projection of the distribution at the screen in the dispersive arm. For a correct calculation the bunch size, the divergence and their correlations at the entrance of the dipole should be known. They are not measured. If they are not taken into account the difference will be of the order of 3% of the estimated momentum spread.

The measured momentum will be smeared out due to the finite transverse emittance of the electron beam at the entrance of the dipole. Considering the expected emittances the momentum resolution will be better than 0.5% of the measured electron energy.

3. Bunch length measurement

The electron bunch length has to be converted into a photon bunch of corresponding length. It will be measured using a streak camera system. Therefore it needs a radiation process with enough photons being produced. Good time resolution is necessary. We will use Cherenkov radiators in order to obtain adequate photon yields. Aerogel and special machined quartz plates are possible options to produce a photon beam with the needed properties [4].

The vacuum properties of aerogel have been tested

among other things by measuring the gas load coming from aerogel. A calculation of the pressure distribution of the whole injector estimates its influence on the pressure in the cavity section. The calculation shows that the gas load coming from the aerogel should be in the range of $10^{-6}mbar\ l/s$ or better to avoid damage of the Cs_2Te photo cathode. Tests with aerogel at different temperature shows that a temperature up to $200^\circ C$ can be allowed (figure 2). This can be ensured by adjusting the pulse train length.

4. Measurement of longitudinal phase space

To measure the longitudinal phase space the streak camera will detect photon beams from a Cherenkov radiator in the dispersive arm so that both distribution of electron momentum and longitudinal profile can be measured simultaneously. To obtain good time resolution for aerogel a slit mask before the radiator will be inserted to get small transverse bunch sizes. Therefore the whole energy spread is measured by moving the slit mask in the transverse direction.

REFERENCES

1. F. Stephan et al., Photo Injector Test Facility under Construction at DESY, FEL 2000, Durham.
2. J. Bähr et al., Diagnostics for the Photo Injector Test Facility in DESY Zeuthen, DIPAC 2001, Grenoble.
3. I. Bohnet et al., Photo Injector Test Facility in the Commissioning Phase at DESY Zeuthen, FEL 2001, Darmstadt.
4. Q. Zhao et al., Design of the Bunch Length Measurement for the Photo Injector Test Facility at DESY Zeuthen, PAC 2001, Chicago.

Undulator systems for the TESLA X-FEL

J. Pflüger, M. Tischer
Hamburger Synchrotronstrahlungslabor, HASYLAB
Notkestr. 85
22603 Hamburg, Germany

Abstract

A large X-ray FEL lab is under consideration within the TESLA project and is supposed to be operated in parallel with the TESLA linear collider. There will be five SASE FELs and five conventional spontaneous undulators.

A conceptual design study has been made for the undulator systems for these X-FEL's. It includes segmentation into 6.1m long undulator 'cells'. Each consists of a 5m long undulator 'segment', a separate quadrupole, one horizontal and one vertical corrector, and a phase shifter. These items are presented and discussed.

PACS Code: 41.60.Cr, 75.50 Ww

Introduction

Together with the TESLA linear collider a large X-FEL lab is planned which makes use of a part of the TESLA main linac. The whole project is described in detail in ref. /1/. The basic layout of the FEL lab is shown in Fig.1. This contribution only deals with the undulators, which for SASE FELs in the X-ray regime need total lengths exceeding 300m. Long undulators like these cannot be built in one piece: They have to be subdivided into 'undulator segments' of suitable length. Additional components for electron beam focusing, steering and detection and phase correction are needed as well. They are placed in between the segments. Together they form an 'undulator cell'. An 'undulator system' for the TESLA X-FEL is an array of up to 53 of such cells.

Together with Fig.1, Table 1 gives an overview over their parameters. Permanent magnet (PM) technology will be used exclusively. Five SASE FELs are planned in total. Four of them, SASE1 through SASE4 are primary FELs using the fresh TESLA electron beam. They produce linearly polarized light and operate primarily around the 0.1nm wavelength regime. There will be a secondary FEL, SASE5, which will be a helical one. It will reuse the beam with an somewhat increased energy spread after the passage through SASE3 and will operate in the soft X-ray regime at wavelengths up to 2.5nm. In addition, there will be five spontaneous radiators, U1 through U5, which will use the spent electron beam of the remaining three SASE FELs. As can be seen in table 1, there will be only four different types of devices, which reduces the magnetic design effort.

The most expensive part of an undulator is the magnetic structure. Fortunately there has been a tremendous development of PM based insertion device technology over the past 20 years when these devices came into use as intense sources of SR. An enormous progress has been made in their design, construction and optimization. There are now well established state of the art techniques to produce high quality insertion devices. With only a few exceptions, nowadays PM technology is used throughout. The undulator systems for the X-ray FEL will benefit from these developments a lot. Thus, the technology is available. The real innovative challenge is, however, the construction of the immense number of undulator segments in sufficient quality, in reasonable time and at reasonable cost.

Hardware Setup

Overview

Three cells of an undulator system are shown in Fig. 2. In between two neighboring undulator segments additional components are arranged: A phase shifter to adjust the proper interference condition between radiation emitted by adjacent segments, a quadrupole for electron beam focusing, horizontal and vertical correctors, and a beam position monitor. In total an intersection is 1.1m long. The quadrupoles are parts of the FODO lattice, i.e. a sequence of focusing and defocusing quadrupoles, which limit the beam size over whole length of the undulator. The distance between two of them is 6.1m. This allows for 5m long undulator segments. The β -function in the undulator sections is large enough so that the modulation caused by the FODO lattice is moderate /2/.

Wavelength tunability, i.e. gap tuning is required for three of the SASE undulators and the spontaneous radiators as well. This has two consequences: First, in the case of SASE undulators the saturation length is increased because the shortest wavelength at which the FEL is to operate is at the upper gap of the tunability range and thus determines the system length. Second, the phase matching of the photon beam between different segments becomes gap dependent. If the undulator gap and therefore the radiation wavelength is changed the interference condition is changed too. With the help of a suitably designed and excited small magnetic chicane called phase shifter the electron beam can be delayed in such a way that proper phasing is preserved.

Mechanical design

A standard gap separation drive and support system has been developed in a conceptual design study /3/. It considers the principles of economic manufacturing of large quantities, while tough requirements on mechanical accuracy have to be maintained. The 3D view in Fig. 3 shows how these ideas could be realized. In order to have a relative stability of the 1st harmonic better than the Pierce parameter ρ , girder deformation under changing load conditions (gap change) has to be limited to at

most $\pm 4\mu\text{m}$. Consequently a voluminous I-beam profiles with dimensions $550 * 200 * 100 \text{ mm}^3$ are used. Using a four point support further limits girder deflection. The same profile is also used for the support columns and the floor stands. This is much simpler to build than a welded structure and has the same or even improved mechanical stability. In total 4700m with a weight of about 1900 tons are needed for the 281 support systems for the TESLA FELs. Only little machining is required on the columns. Standard guiding elements may be used. There are four individual gap drive motors which are electronically synchronized by a control unit. Motors and their motion control units are part of the control system /4/. In order to get absolute gap information with micrometer accuracy a separate frame is used to support absolute length encoders. In this way the exact girder position close to the corresponding drive motor can be measured without errors induced by deformation of the girder support or by the support structure. The gap adjustment accuracy is better than $\pm 1\text{-}2\mu\text{m}$. More details are found in ref. /4/.

Linear Magnetic structures

The FELs in the X-ray range will be equipped with planar devices based on NdFeB PM hybrid technology. Circularly polarized light can be produced using quarter wave plate X-ray optics, which now become quite common in the hard X-ray regime /5/. Thus, helical undulators are not required in this photon energy range. There will be three different planar types, with period lengths of 30, 45 and 60mm. A magnetic prototype has been designed for the SASE1 undulator /6/. At a gap of 12mm and a period length of 60mm the peak field is 1.33 T. At 25GeV and a gap of 22mm, this device would radiate at 0.1nm and at 12mm gap at 0.35nm. The width of poles and magnets was determined such that a transversal good-field-region of $\pm 1 \text{ mm}$ results in which the relative field variation is less than ρ , i.e. $4.2 \cdot 10^{-4}$ in the open gap position. In this way requirements on horizontal alignment of the undulator segments are reduced without affecting the FEL process. The maximum peak field is obtained for a pole dimension of $40 \times 8 \times 55 \text{ mm}^3$ (width \times length \times height) and $70 \times 22 \times 65 \text{ mm}^3$ for the magnet dimension. The field of an undulator segment has even symmetry so that the 2nd field integral can be brought to zero with a simple half pole. The gap dependence of the 1st field integral has been reduced to below 0.05 Tmm by optimizing the length and vertical position of the last magnet, the height of the last pole as well as the width of the 2nd last pole. The remaining dependence can be reduced further using appropriate shims or with the help of active correctors, which are available in the intersections anyhow.

Planar helical magnetic structure

For SASE 5 a helical structure is planned. In the soft X-ray range, above 0.4nm, no optical alternative to the generation of circularly polarized light exists. An APPLE II type undulator is proposed /7/, which is a planar structure thus allowing good lateral access for measurements and the insertion of

vacuum chambers. Among all planar proposals for producing helical fields it offers the highest field and the largest variation of polarization properties. A prototype design for the SASE5 undulator system at TESLA including polarization characteristics was worked out based on extensive experience at BESSY /8,9/. Although the saturation length of a helical undulator in general is shorter than that of a planar device, helical undulators require considerably more mechanical effort than a planar ones.

Undulator Intersections

Fig 4 shows a 3D view of an undulator intersection embedded between two neighboring undulator segments. The phase shifter is seen to the left. A preliminary design is presented in ref /10/. It consists of three horizontal magnets. The length of the center one is doubled because it needs twice the strength. Horizontal correction may be integrated in one of these magnets. The vertical corrector, which is identical to the short phase shifter magnets but rotated by 90° is seen to the right. In between there is a quadrupole with a 15mm bore with a maximum gradient of 100T/m. Its magnetic length is 0.2m only, its total length is about 0.26m. With these quadrupoles a minimum β function of less than 15m at 25GeV can be obtained.

Although SASE2 and SASE3 are operated at a fixed gap, they should be gap adjustable too. There are good reasons to do so:

1. The radiation wavelengths of different segments have to be tuned with an accuracy better than ρ , which is in the order of $3.6 \cdot 10^{-4}$ (see table 1). As a consequence in different segments gap control with an accuracy of $\Delta g < \approx \pm 2 \mu\text{m}$ or better is needed. This accuracy cannot be perpetuated in a truly fixed gap device. Although the field might be precisely adjusted in the lab it is hard to preserve on this level of accuracy. So, some fine adjustment has to be provided anyhow.
2. In order to compensate for the average energy loss of the electron beam along the undulator system, a taper has to be applied. It increases efficiency and maximizes the output intensity. Such a taper will be effectively a step taper, the gap will be changed in very fine steps from one undulator segment to the next: It is very advisable to have this taper adjustable in order to easily optimize output intensity.
3. A segment can effectively be switched off by fully opening its gap. In this way the effective length of the undulator system can be varied. For diagnostic reasons this option might become very important. In ref /11-13/ a 'photon beam based' alignment procedure is described. The electron beam orbit, the proper radiation wavelength of each segment and the phasing can be accurately controlled in this way. Thus this diagnostic tools will play an important role in optimizing emission properties.
4. Experience at the TESLA Test Facility (TTF) has shown that high radiation levels inside the undulator region may be created if the beam is missteered, but very moderate doses can be

obtained during routine operation with a well adjusted beam. So most of the radiation exposure originates during setup and/or commissioning of the machine. By opening the gap this hazard to the magnet structures can be minimized.

In the fixed gap devices two of the three phase shifter magnets can be omitted. Only one magnet is needed for horizontal correction.

Summary and Outlook

The undulator systems for the TESLA X-FELs have been outlined. PM based magnet technology using NdFeB material will be used. Full use can be made from the achievements on PM based magnet technology for insertion devices for the 3rd generation SR sources. A new dimension is however the large number of segments, which requires new and efficient ways of production. The potential layout of a production plant for TESLA has recently been worked out in a study /14/. It also includes the project management structure, which is needed, to organize and synchronize the manufacturing and assembly of sub tasks, such as girders, support mechanics, motion control components etc. These issues will become very important for the production of the undulator systems of the TESLA X-FELs.

Acknowledgement

We gratefully acknowledge stimulating discussions with J. Bahrtdt, P. Elleaume, E. Gluskin, U. Hahn, G. Materlik and J. Rossbach.

References

References marked with * are available in the WWW under: <http://tesla.desy.de>

1. TESLA Technical Design Report Part V: The X-ray Free Electron Laser , G. Materlik, T. Tschentscher, Editors, DESY 2001-011, ECFA 2001-209, TESLA FEL 2001-05, March 2001, *
2. J. Pflüger, Nucl. Instr. and Methods A445, (2000) 366
3. M. Rüter, J. Pflüger, TESLA-FEL 2000-07 *
4. H. H. Radszuweit, J. Krunkowski, J. Pflüger, M. Tischer, TESLA-FEL 2000-09, in german *
5. C. Giles et. al Rev. Sci. Instr. 66 (1995) 1518
6. M. Tischer, J. Pflüger, TESLA-FEL 2000-12 *
7. S. Sasaki, Nucl. Instr. and Methods A347 (1994) 83
8. J. Bahrtdt, W. Frentrup, A. Gaupp, M. Scheer, W. Gudat, G. Ingold, S. Sasaki, Proceedings of the SRI2000, Aug 21-25 2000, Berlin, Germany
9. J. Bahrtdt, A. Gaupp, U. Englisch, W. Frentrup, M. Scheer, TESLA-FEL 2000-11 *
10. J. Pflüger, TESLA-FEL 2000-08 *
11. P. Elleaume, J. Chavanne, B. Faatz, TESLA-FEL 2000-16, Nucl. Instr. Meth. A455, (2000) 503 *
12. M. Tischer, P. Illinski, U. Hahn, J. Pflüger, H. Schulte-Schrepping, TESLA-FEL 2000-13 *

13. M. Tischer, P. Illinski, U. Hahn, J. Pflüger, H. Schulte-Schrepping, these proceedings
14. R. Cremer, F. J. Börgemann, J. Pflüger, M. Tischer, TESLA-FEL 2000-10 *

Figure Captions

- 1 Schematic layout of the X-FEL laboratory at TESLA.
- 2 Three 5m long undulator segments with intersections give an impression how a full system with up to 54 segments will look like
- 3 Standard undulator segment for the TESLA undulator systems
- 4 Components in the intersection between undulator segments

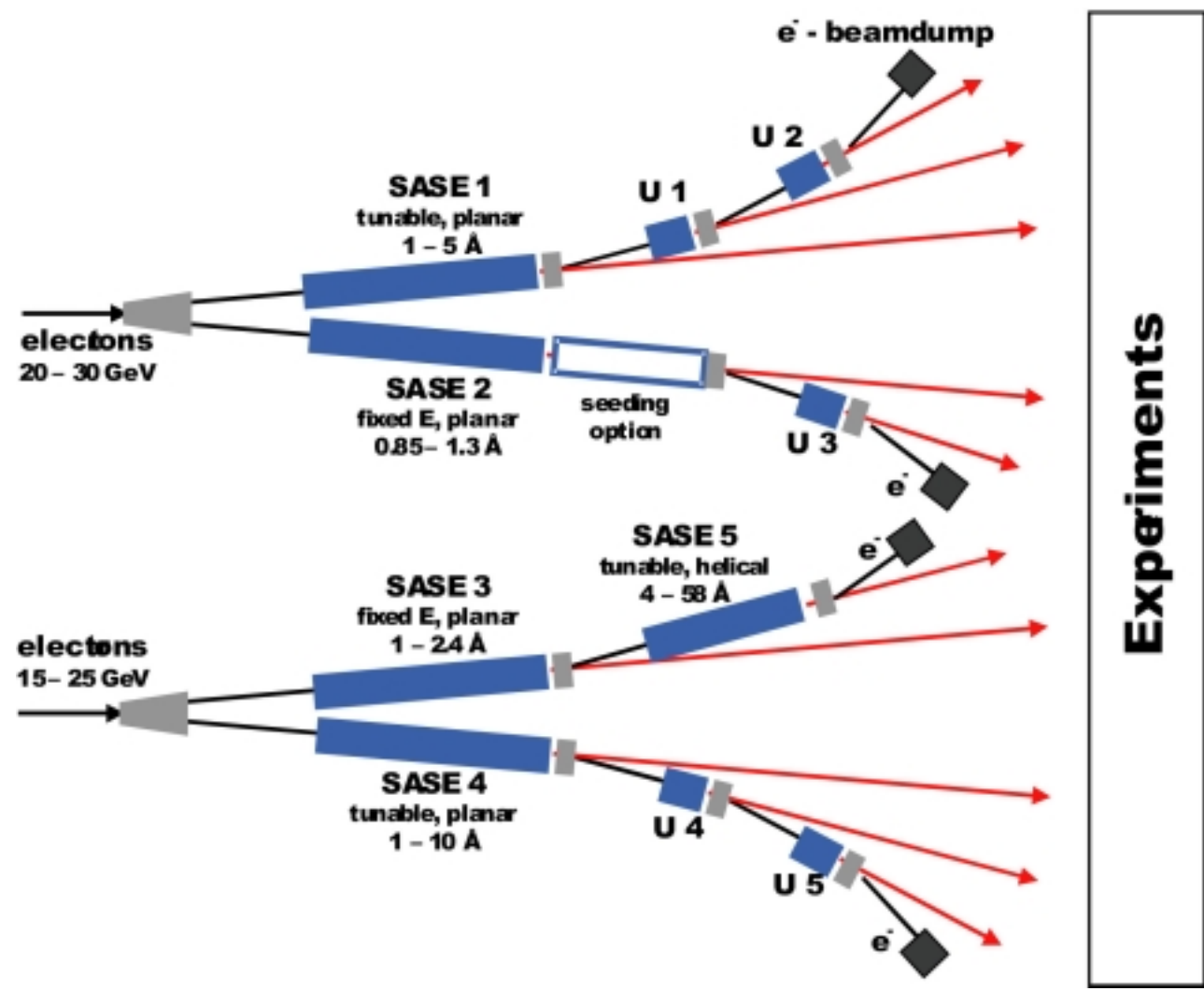
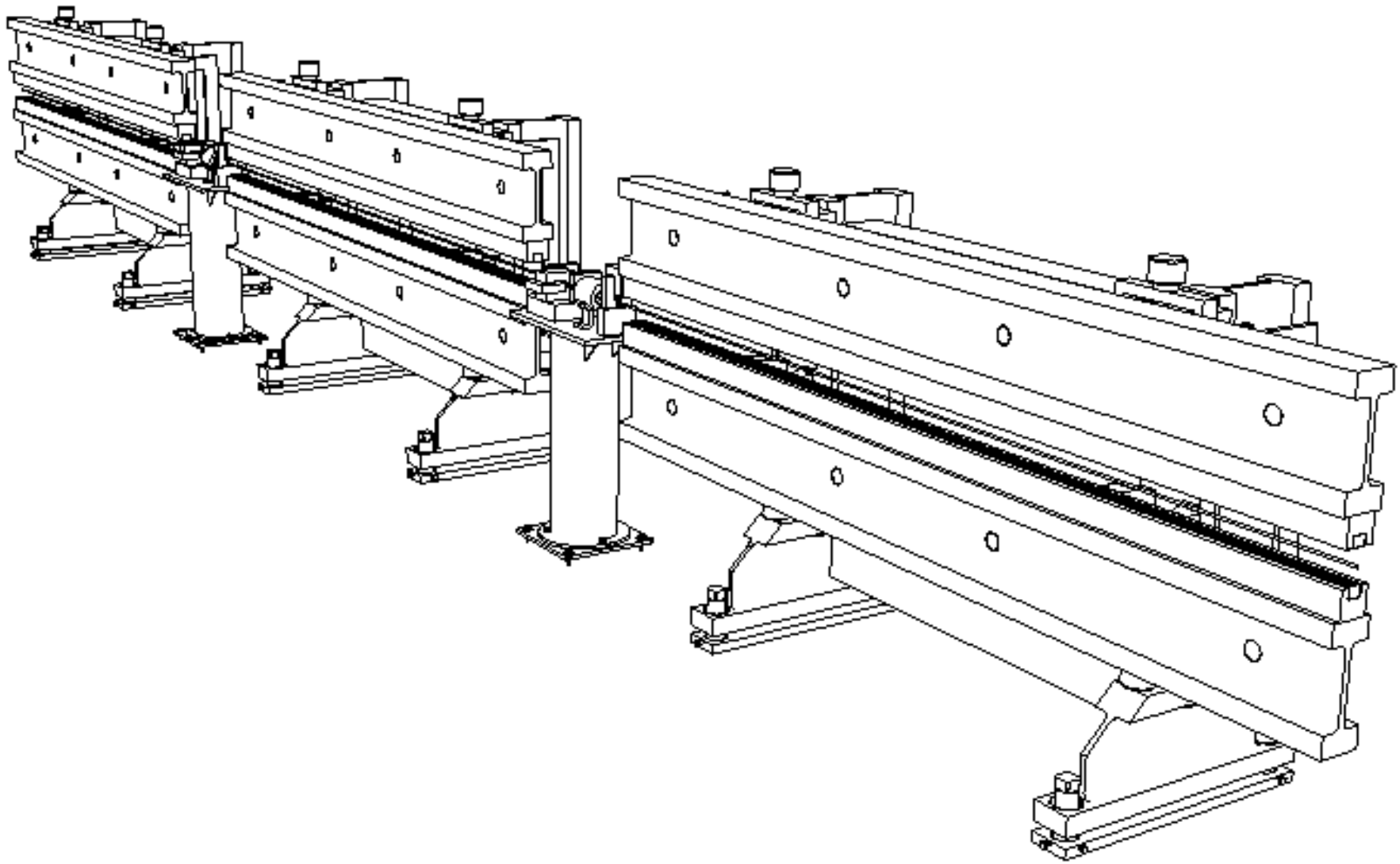


Fig 1



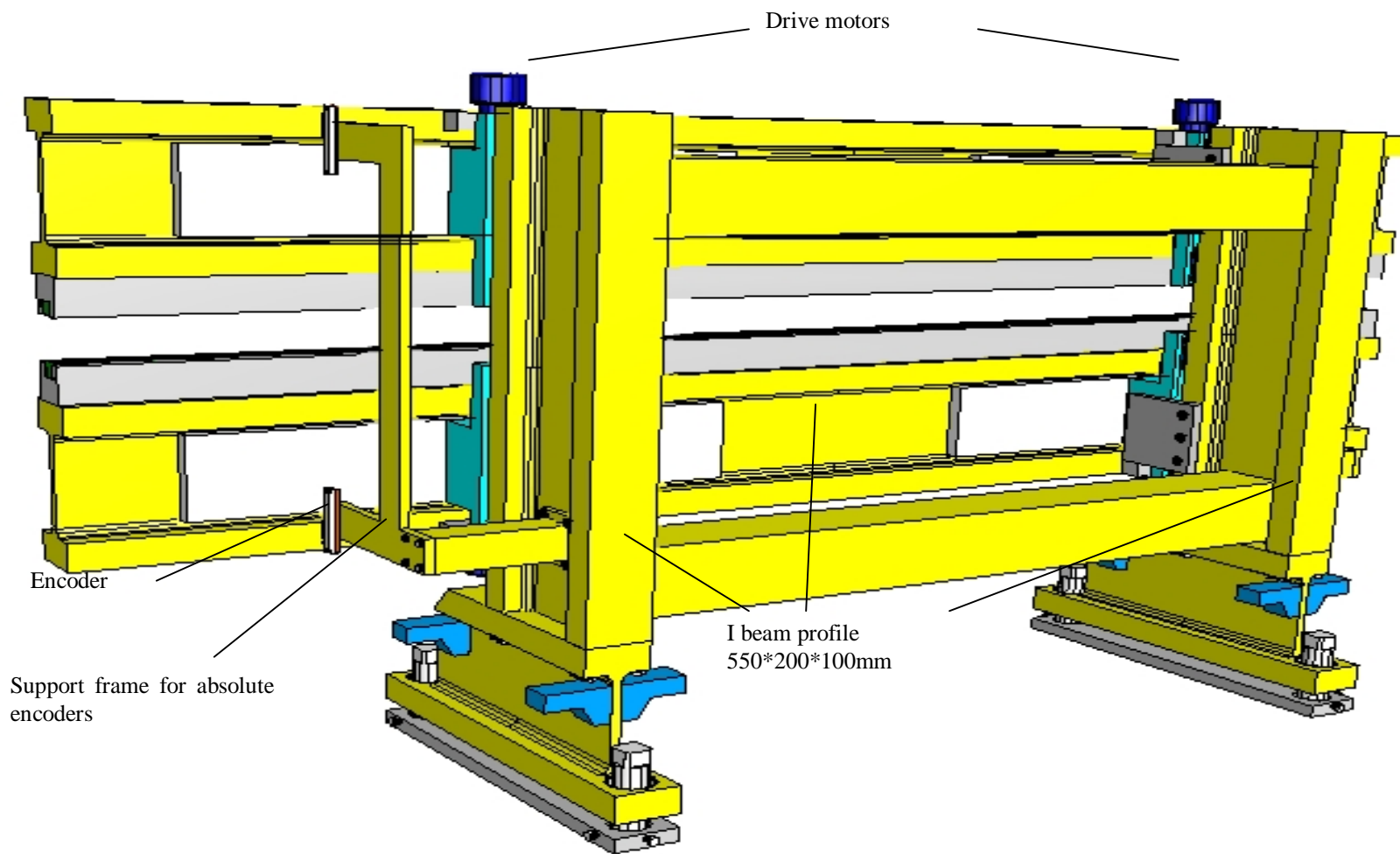


Fig 3

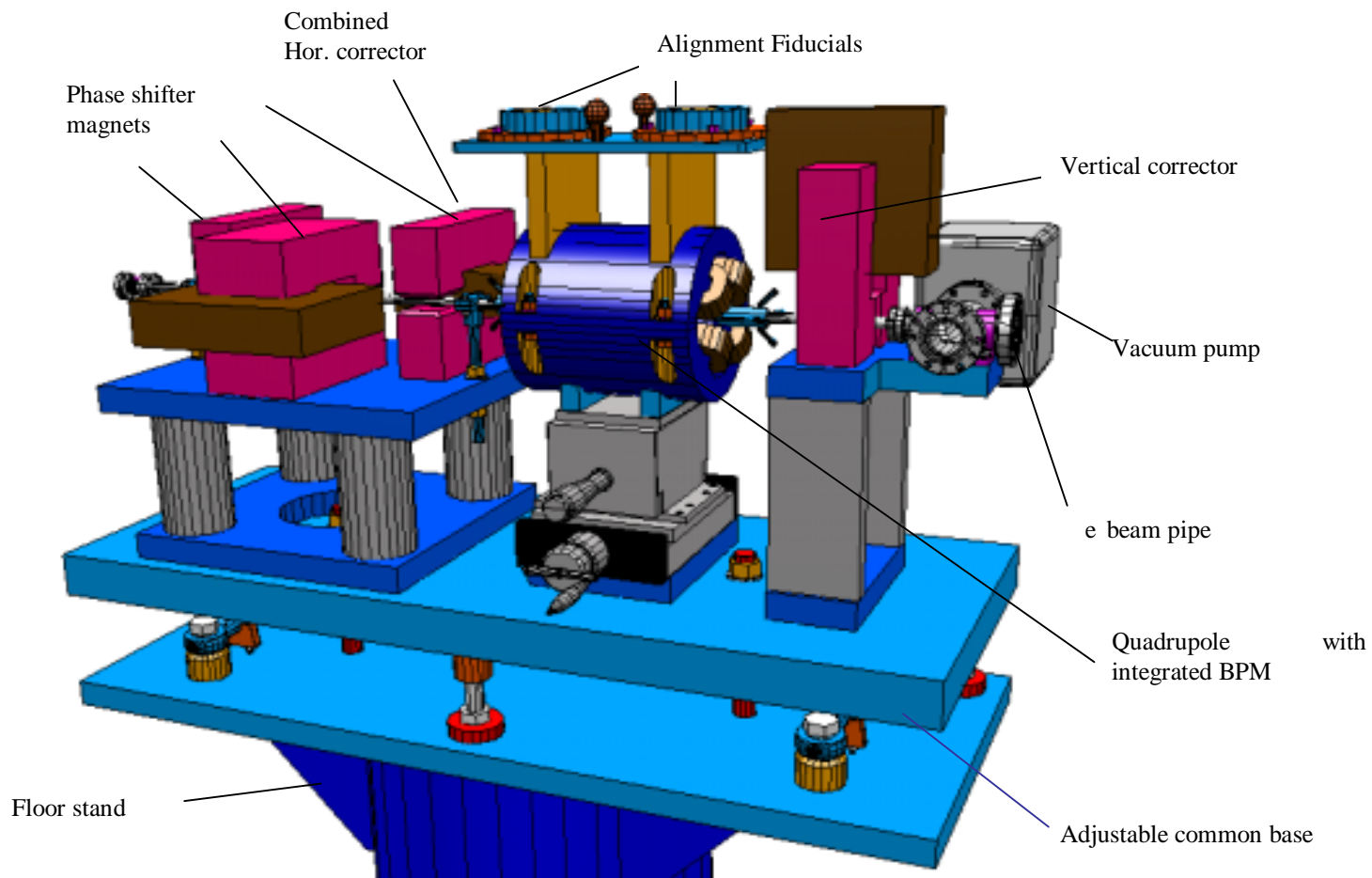


Fig 4

Device	Type	E [GeV]	Wavelength Range [nm]	λ_0 [mm]	ρ^* [10^4]	K_{Max}	B_{Max} [T]	Gap_{Min} [mm]	β [m]	L_{sat}^+ [m]	L_{Tot}^{++} [m]	# of Seg-ments**
SASE1	planar	25	0.1-0.35	60	4.2	7.5	1.33	12	45	220	323.3	53
SASE2	planar	25	0.085	45	3.6	4.0	0.95	12	45	210	311.1	51
SASE3	planar	23	0.10	45	3.8	4.0	0.95	12	45	185	274.5	45
SASE4	planar	25	0.3-1.0	60	4.2	7.5	1.33	12	45	220	323.3	53
SASE5	helical	23	0.4-2.5	107	14.5	9.6	0.96	12	15	120	176.9	29
U1-U5 +++	planar	30	0.0083-0.025 0.0028-0.0083	30	----	3.1	1.10	6	45	50.0 250 total	61.0 305 total	10 50 total
Sum										1405	1714.1	281

+ The saturation length L_{sat} is taken as the required net magnetic length of the undulator

++ The total length L_{tot} of an undulator system includes the saturation length plus 1.1m for intersections (Quadrupoles, phase shifters, correctors, diagnostics pumps etc) and 20% contingency for field errors, misalignment etc. For the spontaneous radiators no contingency for the device length is considered.

+++ For the spontaneous radiators U1-U5 the wavelength range given is for the 1st and 3rd. harmonic. Here L_{Sat} represents the magnetic length of a device. The summation in the bottom line includes 5 devices.

* For SASE1-4 a normalized emittance ϵ_n of $1.6 \cdot 10^{-6}$ m, an energy spread of 2.5MeV and a peak current of 5000A is used. An energy spread of 6.0 MeV is assumed for SASE5, which takes into account the energy spread caused by SASE3. ρ is always calculated for the shortest wavelength, i.e. the largest possible gap.

** Length assumptions: Undulator segment : 5.0m ; Intersection : 1.1m ; resulting cell length : 6.1m ;

Table 1 : Parameters for the 10 undulator systems planned for the TESLA X-FEL Laboratory. λ_0 denotes the undulator period length, ρ the Pierce parameter, B_{Max} , K_{Max} the maximum peak field and undulator deflection parameter at the minimum gap position, Gap_{Min} , respectively, β the average β function in the undulator region. See also the footnotes.

Status of the 3D Time-Dependent FEL Simulation Code GENESIS 1.3

S. Reiche^a, B. Faatz^b

^aDepartment of Physics & Astronomy, UCLA, Los Angeles, CA 90095-1547

^bDeutsches Elektronen Synchrotron, Notkestr. 85, 22607 Hamburg

Since its release in 1999 the 3D time-dependent simulation code GENESIS 1.3 has become a helpful tool for the design-studies and analysis of a single-pass Free-Electron Lasers experiments. With the latest version new features have been added such as support for wake-fields and incoherent spontaneous radiation. In addition the more modular structure of the open-source code and the improved support of external input files allow a better understanding of the code, supporting users who want to add new features to the code.

1. Introduction

Numerical simulations have become an essential part of any FEL project. They are used to either conduct design-studies for proposed experiments or to compare experimental results with the underlying theory embedded in the codes. Numerous codes have been written focusing on the specific FEL interaction between electron beam and radiation field within an undulator. Most of them use simplifications such as the steady-state regime or axi-symmetric beams.

Since its first release the FEL simulation code GENESIS 1.3 [1] is used at various FEL labs around the world and extends the set of time-dependent FEL codes [2,3] by treating the FEL interaction self-consistently in all dimensions. It has been successfully benchmarked with FEL experiments [4] and other codes [5].

2. The Physical Model

The core of the physical model in GENESIS 1.3 is a finite-difference based solver for the eikonal FEL field equations [6] using the alternating direction implicit (ADI) method on a Cartesian 2D mesh. A 4th order Runge-Kutta solver integrates the equation of motion for the electron energy and phase while a symplectic solver tracks the transverse variables through the magnetic lattice of the undulator.

Two new features are incorporated with the propagation of the electron beam. The effect of energy loss due to spontaneous radiation and the growth of the energy spread due to the quantum fluctuation of the spontaneous radiation follow an analytical model [7] and is applied to the particle distribution without introducing unphysical bunching effects in the longi-

tudinal phase space.

The second feature is the effect of wake fields on the electron beam which is mainly modeled by a mean energy loss per integration step. The wake-field potential has to be calculated prior to the run of GENESIS 1.3 and supplied by an external file. Neither the choice of the wake field model nor the explicit calculation of the wake field potential is part of the GENESIS 1.3 distribution and has to be done by 3rd party programs.

3. Interface

The list of input parameter has been extended to roughly 100 parameters, mostly replacing less intuitive parameters. Still the single input is only capable to describe an FEL under certain approximations or assumptions such as predefined bunch profiles or fixed undulator and focusing lattice. To allow more flexibility for the user the GENESIS 1.3 input has been extended to multiple input files, each describing a specific part of the simulation. In particular it allows an easy interface to other simulation tools for e.g. start-end or two stage FEL simulations.

The magnetic field can be describe up to the level of each individual undulator pole and includes the main undulator field, arbitrary quadrupole and solenoid fields as well as field errors, quadrupole misplacements and corrector magnets. The structure of this ASCII input file can be simplified by formatting commands and comments for easy reading and editing by the user.

Similar, beam parameters as a function of the longitudinal position within the bunch as well as entire sample distributions of the complete 6D phase space can be imported into GENESIS 1.3 to model the elec-

tron beam with a high level of detail and flexibility.

Several external programs have been written to support the use of GENESIS 1.3. They simplify the set up of input decks, calculate analytical results or supply correct magnet strength compensating field errors.

4. Outlook

GENESIS 1.3 is written in FORTRAN, which implies two major drawbacks. First, the size of the memory demand is determined during compilation time. Thus the efficiency of the memory usage is low. In particular the array containing the slippage field is the dominant part of the high memory demand of GENESIS 1.3, although not used for steady-state simulations. The other drawback is the poor support of FORTRAN for string processing. As a consequence the functionality of the external input files are limited.

Those problems are solved if the code is converted to C or C++, using dynamical allocation of memory and a wide library support for input and string parsing. It is a prerequisite step for extending the input and output to other file formats. Two promising formats are SDDS [8] and XML [9]. The first allows a better interface to other codes such as ELEGANT [10] as well as the support by an extensive library to process and display the GENESIS 1.3 output. XML is currently the most promising standard for any kind of ASCII documents. It automatically guarantees validity of any input or output file due to its strict format and syntax requirement. GENESIS 1.3 files can rely on compability to any other program supporting the XML standard.

The main algorithm of GENESIS 1.3 in time-dependent mode requires only to pass a limited amount of information to adjacent slices. Thus GENESIS 1.3 can be ported to a parallel architecture without any major modification in the code. Using the message-passing interface (MPI) [11] for synchronizing the nodes of the parallel computer and passing the required data to the next nodes will significantly reduce the computational time for CPU intensive time-dependent simulations.

5. Acknowledgment

The authors would like to thank W.M. Fawley, M. Borland, P. Elleaume, R. Bakker and J. Diemer for their helpful discussion on GENESIS 1.3.

REFERENCES

1. S. Reiche, Nucl. Inst. & Meth. **A429** (1999) 243
2. W.M. Fawley, *An Informal Manual for GINGER and its Post-processor XPLOTGIN*, LBID-2141, CBP Tech Note-104, UC-414, 1995
3. E.L. Saldin, E.A. Schneidmiller and M.V. Yurkov, Nucl. Inst. & Meth. **A429** (1999) 233
4. A. Murokh, *Measuring VISA-FEL radiation and electron beam properties inside the undulator*, presented at this conference.
5. S.G. Biedron *et al.*, Nucl. Inst. & Meth. **A445** (2000) 110
6. R. Bonifacio, C. Pellegrini and L. Narducci, Opt. Comm. **50** (1984) 373
7. E.L. Saldin *et al.*, Nucl. Inst. & Meth. **A381** (1996) 545
8. M. Borland, *A Self-Describing File Protocol for Simulation Integration and Shared Postprocessors*, Proc. 1995 PAC, Texas, (199 6) 2184
9. *Extensible Markup Language (XML) 1.0 (Second Edition)*, W3C, eds. T. Bray, J. Paoli, C.M. Sperberg-McQueen, E. Maler, (2000) (<http://www.w3.org/TR/REC-xml>)
10. M. Borland, Proc. of the ICAP-2000 Conference
11. *Message Passing Interface Forum. MPI: A message-passing interface standard*. Computer Science Dept. Technical Report CS-94-230, University of Tennessee, Knoxville, TN, 1994

An Analytical Description of Longitudinal Phase Space Distortions in Magnetic Bunch Compressors

E.L. Saldin ^a, E.A. Schneidmiller ^a, M.V. Yurkov ^b

^a*Deutsches Elektronen-Synchrotron (DESY), Notkestrasse 85, D-22607 Hamburg, Germany*

^b*Joint Institute for Nuclear Research, Dubna, 141980 Moscow Region, Russia*

Abstract

In this paper we consider a possible mechanism of strong distortions of longitudinal phase space due to collective effects in an electron bunch passing a magnetic bunch compressor. Analytical expressions are derived for the case of a linear compression. The main emphasis is put on analysis of coherent synchrotron radiation (CSR) effects.

1 Introduction

Magnetic bunch compressors are designed to obtain short electron bunches with a high peak current for linac-based short-wavelength FELs [1–5] and future linear colliders [5–7]. The basic principle of compression is very simple. A relativistic electron bunch accumulates energy chirp while passing RF accelerating structures off-crest and then gets longitudinally compressed due to an energy-dependent path length in the magnetic compressor (for instance, in a chicane). Since, however, electron bunches are very short and intensive, collective effects like coherent synchrotron radiation (CSR) [8] can seriously influence beam dynamics in compressors [9].

In the recent experiments with bunch compressors [10–12] the fragmentation of longitudinal phase space has been observed. The self-consistent simulations [13] of beam dynamics in the TESLA Test Facility (TTF) bunch compressor chicane (BCC), taking into account CSR effects, have also shown phase space fragmentation. It has been explained by strong enhancement of CSR effects due to the locally peaked (non-Gaussian) density distribution created during compression process because of RF nonlinearity (see also [14]).

It has been mentioned in [13] that another mechanism can be considered which is also relevant for the ideal linear RF modulation (or, even without modulation). Namely, high-frequency components of the beam current spectrum (higher than

typical inverse pulse duration) cause energy modulations at the same frequencies due to wakefields. The energy modulation is converted into an induced density modulation while the beam is passing the bunch compressor. If the wakefields are strong enough, the induced modulation can be much larger than the initial one. In other words, the system can be treated as a high-gain klystron-like amplifier. The general tendency is that higher frequencies (to some extent) are going to get amplified stronger so that they may become much better pronounced in comparison with the case of undisturbed compression. Thus, the charge distribution and, more generally, the longitudinal phase space can be essentially modified.

In this paper we study such a mechanism analytically in linear approximation. Since it is difficult to measure (simulate) small high-frequency perturbations in the initial state of the beam, one cannot exactly predict its final state. Thus, our goal is to calculate (estimate) the gain as a function of frequency. If the gain is large then one may expect significant modifications of longitudinal phase space in the bunch compressor, and vice versa. In section 2 we study the dynamical aspect of the problem assuming linear energy chirp along the beam and the given amplitude of parasitic energy modulation at some frequency. In section 3 we consider the case when these energy perturbations are created due to wakefields upstream of bunch compressor and in section 4 we thoroughly study CSR in the bunch compressor chicane.

2 Compression of the beam with linear energy chirp and superimposed sinusoidal modulation

In this paper we consider 1-D model of the electron beam neglecting all the transverse effects. An undisturbed phase space distribution of the beam with dc current, linear energy chirp along the beam and Gaussian energy spread can be described with the following function:

$$f(s, \delta\gamma) = \frac{I_0}{\sqrt{2\pi}\sigma_\gamma} \exp\left[-\frac{(\delta\gamma - h\gamma_0 s)^2}{2\sigma_\gamma^2}\right], \quad (1)$$

where s is the coordinate along the beam (particles with positive values of s are placed behind the particle with $s = 0$), $\gamma_0 = \mathcal{E}_0/(mc^2)$ is the nominal energy in units of the rest energy, m is electron's mass, c is the velocity of light, $\delta\gamma = (\mathcal{E} - \mathcal{E}_0)/(mc^2)$ is the energy deviation from the nominal value, $\sigma_\gamma = \sigma_\mathcal{E}/(mc^2)$ is the rms local energy spread, $h = d(\delta\gamma)/(\gamma_0 ds)$ describes linear energy chirp along the beam, I_0 is the beam current. Normalization is chosen in such a way that after integration over $\delta\gamma$ we get the current. We assume γ_0 to be large and consider small energy deviations $\delta\gamma \ll \gamma_0$ although formally we let $\delta\gamma$ extend from $-\infty$ to ∞ . The model of dc current allows us to exclude edge effects from consideration and to deal with small sinusoidal modulations.

To describe phase space transformation in the bunch compressor we assume a linear dependence of path length S in the compressor on $\delta\gamma/\gamma_0$ described by compaction factor¹

$$R_{56} = \frac{dS}{d(\delta\gamma/\gamma_0)} = \frac{ds}{d(\delta\gamma/\gamma_0)}.$$

Then a particle position in the beam before and after compression, s_i and s_f , are connected by

$$s_f = s_i + R_{56} \frac{\delta\gamma}{\gamma_0}.$$

Therefore, to describe the final state of the beam we should substitute s in (1) by $s - R_{56}\delta\gamma/\gamma_0$. Then the new distribution will have the form of (1) where I , σ_γ , and h are substituted by CI , $C\sigma_\gamma$, and Ch , respectively. Here C is the compression factor:

$$C = \frac{1}{1 + hR_{56}}.$$

For compression one should provide $hR_{56} < 0$. For instance, $R_{56} < 0$ for the chicane so that h has to be positive in this case. In addition, in this paper we restrict our consideration by the condition $1 + hR_{56} > 0$, i.e. the beam is undercompressed.

Now let us consider an energy modulation at some frequency ω on top of the linear chirp. In front of the bunch compressor the phase space distribution has the form:

$$f(s, \delta\gamma) = \frac{I_0}{\sqrt{2\pi}\sigma_\gamma} \exp \left\{ -\frac{[\delta\gamma - h\gamma_0 s + \Delta\gamma \sin(ks)]^2}{2\sigma_\gamma^2} \right\},$$

where $k = \omega/c$ and $\Delta\gamma$ is the amplitude of energy modulation. As it was done above, we substitute s by $s - R_{56}\delta\gamma/\gamma_0$ to describe the change of distribution function in the bunch compressor. Then we integrate over $\delta\gamma$ in order to get current as a function of s :

$$I(s) = \frac{I_0}{\sqrt{2\pi}\sigma_\gamma} \int_{-\infty}^{\infty} d\delta\gamma \exp \left\{ -\frac{[\delta\gamma(1 + hR_{56}) - h\gamma_0 s + \Delta\gamma \sin(ks - kR_{56}\delta\gamma/\gamma_0)]^2}{2\sigma_\gamma^2} \right\}$$

¹ Compaction factor is generally defined for momentum deviations $\delta p/p_0$. For considered here ultrarelativistic case $\delta p/p_0 = \delta\gamma/\gamma_0$.

After change of variables $x = [\delta\gamma(1 + hR_{56}) - h\gamma_0 s]$ the integral takes the following form:

$$I(s) = \frac{CI_0}{\sqrt{2\pi}\sigma_\gamma} \int_{-\infty}^{\infty} dx \exp \left\{ -\frac{[x + \Delta\gamma \sin(Cks - CkR_{56}x/\gamma_0)]^2}{2\sigma_\gamma^2} \right\}$$

The integral of such a form is known to describe the process of density bunching starting from initial sinusoidal energy modulation but without linear energy chirp (see, for instance, [15]). Making integration and Fourier expansion, one gets:

$$I(s) = CI_0 \left[1 + 2 \sum_{n=1}^{\infty} J_n \left(nCkR_{56} \frac{\Delta\gamma}{\gamma_0} \right) \exp \left(-\frac{1}{2} n^2 C^2 k^2 R_{56}^2 \frac{\sigma_\gamma^2}{\gamma_0^2} \right) \cos(nCks) \right]. \quad (2)$$

Here J_n is the Bessel function of n th order. Without compression ($h = 0$, $C = 1$) the expression (2) is reduced to the well-known one [15].

Analyzing (2) we see that the frequency range (of initial modulation), in which the beam can be effectively bunched, is limited by $k \leq (CR_{56}\sigma_\gamma/\gamma_0)^{-1}$. Within this range the condition $Ck|R_{56}|\Delta\gamma/\gamma_0 \geq 1$ means that the beam is completely bunched and the phase space is fragmented. For $k \simeq (CR_{56}\sigma_\gamma/\gamma_0)^{-1}$ this happens when $\Delta\gamma \geq \sigma_\gamma$. It is worth mentioning that σ_γ always stands for the initial energy spread (before compression).

In this paper we will use linear approximation assuming that $Ck|R_{56}|\Delta\gamma/\gamma_0 \ll 1$. This leaves us with only the first harmonic of the beam current ($J_1(X) \simeq X/2$):

$$I(s) \simeq CI_0 [1 + \rho_{\text{ind}} \text{sgn}(R_{56}) \cos(Cks)] , \quad (3)$$

where $\text{sgn}(R_{56})$ is the sign of R_{56} and ρ_{ind} is the amplitude of the first harmonic in the final state of the beam:

$$\rho_{\text{ind}} = Ck|R_{56}| \frac{\Delta\gamma}{\gamma_0} \exp \left(-\frac{1}{2} C^2 k^2 R_{56}^2 \frac{\sigma_\gamma^2}{\gamma_0^2} \right) . \quad (4)$$

We have considered here the model of infinitely long beam. The results of this paper can be used for a bunch with finite length σ as soon as the following condition is satisfied:

$$k\sigma \gg 1 . \quad (5)$$

The influence of beam emittance ϵ on longitudinal dynamics is negligible when

$$k\epsilon S_c/\beta \ll 1 , \quad (6)$$

where S_c is the length of a path through compressor and β is the beta-function.

3 Wakefields upstream of a bunch compressor

Let us assume that upstream of the bunch compressor there is a small density perturbation ρ_i at some frequency:

$$I(s) = I_0 [1 + \rho_i \cos(ks)] . \quad (7)$$

Due to some wakefields upstream of compressor the beam gets modulated in energy at the same frequency with the amplitude $\Delta\gamma$. Describing the action of wakefields by longitudinal impedance $Z(k)$ we can connect the amplitudes of energy and density modulations as follows:

$$\Delta\gamma = \frac{|Z(k)|}{Z_0} \frac{I_0}{I_A} \rho_i , \quad (8)$$

where $Z_0 = 377 \Omega$ is the free-space impedance and $I_A = 17$ kA is the Alfvén current. Then, using (4) we calculate the amplitude of the induced density modulation at the end of bunch compressor. In general case, to find final density modulation ρ_f one should sum up induced modulation and (transformed to the end of compressor) initial one, taking care of phase relations. But in this paper we use approximation

$$\rho_i \ll \rho_{\text{ind}} \ll 1 .$$

In other words, $\rho_f \simeq \rho_{\text{ind}}$ and the gain in density modulation

$$G = \frac{\rho_f}{\rho_i} \simeq \frac{\rho_{\text{ind}}}{\rho_i}$$

is assumed to be high, $G \gg 1$ (otherwise the effect, considered in this paper, is not of great importance). Under this approximation the gain depends neither on phase of $Z(k)$ nor on sign of R_{56} and is equal to

$$G = Ck|R_{56}| \frac{I_0}{\gamma_0 I_A} \frac{|Z(k)|}{Z_0} \exp\left(-\frac{1}{2}C^2 k^2 R_{56}^2 \frac{\sigma_\gamma^2}{\gamma_0^2}\right) \quad (9)$$

For broadband nonresonant wakefields the product $k|Z(k)|$ is usually a growing function of k . For such cases the maximal gain is achieved at

$$k_{\text{opt}}^{-1} \simeq \frac{\sigma_\gamma}{\gamma_0} |R_{56}| C . \quad (10)$$

The optimal final frequency (when the beam is compressed) roughly does not depend on compression factor C . A crude estimate for the maximal gain is

$$G_{\text{max}} \simeq \frac{I_0}{\sigma_\gamma I_A} \frac{|Z(k_{\text{opt}})|}{Z_0} . \quad (11)$$

The term $I_0/(\sigma_\gamma I_A)$ is proportional to a longitudinal brightness (particles density in longitudinal phase space). In practice the phase space distribution can be of complex shape. We note that the local energy spread should be taken for estimations of amplification effect.

4 CSR in the bunch compressor chicane

Wakefields can also exist inside bunch compressors. We consider here coherent synchrotron radiation which is an intrinsic feature of magnetic compressors. CSR effects can be minimized there but not avoided. Recently, CSR-induced beam instability in storage rings has been investigated [16]. That instability develops continuously, in small increments, like most instabilities of relativistic electron beams. We analyze here quite different situation when the longitudinal phase space can be suddenly modified while the electron beam is passing a single element of the beamline. In this sense one can think of such an analogy as a klystron versus a travelling-wave tube.

While the formulae of the previous section are pretty general and do not depend on a type of the bunch compressor, in this section we have to choose a specific model. We consider a symmetric three-dipole chicane² where the first and the last dipoles have the length L_d , and the middle one is as long as $2L_d$. The bending angle in the first dipole θ is small, $\theta = L_d/R \ll 1$ (R is the bending radius), and the total length L_c of BCC satisfies the condition

$$L_c \gg 4L_d. \quad (12)$$

The compaction factor can then be expressed in a simple form: $R_{56} = -L_c\theta^2$. To describe CSR we use the steady-state model neglecting edge effects. The domain of validity of this model can be estimated on the base of results obtained in [17]:

$$L_d \gg (R^2/k)^{1/3} \ln(\gamma_0^3/kR), \quad (13)$$

assuming that inequality $\gamma_0^3/kR \gg 1$ always holds. We neglect the influence on CSR of transverse beam size and of the screening effect of the vacuum chamber requiring that [9,18]

$$(b^3/R)^{1/2} \ll k \ll (\sigma_\perp^3/R)^{1/2}, \quad (14)$$

where b is the transverse size of vacuum chamber and σ_\perp is that of electron beam. Under the conditions (13) and (14) the module of CSR impedance in the first and

² Under limitations, accepted in this section, all the results are valid for a four-dipole chicane, too.

the last dipoles can be expressed as [18]

$$\frac{|Z(k)|}{Z_0} = \frac{2\Gamma(2/3)}{3^{1/3}} \frac{L_d k^{1/3}}{R^{2/3}}, \quad (15)$$

and in the middle dipole it is two times larger. Here $\Gamma(\dots)$ is the complete gamma-function.

The accepted model allows us to simplify calculation of the gain. Indeed, under the condition (12) we neglect longitudinal motion inside the dipoles so that the density bunching happens only between dipoles. On the other hand, based on (13) we neglect CSR-induced energy modulation outside the dipoles. Thus, we separate these two processes.

In the framework of this model we consider the two-stage amplification in the bunch compressor. Indeed, initial density perturbation (7) causes energy modulation according to (8), (15). Then we get induced density modulation at the entrance to the middle dipole. We assume it to be much larger than the initial one. Then partially compressed beam (compaction factor is equal to $R_{56}/2$) in the middle dipole gets again modulated in energy at a new frequency:

$$k_{\text{middle}} = \left(1 + \frac{hR_{56}}{2}\right)^{-1} k = \frac{2Ck}{C+1},$$

where C is the total compression factor of BCC. As a result, we have an induced density modulation at a final frequency Ck in the end of BCC, which is again assumed to be much larger than the modulation in the middle dipole. So, we assume the gain in each stage to be large and neglect phase relations as we did in the previous section.

The calculation of the gain in each stage is similar to that presented in the previous section. The main difference is that now the energy modulation linearly increases inside dipoles. Therefore, a particle with a given energy deviation (at the end of the dipole) gets two times smaller angular kick in comparison with the case when this energy deviation exists in front of the dipole. So, the gain is reduced by a factor of two in each stage. Leaving out the details of calculation, we present here the final result for the BCC gain in density modulation:

$$G\left(\frac{k}{k_{\text{opt}}}\right) = G_{\text{max}} \left(\frac{k}{k_{\text{opt}}}\right)^{8/3} \exp\left\{-\frac{4}{3} \left[\left(\frac{k}{k_{\text{opt}}}\right)^2 - 1\right]\right\}, \quad (16)$$

where the optimal frequency is given by

$$k_{\text{opt}}^{-1} = \sqrt{\frac{3}{8}} |R_{56}| \frac{C(C^2 + 1)^{1/2} \sigma_\gamma}{C + 1 \gamma_0}, \quad (17)$$

and the maximal gain is

$$G_{\max} = ag_0^2 f_1(C) . \quad (18)$$

Here a is numerical constant (e is the base of natural logarithm):

$$a = 2^4 \left(\frac{2}{e^4} \right)^{1/3} \left(\frac{\Gamma(2/3)}{3} \right)^2 \simeq 1.08 ,$$

g_0 is the gain parameter:

$$g_0 = \frac{I_0}{\sigma_\gamma I_A} \left(\frac{\gamma_0}{\sigma_\gamma} \right)^{1/3} \frac{L_d}{(R^2 |R_{56}|)^{1/3}} , \quad (19)$$

and the function of compression factor, $f_1(C)$, has the form:

$$f_1(C) = \frac{2C^{2/3}(C+1)^{1/3}}{(C^2+1)^{4/3}} . \quad (20)$$

Since energy modulations are induced inside bunch compressor, one can also calculate the gain in energy modulation. If there is a small perturbation with amplitude $\Delta\gamma$ in front of BCC, it is converted into the density modulation at the entrance to the middle dipole. There CSR induces energy modulation which is assumed to be much larger than the initial one. Then the beam gets further bunched in density while moving to the entrance of the last dipole. In that dipole the energy modulation is induced (much larger than that in the middle dipole). The gain, defined as a ratio between final and initial amplitudes of energy modulation, is then given by (16) with k_{opt} given by (17). The maximal gain differs from (18) and can be written as

$$G_{\max} = 2ag_0^2 f_2(C) , \quad (21)$$

where

$$f_2(C) = \frac{2C^2(C+1)^{1/3}}{(C^2+1)^{4/3}} . \quad (22)$$

Let us comment on the behaviour of functions $f_1(C)$ and $f_2(C)$. As we have already mentioned, the final optimal frequency is almost independent of compression factor. The initial optimal frequency is lower when the compression factor is larger, i.e. CSR is weaker in the first dipole. In addition, the bunching process is less effective for lower frequencies. This explains why $f_1(C)$ quickly decreases. The counteracting process is the growth of the beam current during compression. In the last dipole CSR effects are stronger for larger compression factor. This is important for the gain in energy modulation. As a result, function f_2 hardly depends

on C in practically interesting region. It is worth mentioning that final density (energy) modulations are defined by the gain and by initial modulations. When C is larger, the gain curve is shifted towards lower frequencies where the components of the beam spectrum are larger, in general. Therefore, one may expect stronger perturbations of the longitudinal phase space in the final state of the beam when compression factor is larger. For the same reason (larger initial modulations) the strongest effect may be observed not at the optimal frequency but at lower frequencies.

References

- [1] J. Andruszkow et al., Phys. Rev. Lett. **85**(2000)3825
- [2] S.V. Milton et al., Nature **292**(2001)2037
- [3] J. Rossbach, Nucl. Instrum. and Methods A **375**(1996)269
- [4] Linac Coherent Light Source (LCLS) Design Report, SLAC-R-521, 1998
- [5] TESLA Technical Design Report, DESY 2001-011
- [6] Zeroth Order Design Report for the Next Linear Collider, SLAC Report 474, 1996
- [7] JLC Design Study, KEK Report 97-1, 1997
- [8] L.V. Iogansen and M.S. Rabinovich, Sov. Phys. JETP **37**(10)(1960)83
- [9] Ya.S. Derbenev et al., "Microbunch Radiative Tail-Head Interaction", DESY TESLA-FEL 95-05, 1995
- [10] M. Hüning, Ph. Piot, and H. Schlarb, "Observation of Longitudinal Phase Space Fragmentation at the TESLA Test Facility", Proc. of the FEL 2000 Conf., Durham, USA, to be published in Nucl. Instrum. and Methods A, 2001
- [11] H.H. Braun et al., Phys. Rev. Special Topics - Accelerators and Beams **3**(2000)124402
- [12] Ph. Piot et al., Proc. of EPAC 2000, Vienna, Austria, p.1546(2000)
- [13] T. Limberg, Ph. Piot, and E.A. Schneidmiller, "An Analysis of Longitudinal Phase Space Fragmentation at the TESLA Test Facility", Proc. of the FEL 2000 Conf., Durham, USA, to be published in Nucl. Instrum. and Methods A, 2001
- [14] R. Li, Proc. of EPAC 2000, Vienna, Austria, p.1312(2000)
- [15] L.H. Yu, Phys. Rev. A **44**(1991)5178
- [16] S. Heifets and G. Stupakov, "Beam Instability and Microbunching due to Coherent Synchrotron Radiation", SLAC-PUB-8761 (2001)
- [17] E.L. Saldin, E.A. Schneidmiller and M.V. Yurkov, Nucl. Instrum. and Methods A **398**(1997)373
- [18] J.B. Murphy, S. Krinsky and R.L. Gluckstern, Part. Acc. **57**(1997)9

Photon Diagnostics for the X-ray FELs at TESLA

M. Tischer, P. Ilinski*, U. Hahn, J. Pflüger, H. Schulte-Schrepping

Hamburger Synchrotronstrahlungslabor HASYLAB, DESY, Notkestr. 85, D-22603 Hamburg, Germany

**Advanced Photon Source, Argonne National Laboratory, 9700 S. Cass Ave., Argonne, IL 60439, USA*

An X-ray diagnostic station will be installed for each of the XFEL undulator beamlines at TESLA. Primary purpose of the X-ray diagnostics is to provide an additional tool for alignment and commissioning of the numerous undulator cells along an XFEL beamline independently from electron beam based alignment procedures. Both methods will complement one another. The X-ray diagnostic station will be a sensitive instrument generating essential input for the undulator control system. The diagnostic station will be located about 120 m downstream from the last undulator cell. Total flux measurements will verify the XFEL's gain. Analysis of the spectral and spatial distribution of the spontaneous radiation of individual or several consecutive undulator segments will be used to optimize angle and position of the electron beam trajectory, to verify the magnetic gap, and to adjust the phase match between two undulator segments. The two latter purposes cannot be served by electron beam based alignment.

PACS: 41.60.Cr; 42.60.Jf; 07.85.Qe

Keywords: X-ray Free Electron Laser; Photon Beam Characterization; Trajectory alignment; Phase tuning; Imaging optics;

1. Introduction

The FEL laboratory at TESLA will provide ten undulator beamlines, five of them will be SASE undulators, the others spontaneously radiating devices. The overall project is defined in the TESLA Technical Design Report (TDR) [1]. The primary SASE undulators are four planar devices operating in the energy range from 2.5 keV to 14.6 keV. An X-ray FEL undulator system is made of up to ~50 short cells of 6.1 m length. Each undulator cell consists of a variable gap undulator segment of 5 m length and a 1.1 m long intersection module containing various items such as a phase shifter, a quadrupole with an integrated BPM, steering coils, and vacuum components. Gap motion and gap dependent settings of phase shifter, steerers, etc. will be managed within each cell by a local control system which is part of a central undulator control unit.

Primary purpose of the X-ray diagnostics is to have an additional tool for alignment and commissioning of the numerous undulator cells along a XFEL beamline independently from the electron beam based alignment procedure [2-4]. Both methods will complement one another as the latter gives no insight into the magnetic gap or the phase match of adjacent undulator segments. Photon diagnostics has successfully been used for the TESLA Test Facility [5], the LEUTL FEL [6], and has been proposed for the LCLS project [7]; preliminary ideas have also been suggested for TESLA [8].

Here, the X-ray diagnostics for undulator system SASE1 is discussed as a prototype representative for all beamlines. It is located about 120 m downstream of the last undulator cell (Fig. 1) and allows to characterize the radiation of an entire undulator system or individual segments and can be used for photon beam based alignment. It consists of a crystal monochromator as a principal unit, an imaging optics and different detector systems such as a CCD array, pin diodes, and a calorimeter. As all undulators will be equipped with a gap drive individual segments can be selected for diagnosis by switching off, i.e. opening the gap of all other segments. This concept of only one common diagnostics for all undulator cells avoids a multiple installation of identical diagnostic devices which all would have to be calibrated against each other. It rather facilitates a precise alignment and setup of the whole undulator system.

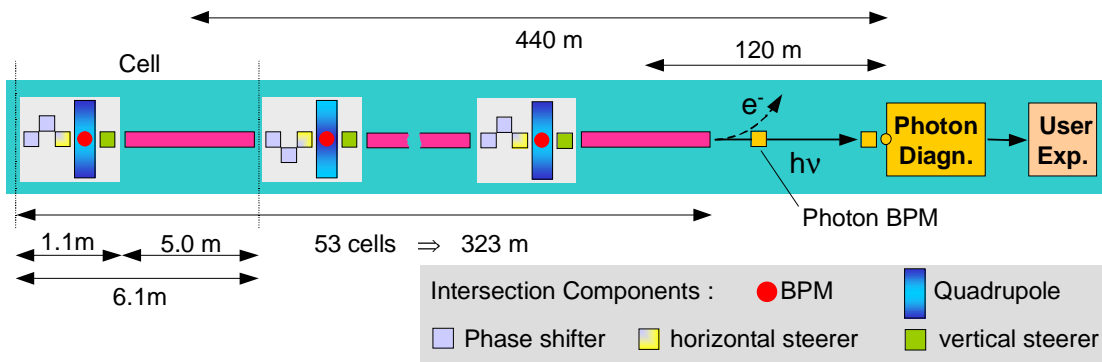


Fig. 1: Schematic outline of a prototype TESLA FEL beamline.

Wavefront calculations have been performed for the parameters of SASE1 [9] using SRW [10] in order to predict the properties of the undulator radiation observed at the diagnostic station. For the ease of comparison all calculations have been performed for an observation point 100 m behind the source. Three major diagnostic issues relate to a proper setup of the undulator cells, namely trajectory alignment, gap adjustment, and phase tuning which are discussed in the following.

2. Trajectory alignment

It has been shown [11] that a random rms quadrupole offset of $1\ \mu\text{m}$ will lead to a FEL gain reduction of $\sim 10\%$. This value, corresponding to a 2nd field integral of $I_2 = 83\ \text{Tmm}^2$, is also considered as upper limit the trajectory displacement within a single undulator segment. The resulting requirement for angular trajectory alignment within a 5 m long undulator segment is $0.2\ \mu\text{rad}$.

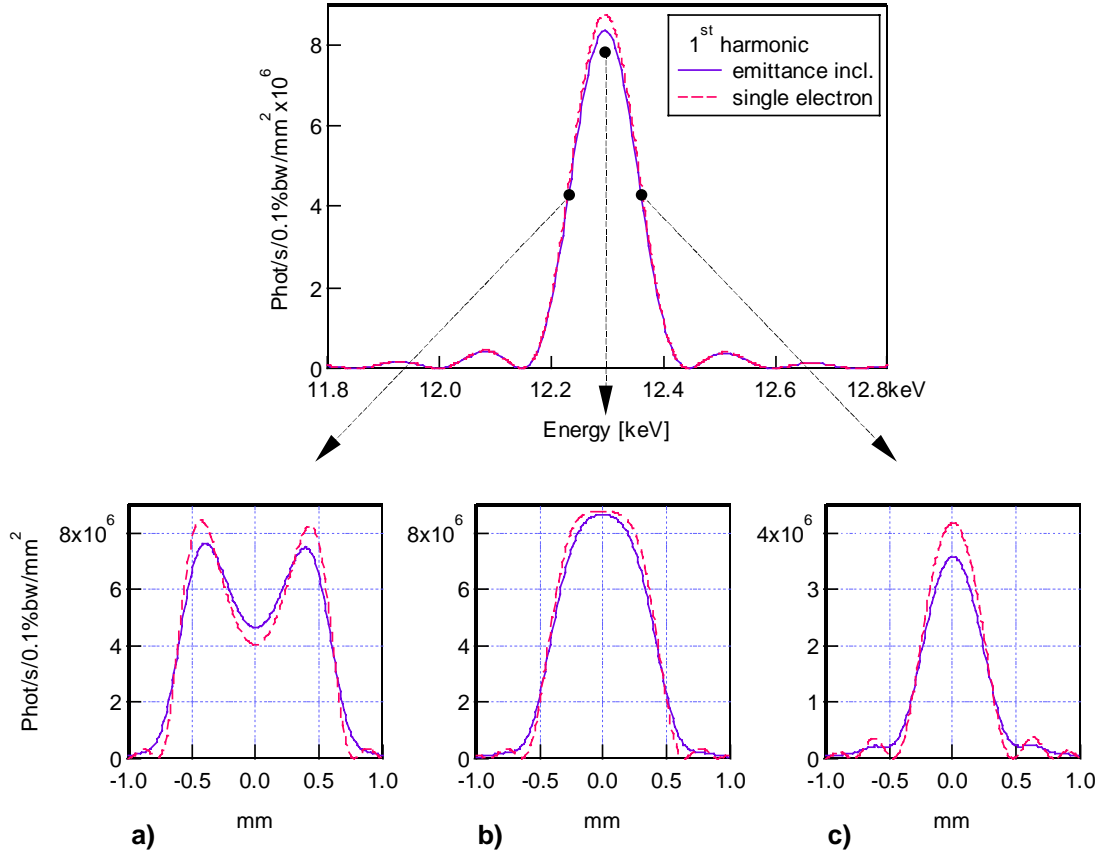


Fig. 2 top part: Energy spectrum of the spontaneous radiation of a single 5 m long undulator segment at a wavelength of $\sim 1\ \text{\AA}$. Solid: emittance effects included, dashed: filament electron beam. Lower part a–c): Profile of the circular beam expected for different observation energies (12.24 keV, 12.30 keV, 12.36 keV) in the vicinity of the undulator peak (arrows).

Spontaneous radiation of the 1st, 3rd or 5th harmonic can be used for the different alignment aspects depending on the required accuracy. The top part of Fig. 2 shows the energy spectrum of the 1st harmonics of a single SASE1 undulator segment for inclusion of the finite emittance (solid) and for a filament electron beam (dashed). As expected, the emittance influence is still small for the (spontaneous) spectrum of the 1st harmonics. The lower part of Fig. 2 displays spatial distributions for slightly different observation energies of the fundamental undulator peak. Detuning of the observation energy towards lower values leads to a broadening accompanied by a splitting of the intensity cone towards a ring. Detuning by $\sim 5\%$ to higher energies (Fig. 2 c) leads to a considerable narrowing of the radiation cone, however to the expense of lower intensity. The center of gravity for all three intensity distributions in Fig. 2 is on the beam axis independent of observing the radiation on- or off-crest of the undulator

spectrum. Therefore the photon beam axis and also the mean undulator trajectory can be detected independently of a possibly incorrect gap setting.

A still smaller spot size is obtained for higher harmonics of the undulator radiation. Fig. 3 compares the spatial distributions for an observation energy detuned by a few ‰ above the higher harmonics peak. As expected the emittance induced portion of the profile broadening becomes more apparent for higher harmonics when the total line width decreases. A full width at half maximum (FWHM) of 330 μm and 280 μm at a distance of 100 m is obtained for the 3rd and 5th harmonic, respectively. Going to even higher energies narrows the spatial distribution only by a negligible amount ($\sim 10\mu\text{m}$) as the photon beam divergence is now dominated by the emittance. Assuming a mean spatial line width of $\sim 330\ \mu\text{m}$, an accuracy of $\sim 7\%$ of the FWHM (working with the 5th harmonics) or correspondingly 20 μm of the obtained spatial distribution has to be achieved in order to cope with the specified angular resolution of 0.2 μrad . The setup described below will meet this requirement.

It is evident that the analysis of the photon spot as a single footprint of the electron trajectory through the undulator cannot distinguish between a shifted and a tilted orbit. Two photon BPMs will be installed in the drift space between undulator exit and the diagnostic station which can also be operated continuously without interference with a user experiment.

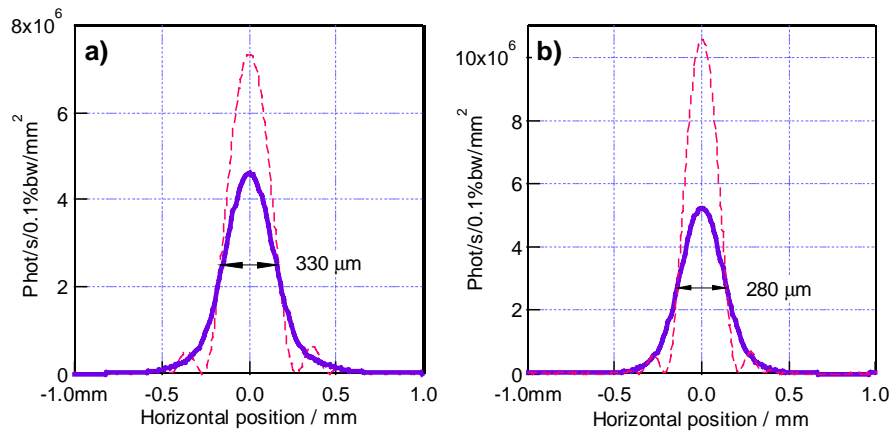


Fig. 3: Intensity profiles of the 3rd (a) and 5th (b) harmonics for the conditions according to Fig. 2c), i.e. an observation energy detuned slightly above the undulator peak.

3. Gap adjustment

One way to adjust the gap of each undulator segment is to take an energy spectrum whose center of gravity defines the energy position of the undulator harmonics for the present gap value which then has to be adjusted. The uncertainty in the measured fundamental energy has to be smaller than the ρ -parameter ($4 \cdot 10^{-4}$), i.e. the undulator harmonics have to be determined with a precision of 18% of the line width.

Alternatively, the gap can be optimized by maximizing the intensity at the desired photon energy which is then kept fixed. Corresponding to the ρ -parameter the precision requirement for the gap adjustment is in the order of $\sim 3 \mu\text{m}$. Fig. 4 displays the intensity obtained for a fixed observation energy at the 5th harmonics (61.5keV) as function of the gap detuning from its nominal value. It can be seen that the observed intensity varies considerably with a small gap misalignment; an intensity drop of $\sim 8\%$ is expected for a gap deviation of $3 \mu\text{m}$. This method will work much faster than the first approach.

Gap tuning of all undulator segments one by one will result in identical fundamental energies of all cells. A tiny taper of the gap along the entire undulator system, which is required to optimize the SASE intensity, has to be fine-adjusted subsequently.

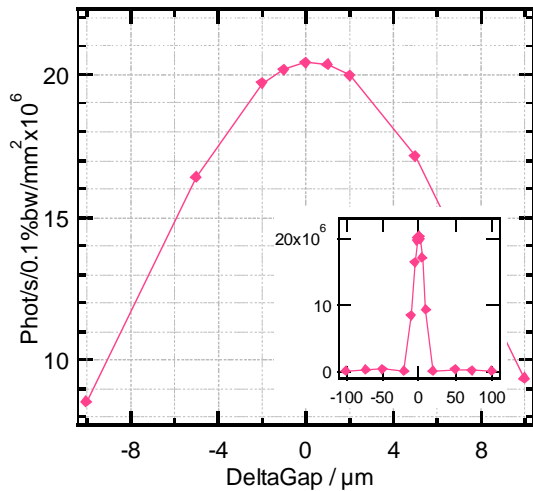


Fig. 4: Photon intensity as function of gap detuning for a constant observation energy of 61.5 keV (5th harm.); the reference gap corresponds to the open gap position (23mm).

4. Phase tuning

Changing the undulator gap will result in a change of the phase relation between two adjacent segments. In order to compensate the wavelength dependent phasing condition, a phase shifter is installed in the intersection module [12]. It consists of a three-magnet chicane which is powered by a gap dependent current, and delays the electron beam so that the radiation from

the following segment is in phase with that of the previous for all wavelengths. The adjustment of the optical phase has to be assured with an accuracy of only $\sim 1\%$ or a few degrees [13].

The determination of the correct phase is based on observing the radiation of two successive undulator segments. The phase relation affects the energy spectrum as well as the spatial distribution of the composed radiation (Fig. 5). For complete phase match the undulator line peaks at E_{fund} . In case of fully destructive interference, the undulator spectrum shows intensity maxima below and above that value. The spatial radiation distribution at $E = E_{\text{fund}}$ is cone-like in the matched phase condition whereas the radiation is emitted in a ring in the destructively interfering case.

The easiest way to monitor the phase is to observe the photon intensity at constant energy $E_{\text{obs}} = E_{\text{fund}}$ while shifting the optical phase in the electron chicane. The detected photon flux shows a cosine dependence with a peak-to-peak amplitude of ~ 400 for a phase advance from π to 2π . This will be sufficient to tune the optical phase within the required accuracy.

5.

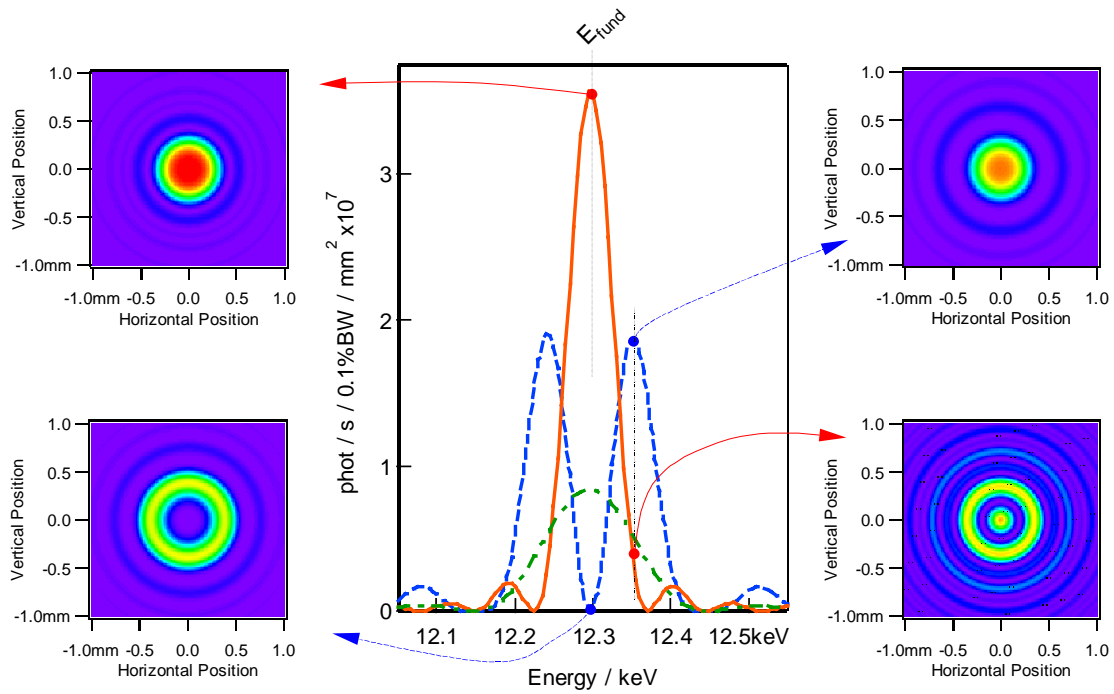


Fig. 5: Spectral distribution of two successive undulator segments (tuned to an energy of 12.3 keV) for a phase difference of 2π (solid) and π (dashed). The corresponding spatial intensity distributions are strongly structured once the detection energy deviates from the undulator fundamental or the phase shift differs from 2π . The spectrum of a single undulator segment is shown for comparison (dot-dash).

Hardware Setup

The photon diagnostic station can be split up into three parts, i.e. the photon beam position monitors, the central imaging station, and a detector unit for observation of integral properties.

Photon BPMs will be used in conjunction with the imaging station to precisely align the trajectories of all undulator segments, in particular to distinguish between transversal and angular displacement. Position-sensitive ionization chambers are present state-of-the-art photon monitors in terms of resolution and are most appropriate for this application as they do not directly interact with the beam. Ionization chambers with so-called backgammon electrodes, which have been developed at Spring8 [14], exhibit a sensitivity of about $1\ \mu\text{m}$ and are ideally suited for our purposes.

The primary part of the photon diagnostic station will image the central cone of the monochromatized undulator beam of one or several undulator segments. It will be possible to observe an image at the energy of the 1st and 5th harmonic of the XFEL undulator through two different viewports. A field of view with a diameter of 5 mm is needed to determine FWHM and shape of the central cone. The undulator beam will be monochromatized using a single crystal Laue-case setup similar to that used at the PETRA-undulator beamline at HASYLAB as shown in Fig. 6. There will be two fixed viewports in order to observe the first and fifth harmonic of the undulator by only rotating the crystal angle. The observation of two angles allows the determination of an absolute energy scale.

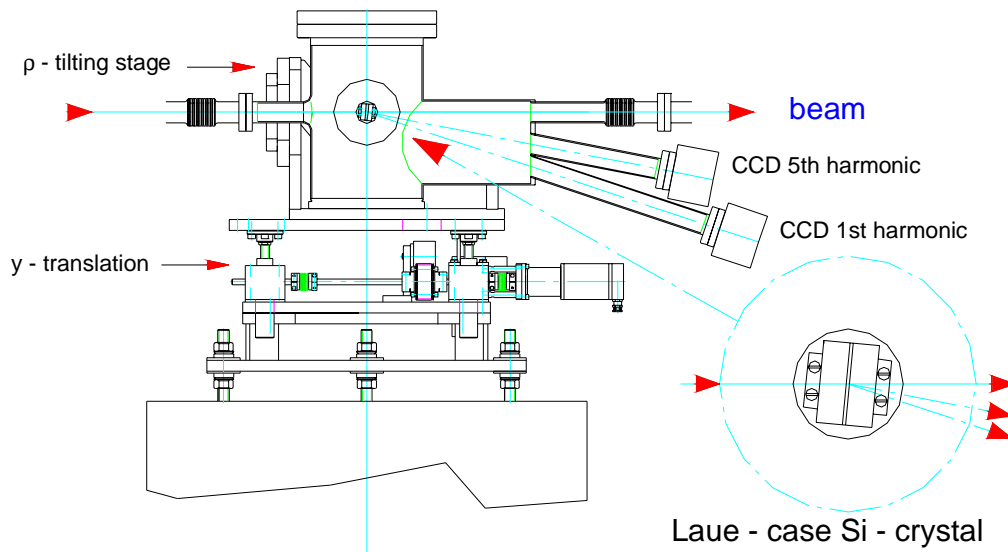


Fig. 6: Schematic view of the diagnostic station setup. A Laue-case silicon crystal monochromatizes the undulator radiation. The central cone will be observed at two photon energies (1st and 5th harm.) through fibre optic viewports coated with fluorescent screens.

Experience with a similar setup at the PETRA beamline [15] with the PETRA storage ring at DESY running at 12 GeV positron energy, shows that the images obtained by a thin Laue-case crystal with a thickness of 200 μm provide a clear picture without additional spots and high energy background. The Laue-case setup is favorable due to the small Bragg angles of 5.49° and 9.17° required for the 5th harmonic using Si(333) and for the 1st harmonic with Si(111), respectively.

An imaging system is proposed composed out of the Laue-case crystal monochromatizing the central cone, projecting it onto a fluorescent screen attached directly onto a fibre optic taper. The fluorescent screen will be either directly coated onto the fibre or be a thin film screen attached to the fibre. This taper is part of a fibre optic vacuum window. At the air side of this window a CCD chip will be directly bonded onto the fibre.

Assuming a field of view of 5 mm^2 and the need for a 12 μm^2 CCD pixel size (16 bit resolution requirement), a taper with an imaging ratio of 1:2.4 (screen side : CCD side) will be installed. The overall resolution of the system using a 1024 \times 1024 pixel CCD chip will be 5 $\mu\text{m}^2/\text{pixel}$. This estimate assumes present day fibre optic tapers with a fibre diameter of 6 μm at the CCD side. A CCD chip with a higher pixel count usually has a larger pixel size and will not give a higher resolution, but will only provide a larger field of view. An option will be replacing the fluorescent screen coating at the fibre end by a doping of the fibre end.

Present day 16 bit resolution CCD systems are driven with a maximum pixel clock of 50 kHz, due to an increase in readout noise at higher clock rates. The dark current in a cooled CCD system is negligible at exposure times in the seconds range. Under these conditions, the setup will be able to provide an image every 20 seconds. A 12 bit system would provide an image in one second or faster, but the dynamic range is too limited to observe the effect of phasing of two undulator segments without changing the exposure time. From our simulations with SRW, we observe a difference in intensity by a factor of 400 while changing the operating conditions from an anti- to a phased mode.

Integral beam properties will be determined in a second station similar to the imaging station described above. The integral power of the spontaneous radiation will be measured with either a pin diode or a calorimeter put into the direct beam. The incident power ranges from about 1 mW (47 mW) for a single pulse to 50 W (2.7 kW) for continuous operation in case of a single (all) undulator segments switched on. Furthermore, a thin diamond crystal in Laue geometry will monochromatize the SASE line to determine the gain and the spectrum. The power in this line will again be measured with either a pin diode or a calorimeter depending on the gain regime of the FEL. The pin diode in the direct beam will then measure the power of the complementary part of the photon spectrum, i.e. the overall background of the SASE line.

References

- [1] TESLA Technical Design Report Part V, Eds.: G. Materlik, T. Tschentscher, TESLA-FEL 2001-05, DESY (2001)
- [2] B. Faatz, TESLA-FEL 2001-04, DESY (2001)
- [3] P. Castro, TESLA-FEL 1997-04, DESY (1997)
- [4] P. Emma, LCLS Technical Notes 00-14, SLAC (2000)
- [5] R. Treusch, T. Lokajczyk, W. Xu, U. Jastrow, U. Hahn, L. Bittner, J. Feldhaus, Nucl. Instr. Meth. A 445, 456 (2000)
- [6] E. Gluskin et al., Nucl. Instr. Meth. A 429, 358 (1999)
- [7] E. Gluskin, P. Ilinski, N. Vinokurov, LCLS Technical Notes 00-13, SLAC (2000)
- [8] P. Elleaume, J. Chavanne, B. Faatz, Nucl. Instr. Meth. A 455, 503 (2000); TESLA-FEL 2000-16
- [9] For all photon spectra calculations the following parameters have been used according to the specifications for SASE1: $E_e = 25$ GeV, $I_e = 1$ nA, $\epsilon_n = 1.6$ mrad mm, $\beta = 45$ m, $\Delta E_e/E_e = 10^{-3}$, $\lambda_U = 60$ mm, $N = 83$ periods, $B_0 = 0.67$ T or $K_{rms} = K_{max}/\sqrt{2} = 2.65$.
- [10] SRW, Version 3.7, ESRF 1997-2000, Authors: O. Chubar, P. Elleaume
- [11] B. Faatz, J. Pflüger, TESLA-FEL 2000-14, DESY (2000)
- [12] J. Pflüger, M. Tischer, TESLA-FEL 2000-08
- [13] B. Faatz, priv. commun.
- [14] K. Sato, T. Kudo, M. Suzuki, T. Ishikawa, Spring8 Annual Report p.181 (1998); K. Sato, H. Tanida, S. Adachi, Proc. SPIE 3774, 114 (1999)
- [15] U. Hahn, H. Schulte-Schrepping, to be published

Statistical properties of SASE FEL radiation: experimental results from the VUV FEL at the TESLA Test Facility at DESY

M.V. Yurkov for TTF FEL Team ¹

*Joint Institute for Nuclear Research, Dubna, 141980 Moscow Region, Russia
Deutsches Elektronen-Synchrotron (DESY), Hamburg, Germany*

Abstract

This paper presents an experimental study of the statistical properties of the radiation from a SASE FEL. The experiments were performed at the TESLA Test Facility VUV SASE FEL at DESY operating in a high-gain linear regime with a gain of about 10^6 . It is shown that fluctuations of the output radiation energy follows a gamma-distribution. We also measured for the first time the probability distribution of SASE radiation energy after a narrow-band monochromator. The experimental results are in good agreement with theoretical predictions, the energy fluctuations after the monochromator follow a negative exponential distribution.

1 Introduction

The correct design of a self-amplified spontaneous emission free electron laser (SASE FEL) and the planning of the equipment and experiments of FEL users depend strongly on an understanding of the radiation amplification process in the

¹ V. Ayvazyan, N. Baboi, I. Bohnet, R. Brinkmann, M. Castellano, L. Catani, P. Castro, M. Dohlus, H.T. Edwards, B. Faatz, A.A. Fateev, J. Feldhaus, K. Flöttmann, A. Gamp, T. Garvey, C. Gerth, V. Gretchko, B. Grigoryan, U. Hahn, C. Hessler, K. Honkavaara, M. Hüning, R. Ischebeck, M. Jablonka, T. Kamps, M. Körfer, M. Krassilnikov, J. Krzywinski, J. Lewellen, M. Liepe, A. Liero, T. Limberg, H. Loos, C. Magne, J. Menzel, P. Michelato, M. Minty, A. Mosnier, U.-C. Müller, D. Nölle, A. Novokhatski, C. Pagani, F. Peters, J. Pflüger, P. Piot, L. Plucinski, K. Rehlich, I. Reygl, A. Richter, J. Rossbach, E.L. Saldin, W. Sandner, H. Schlarb, G. Schmidt, P. Schmüser, J.R. Schneider, E.A. Schneidmiller, H.J. Schreiber, S. Schreiber, D. Sertore, S. Setzer, S. Simrock, R. Sobierajski, B. Sonntag, B. Steeg, F. Stephan, K.P. Sytchev, K. Tiedtke, M. Tonutti, R. Treusch, D. Trines, D. Türke, V. Verzilov, R. Wanzenberg, T. Weiland, H. Weise, I. Will, K. Wittenburg, M.V. Yurkov, K. Zapfe

SASE FEL and the knowledge of the properties of the output radiation. The amplification process in the SASE FEL starts from the shot noise in the electron beam. This implies that the SASE FEL radiation itself is of a stochastic nature. Theoretical investigations [1] predict that the radiation from a SASE FEL operating in the linear regime possesses all the features of completely chaotic polarized radiation. In particular, the probability density function of the energy in the radiation pulse should follow the gamma distribution, and the intensity after a narrow-band monochromator should fluctuate in accordance with a negative exponential distribution.

2 Theoretical background

In the linear mode of operation the SASE FEL can be treated as a narrow band linear device which filters a wide band random input signal – shot noise. A general property of such devices is that an output signal is a Gaussian random process. The properties of SASE FEL radiation can be adequately described in terms of statistical optics: time and spectral correlation functions, probability distributions of finite-time integrals of the radiation power (i.e. energy in the radiation pulse), and probability distributions of the radiation energy after a monochromator. The radiation from a SASE FEL operating in the linear regime falls into the category of statistical optics called completely chaotic polarized light [2]. A detailed study of the statistical properties of the radiation from a SASE FEL is presented in [1]. Here we summarize some results relevant to the SASE FEL operating in the high-gain linear regime:

- The distribution of the instantaneous radiation power P is a negative exponential distribution:

$$p(P) = \frac{1}{\langle P \rangle} \exp\left(-\frac{P}{\langle P \rangle}\right), \quad (1)$$

where $\langle P \rangle$ is the average power.

- Finite-time integrals of the instantaneous power (i.e. energy in the radiation pulse) follow a gamma distribution:

$$p(W) = \frac{M^M}{\Gamma(M)} \left(\frac{W}{\langle W \rangle}\right)^{M-1} \frac{1}{\langle W \rangle} \exp\left(-M \frac{W}{\langle W \rangle}\right), \quad (2)$$

where $\Gamma(M)$ is the gamma function, $M = 1/\sigma_W^2$, and $\sigma_W^2 = \langle (W - \langle W \rangle)^2 \rangle / \langle W \rangle^2$. The parameter M can be interpreted as the average number of “degrees of freedom” or “modes” in a radiation pulse. In the high-gain linear regime the radiation from SASE FEL is almost completely transversely coherent [3], and the value of M is the typical number of spikes in the radiation pulse. When M tends to unity, the distribution (2) tends to a negative exponential distribution (1). When $M \gg 1$, the distribution (2) tends to a Gaussian distribution.

- The probability density distribution of the radiation energy after a monochromator, $p(W)$, is also described rather well by a gamma probability density function. When transversely coherent radiation is filtered by a monochromator, the number of modes gradually decreases with increasing of the monochromator resolution. When the latter value becomes narrower than the width of a spike in the spectrum, the number of modes in the filtered radiation approaches unity, and the fluctuations of the radiation energy are distributed in accordance with a negative exponential distribution (1).

3 Description of the FEL facility

The experimental results presented in this paper have been achieved at the TESLA Test Facility (TTF) Free-Electron Laser at the Deutsches Elektronen-Synchrotron DESY. The goal of the TTF FEL is to demonstrate SASE FEL emission in the VUV and, in a second phase, to build a soft X-ray user facility [4].

The injector is based on a laser-driven $1\frac{1}{2}$ -cell rf gun electron source operating at 1.3 GHz [5–7]. The gun section is followed by a 9-cell superconducting cavity, boosting the energy to 16 MeV. Two superconducting accelerating modules accelerate the electron beam up to an energy of 300 MeV [8]. A bunch compressor is inserted between the two accelerating modules, in order to increase the peak current of the bunch.

The undulator is a fixed 12 mm gap permanent magnet device using a combined function magnet design with a period length of $\lambda_u = 27.3$ mm and a peak field of $B_u = 0.46$ T, resulting in an undulator parameter of $K = 1.17$ [9]. The undulator system is subdivided into three segments, each 4.5 m long. There is a spacing of 0.3 m between adjacent segments for diagnostics. The total length of the system is 14.1 m. The beam orbit straightness in the undulator is determined by the alignment precision of the superimposed permanent-magnet quadrupole fields which is better than $50 \mu\text{m}$ in both vertical and horizontal direction.

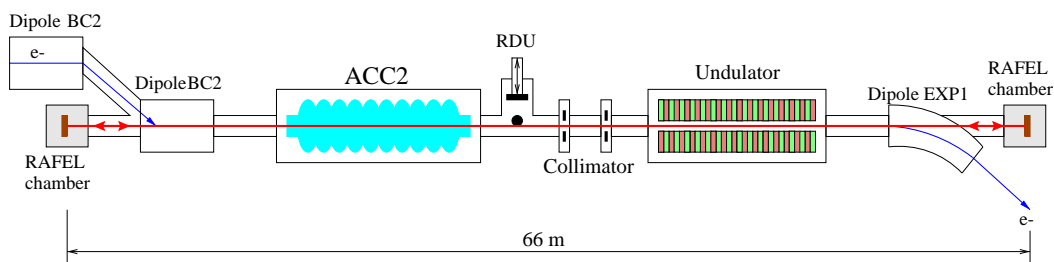


Fig. 1. General layout of the experimental facility. Here BC2 is the bunch compressor, Acc2 is the second accelerating module (120 to 240 MeV), RDU denotes the radiation detector unit (see Sec.4.2 for details). RAFEL chamber downstream the undulator houses a plane SiC mirror, and the chamber in the BC2 area hoses a grating. Both RAFEL chambers are equipped with MCP-based radiation detectors

Table 1
Main parameters of the VUV FEL at TESLA Test Facility

Parameter	Measured value
beam energy	180-270 MeV
rms transverse beam size	$100 \pm 30 \mu\text{m}$
electron bunch charge	1-3 nC
peak electron current	400-600 A
bunch spacing	0.444 ns
number of bunches in a train	24
repetition rate	1 Hz
undulator period, λ_u	27.3 mm
undulator peak field	0.46 T
effective undulator length	13.5 m
radiation wavelength, λ_{ph}	80-180 nm
FEL gain	10^6
spectrum bandwidth (FWHM)	0.6%
FEL radiation pulse energy	10-15 μJ
FEL radiation pulse length	0.5-1 ps
FEL radiation peak power	10-20 MW
FEL radiation peak brilliance	10^{27} phot./sec/mrad ² /mm ² /(0.1% BW.)

4 Experimental study of statistical properties of SASE FEL radiation

The main parameters for FEL operation are compiled in Table 1. Since the first lasing of the SASE FEL at DESY (February 2000) its performance has been gradually improved. The radiation wavelength is continuously tunable in a wide range from 80 to 180 nm [10]. At present the SASE FEL gain is tuned to the value of about 10^6 , of about one order of magnitude below the gain at saturation. This is a significant improvement compared to the FEL gain of about 3×10^3 obtained last year [11]). The energy in the radiation pulse is about 10-20 μJ , the pulse duration is 0.5-1 ps, the peak and average radiation power are about 20 MW and 0.2-0.3 mW, respectively. The peak brilliance is about 10^{27} phot./sec/mrad²/mm²/(0.1% BW.).

The stable operation of the facility has enabled us to perform detailed studies of the statistical properties of the radiation from the SASE FEL operating in the high-gain linear regime. The FEL radiation has been monitored with an MCP-based detector consisting of a thin gold wire scattering a tiny fraction of the SASE FEL radiation onto a micro-channel plate (MCP) [12]. The dynamic range of the detector is about eight orders of magnitude which covers the whole operating range of a SASE FEL (from spontaneous emission up to saturation). The scheme of experiment is presented in Fig. 1.

4.1 Fluctuations of the energy in the radiation pulse

Measurements of the energy in the radiation pulses have been performed by the MCP-based detector installed downstream the undulator in the RAFEL chamber (see Fig. 1). The accelerator has been operated with 24 bunches in a train (1.8 nC bunch charge, 0.444 ns bunch separation) at 1 Hz repetition rate. The radiation detector measured energy for every bunch with relative accuracy of better than 5%. Fluctuations of the output radiation energy occur from train-to-train and bunch-to-bunch within a train. In general they may be caused not only by statistical fluctuations of the SASE FEL radiation, but also by unstable operation of the accelerator. During the experiment we performed simultaneous measurements of individual bunch charges and offsets at the undulator entrance, the most critical beam parameters influencing the FEL process. The analysis of the results shows that the machine fluctuations were small and we did not find a significant correlation between a variation of the above mentioned parameters and the output radiation energy. Thus, we conclude that the measured fluctuations of the radiation energy in the bunch are dominated by the statistical properties of the SASE FEL radiation. During the experiment we stored information on 2000 macropulses and plotted the probability distributions of the radiation energy. Figure 2 illustrates relevant distributions for different bunch positions in the train. The solid curves represent the gamma-distribution (2). The parameter $M = 1/\sigma_W^2$ has been calculated from the experimental data. It is seen that there is good agreement of the measurements with theoretical predictions. Figures 3 and 4 shows the average radiation energy and parameter M along the train.

The determination of the parameter M gives us valuable information about the properties of the radiation pulse in time domain which can not be measured directly. Indeed, typical pulse duration of SASE FELs is about a fraction of a picosecond. The resolution time of modern fast photoelectric detectors is much larger than this value, about a fraction of nanosecond, which allows to measure only total energy

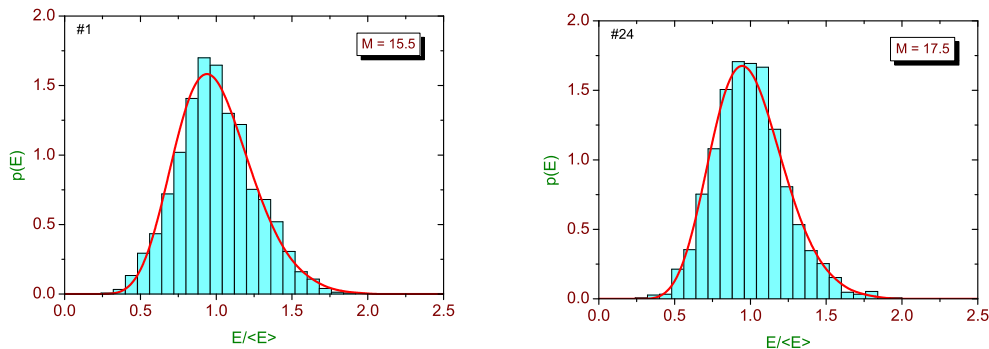


Fig. 2. Probability distribution of the energy in the radiation pulse. Left and right plots correspond to the first and the last bunch in the train, respectively. Solid curves: gamma-distribution.

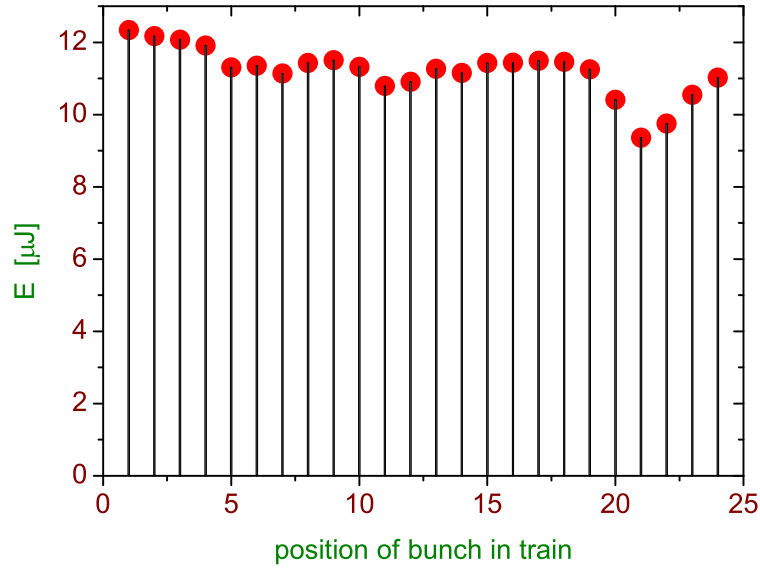


Fig. 3. Average energy in the radiation pulses versus position of the bunch in the train

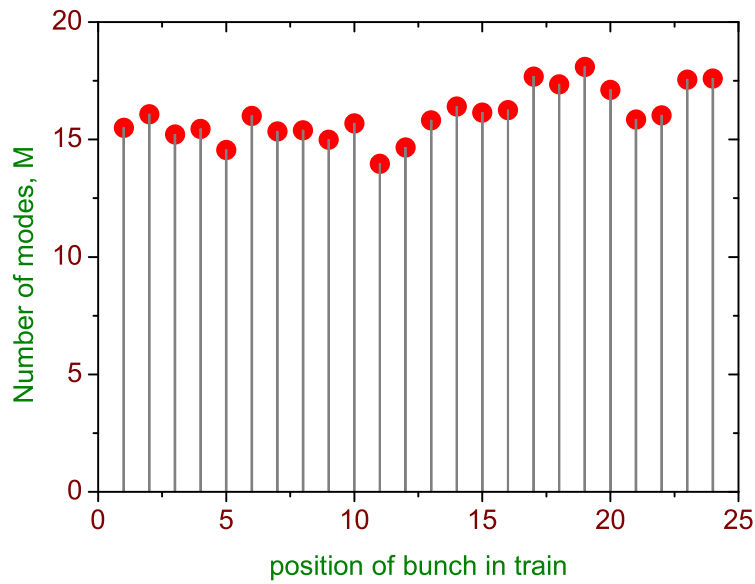


Fig. 4. Number of radiation modes, M , versus position of the bunch in the train

of the radiation pulse. For the SASE FEL operating in the high-gain linear regime the value of M has a direct physical meaning, namely it is about (in average) the number of modes (or spikes) in the radiation pulse in time (or spectral) domain. The typical scale of a spike in the frequency domain is the inverse value of the radiation pulse duration T . The spectral width $\Delta\omega$ of the radiation from a SASE FEL

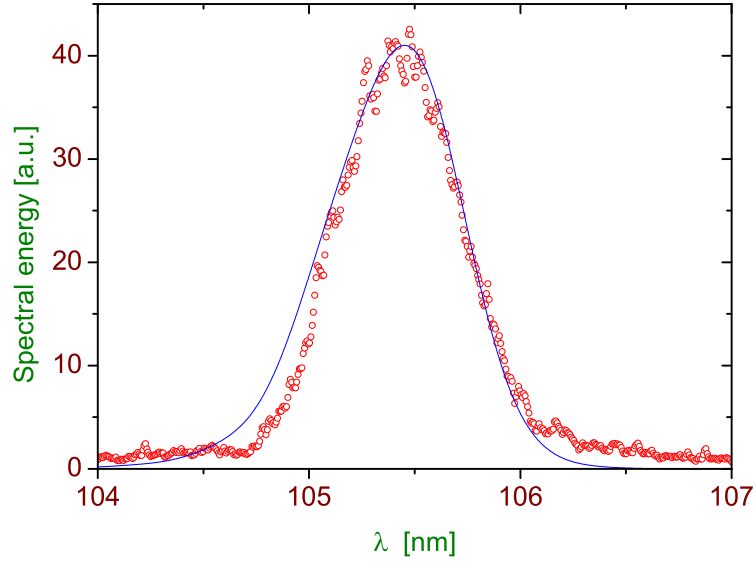


Fig. 5. Single-shot spectrum from TTF SASE FEL (circles). Spiky structure are not seen due to low resolution of monochromator. The solid curve presents the theoretical prediction for the averaged spectrum

can be measured without problems. A relevant measurement for our experiment is presented in Fig. 5. Thus, the radiation pulse length is given by $M/\Delta\omega$. Using the data presented in Figs. 4 and 5, we conclude that the radiation pulse length is about 0.5 ps.

4.2 Fluctuations of the energy after narrow-band monochromator

Measurements of fluctuations of the radiation energy after the monochromator have been performed using a narrow-band monochromator of the RAFEL (Regenerative Amplifier FEL [13]) optical feedback system. The scheme of the experiment is explained in Fig. 1. The SASE FEL radiation emitted by the electron beam is back-reflected by a plane SiC mirror (RAFEL chamber at the right side of the scheme) onto monochromator (RAFEL chamber at the left side of the scheme). The RAFEL monochromator is a spherical grating in Littrow mounting which disperses the light in the direction of the radiation detector unit (RDU) installed 27 meters downstream. The RDU is equipped with an MCP-based radiation detector with a thin ($200 \mu\text{m}$) gold wire which plays the role of an exit slit of the monochromator. The design of a spherical grating in Littrow mounting guarantees a resolution of about $(\Delta\omega/\omega)_M \simeq 10^{-4}$ which is less than typical scale of the spike in spectrum $\Delta\omega/\omega \simeq 3 \times 10^{-4}$ (this value is given by the SASE radiation spectrum width divided by the number of modes M). The experimental procedure is the same as being described in the previous section. We stored information on 300 radiation pulses passed monochromator and plotted a histogram of the probability distribu-

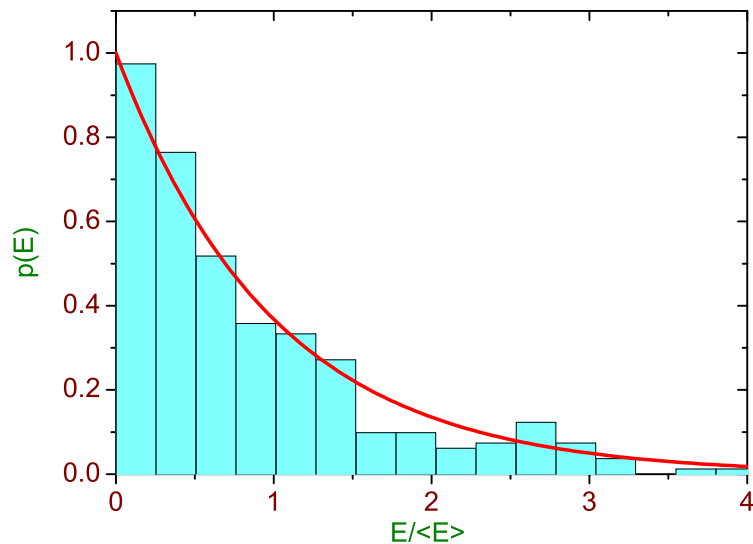


Fig. 6. Probability distribution of the energy in the SASE radiation pulse after narrow-band monochromator. Solid line: negative exponential distribution

tion of the radiation energy in the pulse. The solid curve in Fig. 6 represents the negative exponential distribution (1). It is seen that there is good agreement between experimental and theoretical results.

References

- [1] E.L. Saldin, E.A. Schneidmiller and M.V. Yurkov, *Opt. Commun.* **148**(1998)383
- [2] J. Goodman, *Statistical Optics*, (John Wiley and Sons, New York, 1985)
- [3] E.L. Saldin, E.A. Schneidmiller, and M.V. Yurkov, *Opt. Commun.* **186**(2000)185
- [4] J. Rossbach, *Nucl. Instr. and Meth. A* **375**, 269 (1996)
- [5] J.-P. Carneiro, et al., *Proc. 1999 Part. Acc. Conf.*, New York, 2027-2029 (1999)
- [6] P. Michelato, et al., *Nucl. Instr. and Meth. A* **445**, 422 (2000)
- [7] I. Will, S. Schreiber, A. Liero, W. Sandner, *Nucl. Instr. and Meth. A* **445**, 427 (2000)
- [8] H. Weise, *Proc. 1998 Linac Conf. Chicago*, 674-678 (1998)
- [9] J. Pfüger, *Nucl. Instr. and Meth. A* **445**, 366 (2000)
- [10] J. Rossbach et al., report at FEL2000 Conference, *Nucl. Instr. and Meth. A*, in press
- [11] J. Andruszkow et al., *Phys. Rev. Lett.* **85**(2000)3825

- [12] B. Faatz et al, "Use of micro-channel plate for nondestructive measurement of VUV radiation from SASE FEL at the TESLA Test Facility", Presentation at FEL2001 Conference
- [13] B. Faatz et al., Nucl. Instrum. and Methods **A429**(1999)424